The Pennsylvania State University

The Graduate School

Department of Civil and Environmental Engineering

AN INTEGRATED HYDROLOGIC MODEL FOR MULTI-PROCESS SIMULATION USING SEMI-DISCRETE FINITE VOLUME APPROACH

A Thesis in

Civil Engineering

by

Yizhong Qu

Submitted in Partial Fulfillment
of the Requirements
for the Degree of

Doctor of Philosophy

December 2004

We approve the thesis of Yizhong Qu.

Date of Signature

Christopher J. Duffy
Professor of Civil Engineering
Thesis Advisor
Chair of Committee

Qiang Du
Professor of Mathematics

Arthur C. Miller
Distinguished Professor of Civil Engineering

Paul E. Plassmann
Associate Professor of Computer Science and Engineering

Patrick M. Reed
Assistant Professor of Civil Engineering

Andrew Scanlon
Professor of Civil Engineering
Head of the Department of Civil and
Environmental Engineering

The thesis of Yizhong Qu was reviewed and approved* by the following

Christopher J. Duffy
Professor of Civil Engineering
Thesis Advisor
Chair of Committee

Qiang Du
Professor of Mathematics

Arthur C. Miller
Distinguished Professor of Civil Engineering

Paul E. Plassmann
Associate Professor of Computer Science and Engineering

Patrick M. Reed
Assistant Professor of Civil Engineering

Andrew Scanlon
Professor of Civil Engineering
Head of the Department of Civil and Environmental Engineering

*Signatures are on file in the Graduate School.

ABSTRACT

This thesis presents (1) a strategy to build an integrated hydrologic model using the semi-discrete finite volume approach; (2) the development of the Penn State Integrated Hydrologic Model (PIHM), an implementation of above theory with object-oriented data-model; (3) the verification and field application of PIHM to Shale Hills experiment in central Pennsylvania.

Numerical simulation of coupled non-linear hydrologic processes requires an efficient and flexible approach to solve a mixture of governing partial differential equations (PDE) and ordinary differential equations (ODE). A new strategy for integrated hydrological modeling is proposed in this thesis. First, those PDE's are reduced to ODE's using the semi-discrete finite volume method (FVM). This leads to a local ODE system (referred to as the model kernel). The kernel is distributed on an unstructured triangular irregular network (TIN) constructed from domain decomposition using Delaunay Triangulation. The global ODE system is formed by combining all local ODE systems over the entire domain and the system is solved with an efficient ODE solver. This strategy is designed to capture "dynamics" in multiple processes while maintaining the conservation of mass at all cells, as guaranteed by the finite volume formulation. A hypothetical test case is presented to demonstrate the flexibility and utility of this model.

The implementation and code verification of the above strategy, PIHM, is also discussed in this thesis. The model is coded in C with an object-oriented data-model,

one that is widely used in geographic information system (GIS) literature. The goal of the data structure used here is to ultimately connect the model and the solver with a GIS pre and post processors in a seamless manner, e.g. without the intermediate text files. In a seamless hydrologic modeling strategy, the numerical model and its pre/post-processor operate on the same data-model (referred to as a geo-database), which enables faster access of raw data and supports advanced user inquiries and visualization of the model results. The PIHM code is verified against analytic solution and other hydrologic models for several cases. For groundwater flow alone, the model converges to analytic solutions for radial groundwater flow to a well. For surface overland flow and channel routing within a v-shaped catchment, PIHM agrees well with other models using finite difference and finite element methods.

The first field application of PIHM is the Shale Hills Experiment (http://www.cee.psu.edu/Shale Hills/). In 1974, a field experiment is conducted at the Shale Hills, a watershed in central Pennsylvania, to investigate the hillslope runoff response to multiple rainfall events. The data reveals that more than 37% of rainfall is stored in the aquifer during each rainfall event. It was also shown experimentally that groundwater recharges and relaxes over a fairly long time scale (~weeks). The actual percentage of rainfall stored in the aquifer during rainfall events depends on the antecedent soil moisture, e.g. the initial conditions for soil moisture. Since the antecedent soil moisture builds up gradually during the series of storms, the runoff response increases noticeably in Shale Hills experiment. The ephemeral channel in the upland region of the watershed at Shale Hills expands and shrinks during rainfall events. The flowing portion of the stream cannot be pre-determined, and represents a physical process that challenges current models that do not fully-couple channel routing with overland and groundwater flow. It is well-resolved in the simulation with the new approach proposed in this thesis. PIHM results clearly reflect the change in channel length and agree well with experiment observations. Both field data and numerical results agree that all of three major rainfall-runoff generation mechanisms take place at Shale Hills. Among them, saturation overland flow is the most important contributor to the total runoff. With this feedback mechanism, subsurface hydrologic processes modulate surface runoff generation where the water table saturates the surface. The area of saturation is interpolated from soil moisture numerical results captures soil moisture building up during the entire simulation. The numerical results reveal that the saturation area is discontinuous and after each successive storm event, evolves from a disconnected patchwork of saturated elements to a highly connected network of saturated elements in what might be called "patch dynamics". Much of this effect is the result of local complex terrain as the hydraulic conductivity used is relatively homogeneous. Although the application is for a small (~20 acre) watershed, it demonstrates the magnitude and timing of feedback processes when full coupling of all physical processes are implemented in the model.

TABLE OF CONTENTS

LIST OF FIGURES

CHAPTER 2

CHAPTER 3

CHAPTER 4

LIST OF TABLES

CHAPTER 3

CHAPTER 4

ACKNOWLEDGEMENTS

First, I would like to express my sincerest gratitude to my advisor, Dr. Christopher, J. Duffy for his financial support, insightful guidance and constant encouragement. As his student, I have been very fortunate to enjoy a generous and patient academic environment he created for the last four years.

I would like to thank Dr. Qiang Du and Dr. Patrick M. Reed for their constructive comments on this research. I would also like to thank Dr. Paul E. Plassmann for his recommendation of SUNDIALS package. Special thanks are also given to Dr. Arthur C. Miller for his suggestion about channel routing process.

I am very thankful for many friends and colleagues who have helped me and enrich my experiences in Happy Valley. Special thanks are given to Guobiao Huang, Yilin Fang, Jun Sun, Yong Tang and all my tennis partners. I am also grateful to Kris Sedmera and Martha Sedmera who had helped me a lot when I first came to the United States in 2000.

I am deeply indebted to my parents, Zhi Qu and Guizhen Wang for their wisdom and constant belief that higher education will make my life better. Finally, I want to thank my wife, Weixiu Luo, for her love, encouragement and for being a wonderful wife. Her confidence in me has always been the most important sources of my momentum.

CHAPTER 1
INTRODUCTION

There have been many successful hydrologic models which focus on simulating a single hydrologic process. Recently, modelers have been challenged to simulate multiple processes in order to satisfy the growing demand for comprehensive hydrologic and climate forecasts. One such demand has been to evaluate the importance of the fully coupled processes to provide accurate long term water resource predictions. For instance, overland flow, as it converges to a stream channel, may also infiltrate into the soil. This infiltration increases the soil moisture and will recharge the underlying water table, which in turn augments the stream-flow over a longer time scale. Another example is a flood-wave within the channel dynamically interacting with the adjacent aquifer while the flood event is routed down stream. It is often referred as the “bank storage effect”. Another very important demand has been to couple hydrologic models with general circulation model (GCM) in large scale climate change simulations. In cases where spatially distributed results are required, it is necessary that the hydrologic model simulate the soil moisture, groundwater level as well as stream flow hydrograph at outlet of the watershed.

Numerical simulation of coupled nonlinear hydrologic processes requires an efficient and flexible approach. There have been several hydrologic models developed to simulate multiple processes with various approaches. MIKE-SHE (Abbott 1986) is a comprehensive deterministic, distributed and physically-based modeling system for the simulation of major hydrological processes occurring in the land phase of hydrologic cycle. It simulates water movement, water quality and sediment transport in different modules. Each process has its independent governing equation and solution technique (Singh, 1995). The coupling techniques used in MIKE-SHE can generally be described as boundary condition forcing, i.e., one process is coupled to others by providing boundary conditions or as external driven forcing. This approach is also called "weak coupling". A control unit (frame) is run to control time steps of the components and unilateral data exchange among the modules. An aquifer-river exchange component is designed to handle bilateral interactions between river and aquifer.

There have been fully coupled integrated hydrological model developed (VanderKwaak, 1999; Panday and Huyakorn, 2004). In these approaches, Saint Venant equations are approximated with the same form as Richard's equation (nonlinear diffusion equation) so that they can be conveniently assembled into one mass matrix using finite element method (FEM) or finite difference method (FDM). In the fully coupled technique, flux across the land surface is a natural internal process allowing water to move between the surface and subsurface flow systems as governed by local flow hydrodynamics, instead of using artificial boundary conditions at the interface. For a fully integrated approach, the system of equations is linearized using Newton-Raphson schemes, and solved in an iterative fashion at every time step. However, for integrated models using this strategy it is difficult to incorporate all processes into one single solution matrix without significant approximation. For instance, in the mountainous region where channel slope is steeper and the diffusion wave approximation is not suitable, other approximations, such as the kinematic wave approximation, cannot be incorporated by these approaches.

In this thesis, a new strategy for integrated hydrological modeling is proposed using the semi-discrete finite volume method (FVM). The idea is to first semi-discretize all governing PDE's into ODE's, then solve a global system of ODE's using a state-of-art ODE solver. This strategy has several advantages. First, the user can incorporate the desired number of processes simply by setting on/off switches prior to simulation. Second, trial constitutive relationships are easily applied and tested with numerical experiments. For instance, either the diffusive wave or the kinematic wave approximation can be applied to the St. Venant equations, depending on the application. Finally, the control volume can be any shape as long as the orthogonal flux across element boundary can be evaluated with the FVM. This approach requires a sophisticated algorithm for domain decomposition which will be discussed in detail later.

This thesis consists of three research papers designated by chapters. Chapter 2 is the first paper and it presents the theoretical approach with a hypothetical watershed example to show the dynamics and utility of full model integration. It was submitted to Water Resource Research in October 2004. Chapter 3 presents the Penn State Integrated Hydrologic Model (PIHM), the C code implementation of the theory with an object oriented data-model. Several cases are shown for verification of the components in the model in this chapter. Chapter 3 is intended to be submitted to

Computers and Geosciences. Chapter 4 presents a real application of PIHM to Shale Hills Experiments, PA. This paper is intended to be submitted to Hydrological Processes.

REFERENCES

Abbott, M.B., Bathurst, J.A., Cunge, P.E., 1986. An Introduction to the European Hydrological System-Systeme Hydrologicque Europeen "SHE" 1: History and philosophy of a physically based distributed modeling system. Journal of Hydrology, 87, 45-59.

Abbott, M.B., Bathurst, J.A., Cunge, P.E., 1986. An Introduction to the European Hydrological System-Systeme Hydrologicque Europeen "SHE" 2: Structure of a physically based distributed modeling system. Journal of Hydrology, 87, 61-77.

Panday, S., Huyakorn, P.S., 2004. A fully coupled physically-based spatially-distributed model for evaluating surface/subsurface flow. Advances in Water Resources 27, 361-382.

VanderKwaak, J., 1999. Numerical simulation of flow and chemical transport in integrated surface-subsurface hydrologic systems. Ph.D Thesis in Earth Sciences, University of Waterloo, Waterloo, Ontario, Canada, 217pp.

Singh VP (editor), Computer Models of Watershed Hydrology, Water Resources Publications, 1995

CHAPTER 2
AN INTEGRATED HYDROLOGIC MODEL FOR MULTIPLE PROCESS SIMULATION

Yizhong Qu[1] and Christopher J Duffy[1]

[1]Department of Civil and Environmental Engineering
The Pennsylvania State University
University Park, PA 16802

ABSTRACT

Major hydrological processes within the terrestrial hydrological cycle operate over a wide range of time scales with interactions among them ranging from uncoupled to strongly coupled. Numerical simulation of coupled nonlinear hydrologic processes requires an efficient and flexible approach. In this paper, a new strategy for integrated hydrological modeling is proposed, which reduces the governing partial differential equations (PDE) to ordinary differential equations (ODE) using the semi-discrete finite volume method (FVM). This leads to a local ODE system referred to as the model kernel, which is distributed on an unstructured triangular irregular network (TIN) constructed from domain decomposition using Delaunay Triangulation. The global ODE system is formed by combining local ODE system over the entire domain and the system is solved with an efficient ODE solver. The finite volume elements are prisms, projected from the TIN generated with constraints. The constraints are related to the river network and watershed boundary, elevation contours, etc. The model is

designed to capture "dynamics" in multiple processes while maintaining the conservation of mass at all cells, as guaranteed by the finite volume formulation. A test case is presented to demonstrate the flexibility and utility of this model.

Key words: integrated hydrologic model, semi-discrete, finite volume method, and multiple processes.

2.1 INTRODUCTION

Governing equations in environmental models typically arise from conservation laws and constitutive relationships. For diffusive processes, a parabolic partial differential equation (PDE) results when a constitutive relationship involves only first order derivatives of the unknown state, while hyperbolic PDE's arise for other constitutive relations. A commonly used numerical approach to solving PDE's is based on the finite element method (FEM), which applies a variational formulation of the PDE. In the spatial domain, continuous trial basis functions are constructed to form a global stiffness matrix, and a linear solver is used to find solutions at nodal values in test space [Johnson, 1990]. In time, simple finite differencing, e.g. backward Euler, is used in many cases. The FEM approach became popular, in recent decades, due to availability of fast iterative solvers [Xu, 1989]. However, its lack of assured mass conservation and inability to handle discontinuous solutions represents a disadvantage in some applications of interest to hydrologists.

In case of finite volume method (FVM), conservation laws are conveniently derived from physical laws in integral form. It approximates the total integral with the average of the state over the control volume [Leveque, 2002]. The volume average is updated and the flux across control volume is determined at each time step in the numerical solution. FVM can effectively handle discontinuous solutions and guarantee mass conservation throughout the simulation for all states while evaluating the flux across element boundaries with appropriate constitutive relationships and desired order accuracy.

Recently, the FVM has been applied to solve energy, solute, and reactive transport equations in chemical engineering, mechanical engineering and electronic engineering [http://www.math.ntnu.no/conservation/]. In hydrology, the FVM has been used to solve the Saint-Venant equations in order to simulate channel and estuarine flow [Sleigh et al., 1998; Garcia-Navarro et al, 1995].

In this paper, the FVM discretization is carried out in two stages. The governing PDE's are first discretized in space, leaving the problem continuous in time. This results in a system of ordinary differential equations (ODE). This approach is often called the "semi-discrete" method or "method of lines" [Madsen, 1975]. An important feature of the semi-discrete approach is that it provides a convenient way to couple mixtures of PDE's and ODE's for multiple processes, which is attractive for multi-process hydrologic applications. In the first stage of discretization, the reduced system of ODE's together with those original ODE's represents all processes within a finite volume/control volume. It is referred to as the "local system" in this paper. The control volume containing the governing equations for multiple processes and the local system of ODE's, together are referred to as the model kernel. In the second stage, combining the local system over the domain leads to a "global" system which is solved with a state-of-art ODE solver.

Computational cost to solve such a system of ODE's is another concern. Because of the multiple time scales in a multi-process model, the resulting system is likely to be “stiff”. That is, one or more processes may have very small damping time constants in the system. For stiff systems, it is necessary to use implicit ODE solvers which require more operations in one time step to meet numerical stability criteria [Ascher and Petzold, 1998]. Fortunately, there are well tested and efficient sequential and parallel implicit solvers, such as the SUNDIAL package [Cohen and Hindmarsh, 1994] for solving highly stiff problems. In general, the semi-discrete finite volume approach is a flexible and efficient strategy for multi-process hydrologic modeling comparable to existing finite difference and finite element codes [Abbott et al., 1986; Yeh, 1987].

2.2 MODEL STRATEGY

2.2.1 Semi-Discrete Approach with FVM

The general form of mass conservation equation of incompressible fluid flow can be written as

$$\frac{\partial \rho}{\partial t} + \nabla \cdot u = 0 \tag{1}$$

where ρ is fractional mass (dimensionless) in an arbitrary control volume, and u is fluid flux [L/T]. Mass conservation implies that the change rate of ρ is exactly balanced by the divergence of the flux. The integral form over the control volume V is given by:

$$\int_V \frac{\partial \rho}{\partial t} dV = -\int_V \nabla \cdot u dV \ . \tag{2}$$

Applying the divergence theorem to the right hand side yields

$$-\int_V \nabla \cdot u dV = -\int_S u \cdot N dS \tag{3}$$

where S is surface of V, and N is the normal vector on S. Combining equation (2) and (3) leads to

$$\int_V \frac{\partial \rho}{\partial t} dV = -\int_S u \cdot N dS \ . \tag{4}$$

Computing the right-hand-side of equation (4) using the finite volume formulation [Leveque, 2002] yields

$$-\int_S u \cdot N dS = \sum_{i=1}^{S} Q_i \qquad (5)$$

where the net flux Q_i across surface i, is positive in and negative out.

Letting the integral form of the left hand side of (4) be $M = \int_V \rho dV$, leads to the semi-discrete form of the mass conservation equation

$$\frac{dM}{dt} = \sum_{i=1}^{S} Q_i \qquad (6)$$

where M is mass storage of control volume. Q_i is evaluated as the normal flux to each surface of the control volume. For simplicity, we classify the flux into inflow and outflow terms,

$$\frac{dM}{dt} = Q_I - Q_O \qquad (7)$$

where Q_I represents summation of inflow and Q_O stands for summation of outflow. The vector form of (7) represents the system of ODE's within a control volume. Substitution of appropriate constitutive equations into (7) allows the flux to be evaluated across the element boundary. We note that the finite volume method guarantees mass conservation for each control volume and it has the convenient ODE form of balance equations for both parabolic and hyperbolic PDE's [Leveque, 2002].

2.2.2 Advantages of the Kernel in Semi-Discrete Approach

Under circumstances where full coupling of multiple hydrologic processes is required, there are several reasons that the model kernel approach described above offers a simple, yet flexible numerical strategy. First, the user can incorporate the desired number of processes simply by setting on/off switches prior to simulation. Second, trial constitutive relationships are easily applied and tested with numerical experiments. Finally, the control volume can be in any shape as long as orthogonal flux across boundary is feasible to be evaluated with the FVM.

In this paper the hydrological processes included in the model are: canopy interception, evapotranspiration, overland flow, infiltration, vertical unsaturated flow, and lateral groundwater flow. The solution domain (e.g. the watershed) is decomposed into a triangular unstructured grid, and the finite volume element is a prism while the channel segment is represented as uniform as shown in figure 1. A prism element may have channel segments along any edge. Details of the governing equations, boundary conditions and interactions are discussed in a later section.

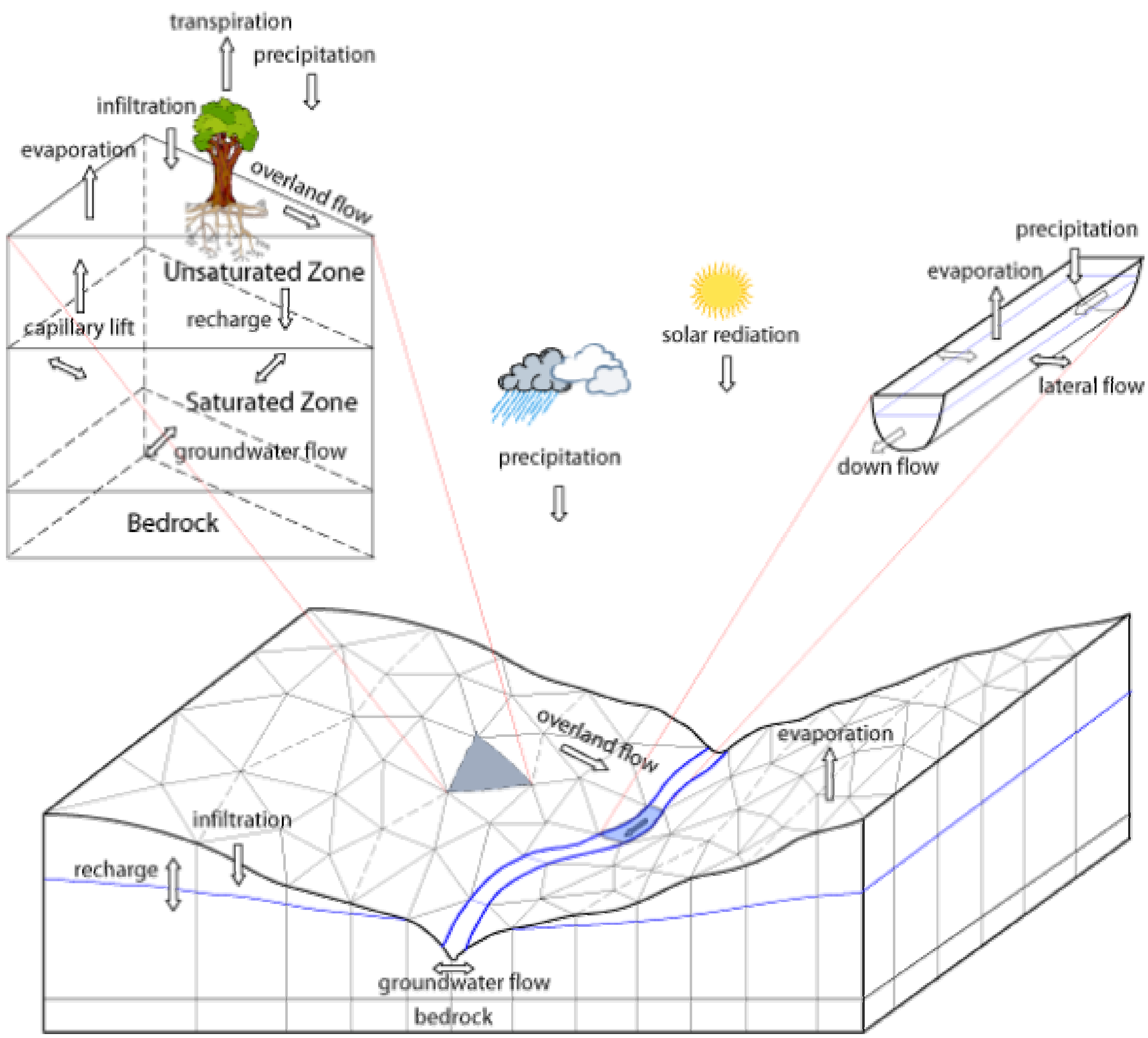

Figure 1 **Spatial decomposition in a hillslope scale example. Basic prism element is shown to the left with multiple hydrological processes. Channel segment is shown to the right. The major hydrologic processes associated with elements and their connections are also shown.**

2.3 BUILDING THE LOCAL ODE SYSTEM

As discussed earlier, the governing equations for hydrologic processes are either PDE's or ODE's. In this case, the model described here assumes 2-D overland flow, 1-D vertical unsaturated flow, and 2-D horizontal saturated groundwater flow. For the channel, 1-D channel routing is assumed. Auxiliary processes for canopy interception, snow accumulation/melting in the model kernel are assumed to be described by ODE's. It should be noted that there are no intrinsic limitations to more complex models assumptions, and the choices evolve from practical considerations of the authors' research.

2.3.1 Semi-Discrete Form of the Governing PDE's

2.3.1.1 Surface overland flow

The governing equation for surface overland flow is the 2D St. Venant equations, given by the equation of continuity

$$\frac{\partial h}{\partial t}+\frac{\partial (uh)}{\partial x}+\frac{\partial (vh)}{\partial y}=q \tag{8}$$

and two momentum equations

$$\frac{\partial (uh)}{\partial t}+\frac{\partial \left(u^2 h\right)}{\partial x}+\frac{\partial (uvh)}{\partial y}+gh\left(S_{fx}+\frac{\partial H}{\partial x}\right)=0 \tag{9}$$

$$\frac{\partial (vh)}{\partial t}+\frac{\partial \left(v^2 h\right)}{\partial y}+\frac{\partial (uvh)}{\partial x}+gh\left(S_{fy}+\frac{\partial H}{\partial y}\right)=0 \tag{10}$$

where $h(x,y,t)$ is the local water depth, and $H(x,y,t)$ is the water surface elevation above an horizontal datum. u and v are flow velocities in x and y directions, respectively. q is areal source term normalized by surface area. g is the gravity constant. S_{fx} and S_{fy} are friction slope in x and y directions, which can be estimated using Manning's equation.

Sleigh et al. [1998] have developed a numerical algorithm solving full St. Venant equation with finite volume method for predicting flow in rivers and estuaries, in which the normal flux vector is calculated using Riemann approach [Leveque, 2002]. Applying semi-discrete approach to equation (8)-(10) results in three unknowns, i.e., h , u_x , u_y , for each element.

One approximation, called the diffusion wave approximation, neglects the inertia terms in the momentum equations in (9) and (10) and uses Manning's formula to estimate friction slopes. The two-dimensional diffusion wave approximation [Gottardi and Venutelli, 1993] is given by

$$\frac{\partial h}{\partial t} = \sum_{i=1}^{2} \frac{\partial}{\partial x_i}\left(hk_i \frac{\partial H}{\partial x_i} \right) + q_e \tag{11}$$

with

$$k_i = \frac{h^{\frac{2}{3}}}{n_i} \frac{1}{\left| \partial H / \partial s \right|^{\frac{1}{2}}} \tag{12}$$

where n is Manning roughness coefficients. s is a vector along the direction of maximum slope.

The 2-D St. Venant equation is simplified to a diffusive wave equation with only one unknown state in equation (11) by introducing a non-linear effective hydraulic conductivity. To evaluate it over an unstructured grid, denote (x_i, y_i, z_i) as local coordinates associated with vertex V_i, where z_i is hydraulic head (see Fig 2). Assume the plane determined by vertex V_2, V_3, V_4 and the triangular element of $D_4D_7D_8$ are identical. The plane is defined by $\begin{vmatrix} x & y & z & 1 \\ x_2 & y_2 & z_2 & 1 \\ x_3 & y_3 & z_3 & 1 \\ x_4 & y_4 & z_4 & 1 \end{vmatrix} = 0$. The hydraulic head gradient along the maximum slope direction of the element $D_4D_7D_8$ can be calculated by $\frac{\partial H}{\partial s} = \frac{s}{\|s\|} \cdot \nabla H = \sqrt{\left(\frac{(y_3 - y_2)(z_4 - z_2)}{(x_2 - x_3)(y_4 - y_2)}\right)^2 + \left(\frac{(x_4 - x_2)(z_3 - z_2)}{(x_3 - x_2)(y_4 - y_2)}\right)^2}$.

Integrating equation (11) over control volume i yields

$$\left(A\frac{\partial h}{\partial t} = \int_\Gamma V \cdot nd\Gamma + \int_v q_e dv \right)_i \tag{13}$$

where V is flux across the element boundary, and n is normal vector to Γ. q_e represents the source and interaction term, including infiltration and surface overland flow/channel interaction.

Rearranging equation (13) and then normalizing by surface area yields

$$\left(\frac{\partial h}{\partial t} = P_o - I - E_o - Q_{oc} + \sum_{j=1}^{3} Q_s^{ij} \right)_i \tag{14}$$

where Q_s^{ij} is surface flow from element i to its neighbor j, evaluated by equation

(11) and (12). P_o , I and E_o are precipitation, infiltration and evaporation respectively. Q_{oc} describes interaction between overland flow and channel routing. Please note all fluxes are normalized by projected surface area of the prismatic element.

The kinematic wave approximation [Eagleson, 1970], defines the stage and discharge in terms of

$$Q = \alpha A^m \tag{15}$$

where α and m are empirical parameters. Combining equation (15) and continuity equation (8) will also result in only one unknown for each finite volume element.

2.3.1.2 Subsurface flow

Combining continuity equation and Darcy's law

$$\frac{\partial \theta}{\partial t} + \nabla \cdot q = 0 \tag{16}$$

$$q = K(\psi)\nabla(\psi + Z) \tag{17}$$

over both saturated and unsaturated zone yields Richards' equation in form of

$$C(\psi)\frac{\partial \psi}{\partial t} = \nabla \cdot (K(\psi)\nabla(\psi + Z)) \tag{18}$$

where θ is dimensionless volumetric soil moisture in control volume. q is flow flux [L/T]. ψ is pressure head [L], and $\psi + Z$ is hydraulic head. $C(\psi)$ is the specific moisture capacity. $K(\psi)$ is the non-hysteretic unsaturated hydraulic conductivity.

Applying the Reynolds transport theorem [Slattery, 1978] and the divergence theorem, Duffy [1996, 2004] integrates Richards' equation within a control volume having both unsaturated zone and saturated zone, and yields a two-state dynamic representation of the volume averaged states

$$A_i^+ \frac{d}{dt}\int_h^{z_s} \theta dz = -\int_{A_i^+} q \cdot \lambda dA + \int_{A_i^0} (q - \theta^+ u) \cdot \lambda dA \tag{19}$$

$$A_i^- \frac{d}{dt}\int_{z_b}^{h} \theta dz = +\int_{\Gamma_i^-} q(h - z_b) \cdot \eta d\Gamma - \int_{A_i^0} (q - \theta^- u) \cdot \lambda dA \tag{20}$$

where A_i^+ is the projected surface area of the unsaturated zone of element i. A_i^- is the projected surface area of the saturated zone element i. Γ_i^- is the perimeter of the saturated zone portion of element i. z_b, h, and z_s are elevation of bedrock, groundwater table and surface respectively. λ and η are normal vectors. $\int_{A_i^0}(q - \theta^- u) \cdot \lambda dA$ is the net vertical flux from or to groundwater table. q represents flux in general. u is the velocity of water table surface.

Rewriting equation (19) and (20) for the prismatic element shown in Figure 1 yields

$$\left(\frac{d\xi}{dt} = I - q^0 - ET_s\right)_i \tag{21}$$

$$\left(\frac{d\zeta}{dt} = q^0 + \sum_{j=1}^{3} Q_g^{\ ij} - Q_l + Q_{gc}\right)_i \tag{22}$$

where ξ [L] is unsaturated moisture storage of element i. ζ [L] is saturated moisture storage. q^0 is internal flux between unsaturated zone and saturated zone, referred to as capillary lift for upward flow from the water table or recharge for downward flow to water table. I and ET_s are incoming infiltration and outgoing evapotranspiration at land surface, respectively. As shown in equation (14), infiltration is generated by precipitation, Hortonian or Dunne overland flow. ${Q_g}^{ij}$ is lateral groundwater flow from element i to its neighbor j. Q_l is vertical leakage through an underlying confining bed. Q_{gc} is discharge/recharge from/to aquifer to/from channel. In this approach all fluxes are normalized by surface area of the element with units [L/T].

For each prismatic element, lateral groundwater fluxes are evaluated using a volume-average version of Darcy's law [Duffy, 2004]. Before normalization, it is in form of

$$ {Q_g}^{ij} = B_{ij} K_{eff} \frac{H_i - H_j}{D_{ij}} \frac{\zeta_i + \zeta_j}{2} \tag{23} $$

where B_{ij} is length of common boundary and D_{ij} is distance between element i and j. $H_i = \zeta_i + z_i$ is hydraulic head where z_i is elevation of datum of element i. The effective hydraulic conductivity K_{eff} is harmonic mean of element i and j. The storage-discharge relation in equation (23) is a non-linear one due to vertical integration. Brandes [1998] also shows by way of numerical experiments that, at the hillslope scale, the integral storage-discharge or "effective" constitutive relationship, is a non-linear function of hydraulic head.

For the internal flux q^0 between unsaturated zone and saturated zone, i.e. recharge or capillary lift, Duffy [2004] has shown that a simplified form based on integration over the finite volume can be approximated by

$$q^0(\xi,\zeta) = K_s \frac{1-e^{-\alpha(z_s-\xi)} - \alpha\zeta}{\alpha(z_s-\xi)-(1-e^{-\alpha(z_s-\xi)})} \tag{24}$$

where K_s is saturated hydraulic conductivity. α is a parameter for the exponential soil model. Z_s is total aquifer depth. We note that the integrated flux at the water table (24) is a nonlinear function of the water table position and the depth of soil moisture above the water table.

2.3.1.3 Channel routing

For channel routing the 1-D St. Venant equations are applied.

$$\frac{\partial h}{\partial t} + \frac{\partial (uh)}{\partial x} - q_l = 0 \tag{25}$$

$$\frac{\partial (uh)}{\partial t} + \frac{\partial (u^2 h)}{\partial x} + gA\frac{\partial H}{\partial x} + gAS_{fx} = 0 \tag{26}$$

where u is flow velocity in x towards the downstream direction. q_l is spatially averaged lateral inflow/outflow. h is local water depth, and H is water surface elevation. S_{fx} is friction slope.

Applying the semi-discrete procedure for the continuity equation involves integration of equation (26) along a (uniform) channel segment

$$\int_{L_i} \frac{\partial A}{\partial t} = \int_{L_i} q_l - \int_{L_i} \frac{\partial Q}{\partial x} \tag{27}$$

where L_i is length of element i. Since

$$\int_{L_i} \frac{\partial Q}{\partial x} = Q_{out} - Q_{in} \tag{28}$$

therefore,

$$\left(\frac{d\varsigma}{dt} = P_c - \sum Q_{gc} + \sum Q_{oc} + Q_{in} - Q_{out} - E_c \right)_i \tag{29}$$

where ς is volumetric water in channel. P_c is precipitation applying to channel element i. E_c is evaporation from channel segment. $\sum Q_{gc}$ is the summation of the lateral interaction between aquifer and channel, which is evaluated by Darcy's law. Q_{oc} refers to interaction between overland flow at surface and channel routing. A weir equation is assumed to connect overland flow and the channel [Panday and Huyakorn, 2004]. Q_{in} is inflow from other channel segments. Q_{out} is outflow to other channel segments. Again, all the fluxes are normalized by segment surface area.

Like 2D overland flow, the kinematic wave or the diffusion wave approximations can also be applied to reduce the complexity of solving full St. Venant equations. For instance, in the kinematic wave approximation, one can simplify the form of the momentum equation by using Manning-type equation (15). In diffusion wave approximation, one can use equation (12).

2.3.2 Processes Governed by ODE's

2.3.2.1 Interception process

In the presence of vegetation and canopy, a fraction of precipitation is intercepted before it impacts the ground. Water intercepted by vegetation is stored in the canopy temporally until it returns to the atmosphere as ET, drains down to surface, or utilized directly by the plant. We assume that spatial interactions between element neighbors are insignificant. Therefore, the governing equation is an ODE of the form

$$\left(\frac{dS_I}{dt} = P - E_I - P_o\right)_i \tag{30}$$

where S_I is interception storage. P is total water equivalent precipitation, E_I and represents evaporation from surface vegetation, P_o is through-fall precipitation, which is also the input of overland surface storage. The upper bound of S_I is a function of vegetation type, canopy density and even the precipitation intensity. When the canopy reaches the upper threshold, all precipitation becomes through-fall.

2.3.2.2 Snowmelt process

The accumulation and snowmelt process is a cold-season counterpart to interception. Here we apply a simple index approach to snow accumulation and melt [Dingman, 1994]. Assuming that vegetation is dormant during the snow season, and while air temperature is below snow-melting temperature T_m, the snow pack will accumulate during precipitation. Likewise, if air temperature exceeds the melting temperature, snow pack melts. The dynamic snowmelt model is given by

$$\left(\frac{dS_{snow}}{dt} = P - E_{snow} - \Delta w\right)_i \tag{31}$$

where Δw is snow melting rate, which is also an input to overland flow. It can be calculated by

$$\Delta w = \begin{cases} M(T_a - T_m), & T_a > T_m \\ 0, & T_a \le T_m \end{cases} \tag{32}$$

where M is melt factor, which can be estimated from empirical formulas [Dingman, 1994], and E_{snow} is evaporation directly from snow.

2.3.2.3 Evaporation and evapotranspiration

Evaporation from vegetation interception, overland flow, snow pack and river surfaces is estimated using the Pennman Equation [Bras, 1990], which represents a combined mass-transfer and energy method.

$$\left(E = \frac{\Delta(R_n - G) + \rho_a C_p (e_s - e_a)}{\Delta + \gamma}\right)_i \tag{33}$$

Potential evapotranspiration from soil and plant is estimated using Pennman-Monteith equation

$$\left(ET_0 = \frac{\Delta(R_n - G) + \rho_a C_p \dfrac{(e_s - e_a)}{r_a}}{\Delta + \gamma(1 + \dfrac{r_s}{r_a})}\right)_i \tag{34}$$

here, ET_0 refers to potential evapotranspiration. R_n is net radiation at the vegetation surface. G is soil heat flux density. $e_s - e_a$ represents the air vapor pressure deficit.

ρ_a is the air density. C_p is specific heat of the dir. Δ is slope of the saturation vapor pressure- temperature relationship. γ is the psychometric constant. r_s and r_a are the surface and aerodynamic resistances. Actual evapotranspiration is a function of potential ET and current plant, climatic and hydrologic conditions, such as soil moisture. In this approach, coefficients are introduced to calculate actual ET from potential following Kristensen and Jensen [1975]. Allen et al. [1998] provides guidelines for computing those coefficients for different vegetation.

Combining equation (14), (21), (22), (29), (30) and (31) together leads to a local system of ODE's representing multiple hydrological processes within element i including the land surface and channel dynamics. Those interactions can be evaluated with constitutive relations in equation (12), (15), (23), (24), (32), (33) and (34). As we mentioned before, one advantage of this strategy is flexibility in these constitutive relationship and there is no intrinsic limitations to other possible forms.

2.4 ASSEMBLE GLOBAL ODE SYSTEM

A global ODE system is formed by assembling all the local system, i.e. the kernel, throughout the entire domain. By this approach, we reduce a mixture of governing PDE's and ODE's representing all hydrologic processes over a domain to a global system of ODE's with respect to a particular domain decomposition. Next we examine an efficient way to decompose the domain, an important step in the model implementation.

2.4.1 Domain Decomposition

In this research the integrated finite volume model applies Delaunay Triangulation [Delaunay, 1934; Voronoi, 1908], an orthogonal-triangular unstructured grid represents the watershed terrain very efficient with fewest number of elements [Polis and McKeown, 1993; Vivoni, 2004], to decompose the 2-D domain surface. A 2-D TIN (triangular irregular network) is formed over the model domain with constraints in order to incorporate watershed boundaries, the stream network, soil type, geology, elevation contours or other features particular to the domain. The grid is then projected vertically to form prismatic volume elements, as shown in figure 1 and 2.

The circum-center assures that the flux across any edge with its neighbor is normal to the common boundary, and is used here to represent each triangle instead of the centroid. For instance, V_1V_2 is normal to D_4D_7 in figure 2. This simplifies evaluation of the flux across each boundary. However, it has the restriction that the circum-center has to remain within the triangle under all circumstances. There are ideas and algorithms [Shewchuk, 1997; Du, 2002] help generate good quality Delaunay triangulation, and make it possible to satisfy the above requirement from a set of points and constraints, in principal.

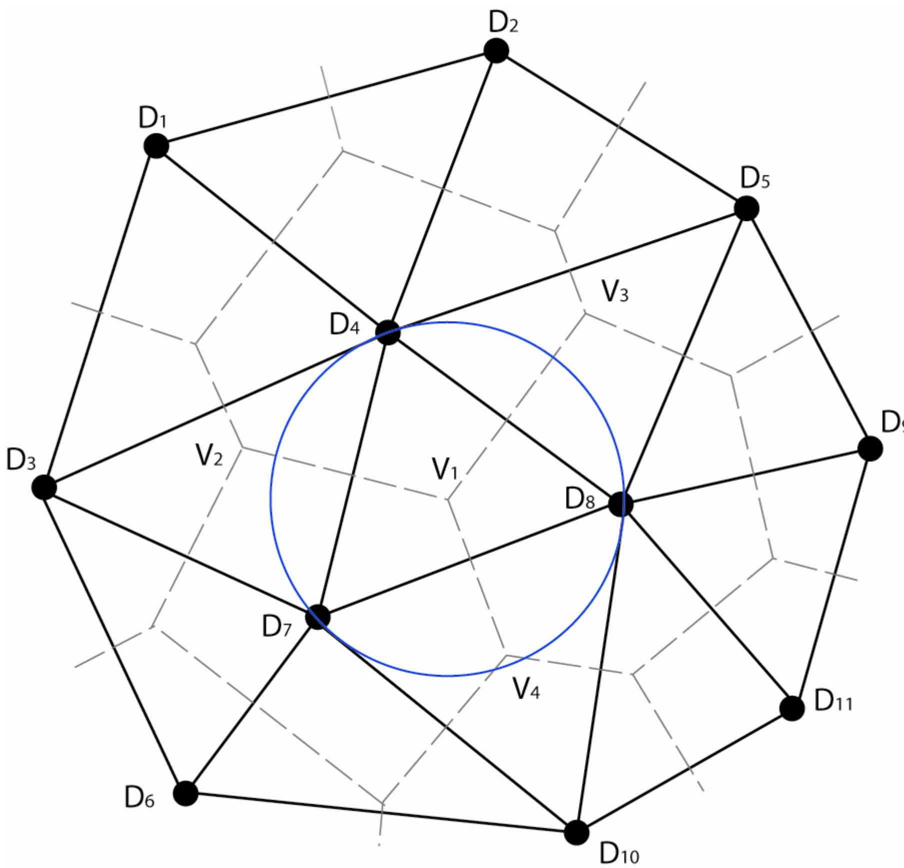

Figure 2 Delaunay triangulation (Delanunay, 1934) and Voronoi diagram (Voronoi, 1908). The solid lines form Delaunay triangulation, and the dashed lines form Voronoi diagram.

TIN generation for the watershed domain starts from a set of user defined control points. Generally, to represent the terrain with the fewest number of triangles, hydrographic points (including gage station and dams etc) and critical terrain points (including local surface maximum/minimum, convexity/concavity, or saddle points) are selected using terrain analysis tools.

It is straightforward to refine a coarse unstructured TIN to produce a finer one. So, at the first stage, the goal of TIN generation is to generate a mesh having as small number of elements as possible and satisfying all requirements (minimum angle, maximum area, and constraints, etc). In large scale applications, this would involve determining the coarsest spatial scale that meets the goals of the hydrologic simulation.

In addition to starting points, we also extract line segments, including catchment boundaries, stream network, elevation contours, etc, as constraints through GIS terrain analysis tools [Tarboton, 1991; Maidment, 2002] so that the domain decomposition follows the natural boundaries. Figure 3 illustrates the sequence of procedures used to generate TIN and estimate parameters for each element in a river basin. The decomposition process involves delineation of the catchments boundary and river network at the desired resolution, which defines the constraint framework.

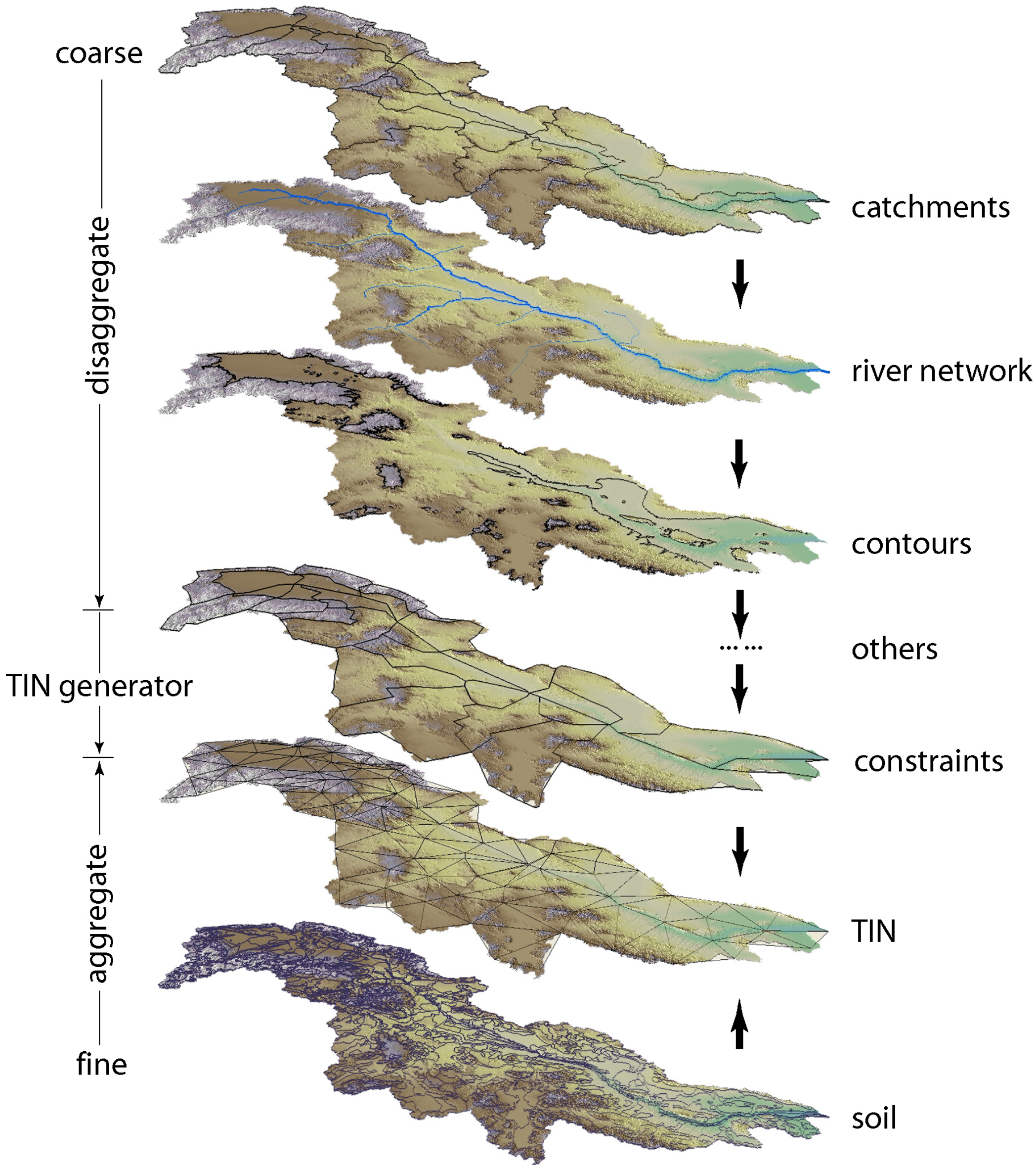

Figure 3 A schematic view of domain decomposition. Within the disaggregating process, catchments boundary, river network and critical terrain points, etc, are introduced as constraints to generation of the TIN. Using GIS tools, detail coverage (soil map) is utilized to determine soil or geologic parameters for each element.

2.4.2 Treatment of Interaction Terms

The central point of the integrated model is that all interaction terms and coupling are specified within the local ODE system and kernel, incorporating equations (14), (21), (22), (29), (30) and (31).

In detail, the interaction item between the overland flow process and subsurface processes, i.e. infiltration I in equation (14) and (21), is expressed by either Horton or Dune runoff generation mechanism. The interaction between overland flow and channel routing, i.e., lateral flow Q_{oc} in equation (14) and (29), is approximated by the weir equation [Panday and Huyakorn, 2004], with free-flowing or submerged conditions. The interaction between the unsaturated zone and saturated zone, i.e. q^o in equation (21) and (22), is expressed by equation (24). The interaction item between aquifer and channel routing, i.e. Q_{gc} in equation (22) and (29) is controlled by volumetric integration of Darcy's law in equation (23).

2.5 SOLVING THE GLOBAL ODE SYSTEM

Combining all local ODE's across the solution domain yields a global ODE system in form of

$$My' = f(t, y, x) \tag{35}$$

where M is the identity matrix, y is n by 1 vector of state variables and x is the forcing. The unknown states are fully coupled on the right hand side. Once the ODE system is formed, it is important to take advantage of the special properties of the problem for an efficient solution.

An explicit solver is always preferred if an acceptable solution can be achieved, since within each time step, an explicit solver requires fewer evaluations of the right-hand-side. However, as noted earlier, the multiple time-scales arising from multiple processes, typically makes (35) a highly stiff system [Archer and Petzold, 1998]. For highly stiff problems, the overall computational cost of an explicit solution may actually be higher than an implicit solver due to stability concerns. Thus, the sequential solver used here is implicit.

The Suite of Nonlinear and Differential/Algebraic equation Solvers [SUNDIALS, 1994], developed at the Lawrence Livermore National Laboratory has been wide applied and extensive testing [http://acts.nersc.gov/sundials/], and is adopted here.

For the initial condition $y(t_0) = y_0$, a multi-step formula is written:

$$\sum_{i=0}^{K1} \alpha_{n,i} y_{n-i} + h_n \sum_{i=0}^{K_2} \beta_{n,i} y'_{n-i} = 0 \tag{36}$$

where α and β are coefficients. For stiff problems, CVODE [Cohen and Hindmarsh, 1994] in the SUNDIAL package uses the Backward Differentiation Formula (BDF) with adaptive time step and method order varying between 1 and 5. Plugging equation (36) into (35) yields a non-linear system of the form

$$G(y_n) \equiv y_n - h_n \beta_{n,0} f(t_n, y_n) - a_n = 0 \tag{37}$$

$$a_n \equiv \sum_{i>0} (\alpha_{n,i} y_{n-i} + h_n \beta_{n,i} y'_{n-i}) \tag{38}$$

Numerically solving equation (37), with some variant of Newton iteration, is equivalent to iteratively solving a linear system of the form

$$\mathrm{M}(y_{n(m+1)} - y_{n(m)}) = -G(y_{n(m)}) \tag{39}$$

where M is $I - h\beta_{n,0} J$ with $J = \partial f / \partial y$.

The GMRES (Generalized Minimal Residual) iterative linear solver in SUNDIAL makes the computational cost of solving the global ODE system a competitive strategy. For additional details the reader is referred to the SUNDIAL website [http://acts.nersc.gov/sundials/].

2.6 EXAMPLE: DYNAMIC WATERSHED SIMULATION

Next we apply the integrated modeling strategy to a storm event in the hypothetical watershed shown in figure 4. In this example, the domain is decomposed into TIN's with 34 nodes and 48 triangles. The watershed has an embedded 2^{nd} order stream channel and the aquifer depth is taken to be 3 meters with horizontal surface and bottom. The boundary condition for the channel is 1.5 m above the base. The aquifer has no-flow boundaries around the perimeter. To demonstrate the complex interaction of surface and subsurface routing, only the upper part (1^{st} –order channel region) of watershed is forced. The forcing is a single storm event. The model assumptions are: 1) evapotranspiration and vegetation storage are omitted; 2) a shallow water table-soil moisture approximation is applied [Duffy, 2004]; 3) the kinematic wave approximation to Saint Venant equations is applied for overland and channel flow.

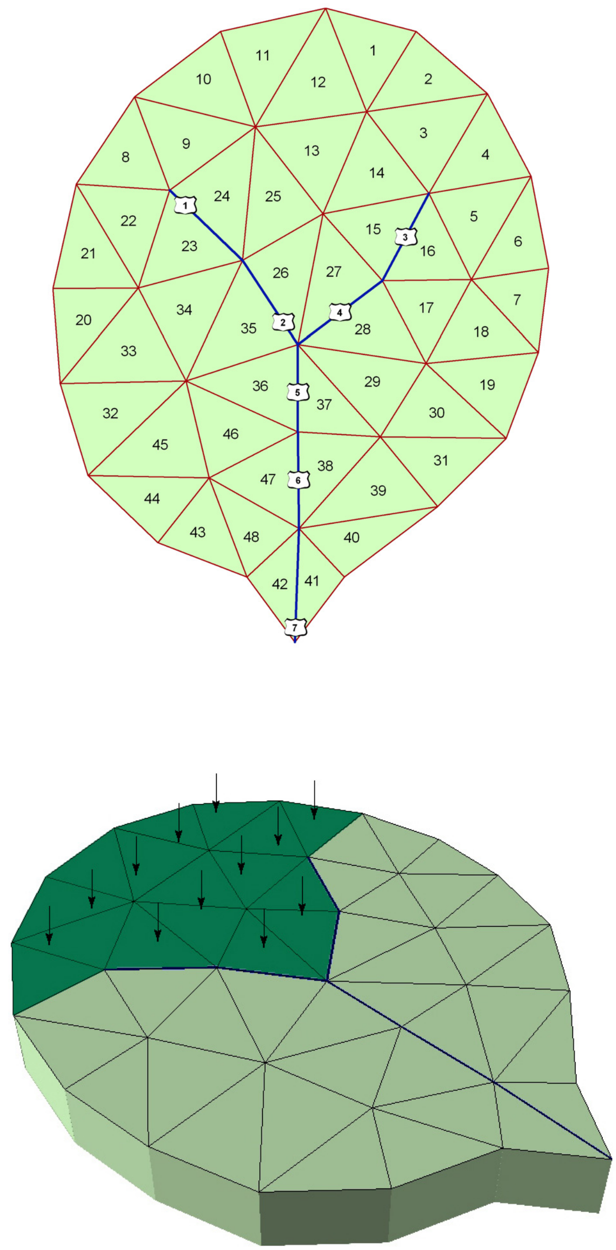

Figure 4 The hypothetical watershed example. The above figure shows its spatial decomposition. The below one shows the forcing applied.

The watershed, shown in Figure 4, has an average element size of ~ 1000 m^2. The total area is 45,175 m^2. The upper region receiving rainfall is 36% of the total watershed area. The watershed is assumed to be homogenous with soil properties $K_{sat} = 0.001 m/s$, $\theta_s = 0.4$, $\theta_r = 0.05$, $\alpha = 1.5$, $n = 1.2$. The river cross-section is rectangular in shape, 2m wide, with the channel bed 1 meter above aquifer bottom.

The initial conditions for groundwater table and stream stage are set at 1.5 m (equilibrium), and the system is solved with CVODE.

The first result of the simulation, shown in figure 5, identifies two stream-flow peaks resulting from a single-peak storm event. The first runoff peak is generated by overland flow resulting from infiltration excess and saturation overland flow. The stream discharge rises instantly when rainfall intensity is greater than infiltration capacity, and relaxes quickly after precipitation event ends. The second peak is due to groundwater base-flow, with a slow relaxation. Note the time axis is on a log scale to show the complete event.

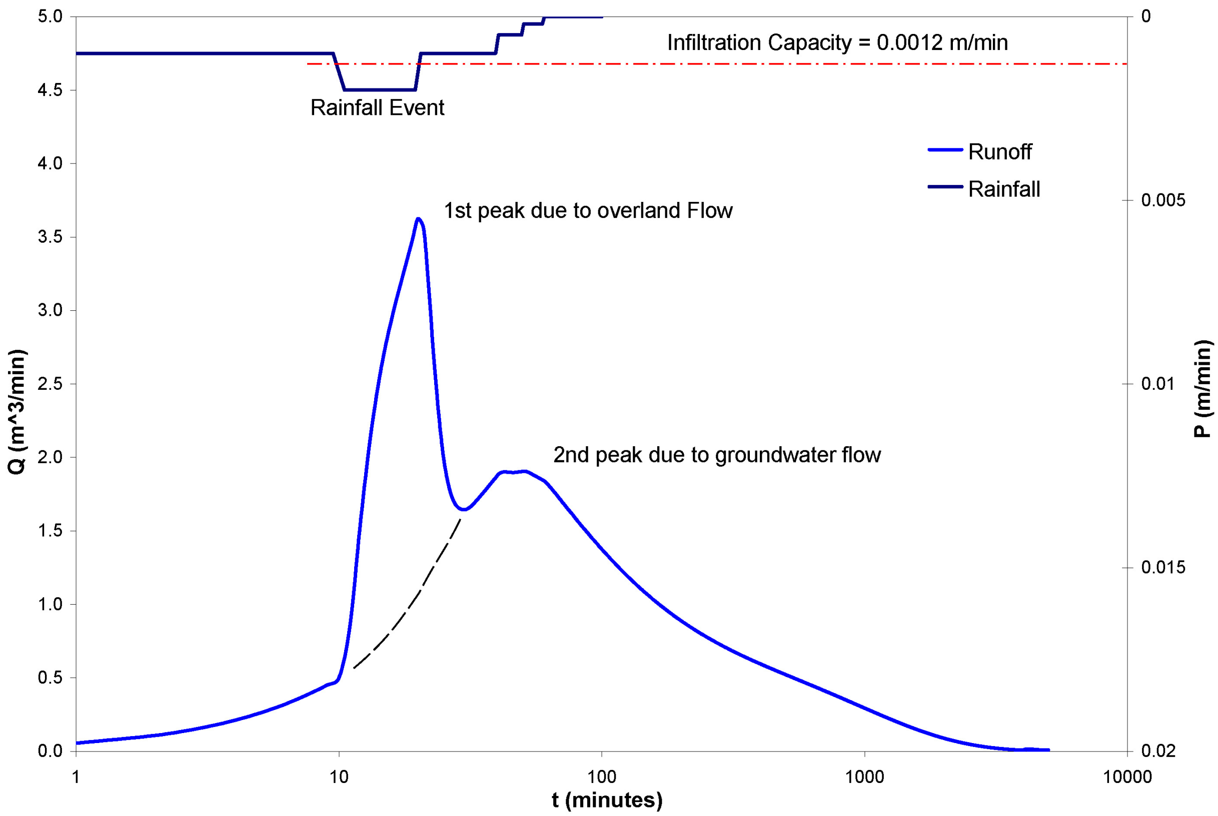

Figure 5 Watershed discharge at the outlet for the rainfall event indicated. The runoff hydrograph has two peaks corresponding to overland flow and groundwater base-flow.

This coupling of fast time scales of surface runoff and the slower time scales of groundwater flow is an important feature of the dynamic watershed response. Figures 6-8, illustrate the groundwater level and river stage relation at various internal locations.

Figure 6 shows the surface water level and the adjacent water table elevations at two locations in the upper part of the watershed. As the groundwater level at element 15 rises due to recharge, the delayed response at element 16 (no recharge) is due to lateral flow and stream-flow losses from the opposite channel bank. As rainfall intensity exceeds infiltration capacity, surface overland flow grows rapidly and stream-flow in channel segment 3 rises quickly. The post-event response at segment 3 is the result of groundwater base-flow from both sides of the channel.

During the storm event runoff, generated within the upper part of the basin, actually recharges the opposite bank where no precipitation fell. Thus the rise and fall of the water table response at 15 (storm recharge) and 16 (channel recharge) are affected by totally different processes during the storm.

Figure 7 illustrates the response of the lower region of watershed. The large early peak in stream-stage at river segment 6 is the result of routing from the upper watershed, with a second peak from upland groundwater base-flow. The aquifer water levels rise entirely due to channel losses during the runoff event. Groundwater which recharged the lower watershed as bank storage during the storm event is gradually released as base-flow to the lower channel after the stream-stage relaxes.

Figure 8 confirms the complexity of aquifer-channel dynamics. In the figure base-flow is plotted at three sites. In the upper region where the rainfall event occurred, the aquifer contributes to the channel at all times indicating areal recharge and base-flow. In the lower region, the channel looses water to the aquifer during the storm, and slowly recovers the same as base-flow after the storm is over. Element 16 (no areal recharge), responds in the same way as the lower watershed element 47, except that channel recharge at this site is quite large during the storm event. Clearly, the dynamics of even this simple example are quite complex and suggest the importance of dynamic coupling to physical interpretation of runoff response.

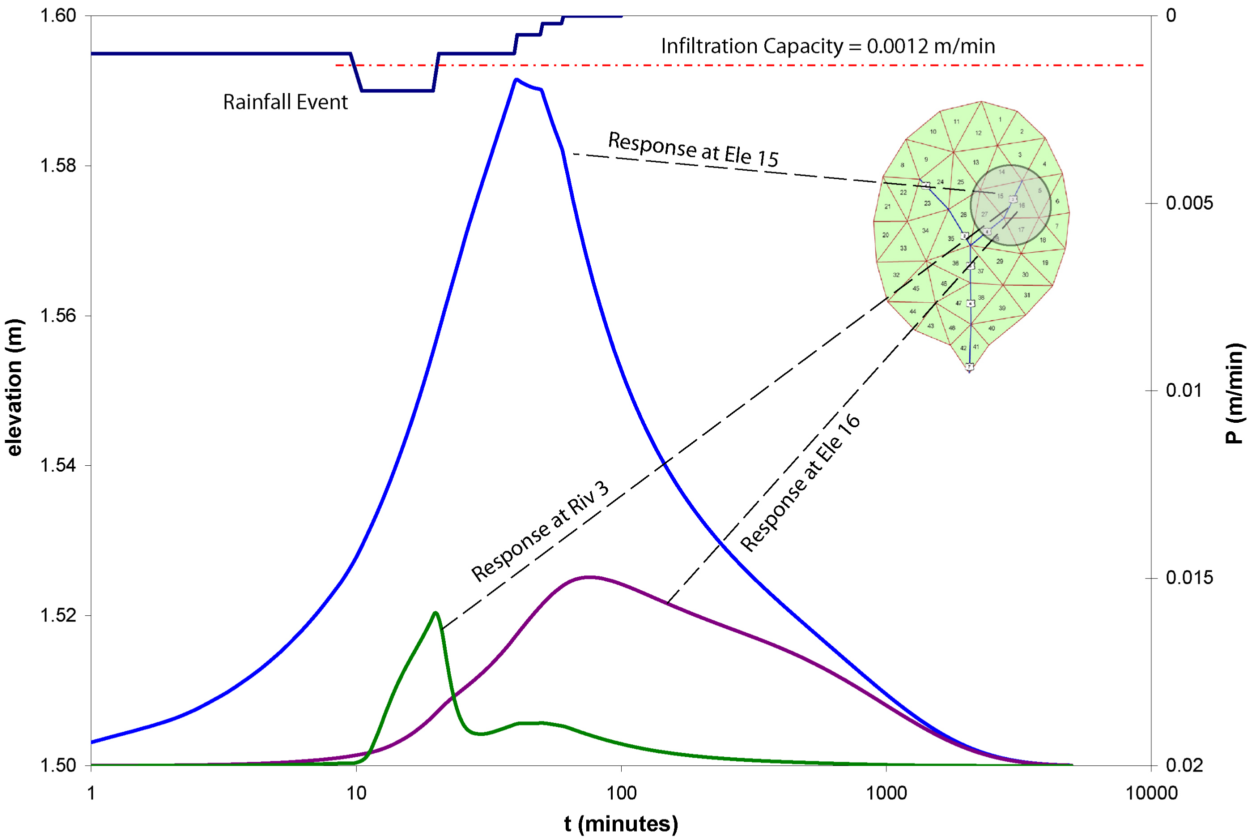

Figure 6 Groundwater elevation and channel stages responses in the upper watershed region.

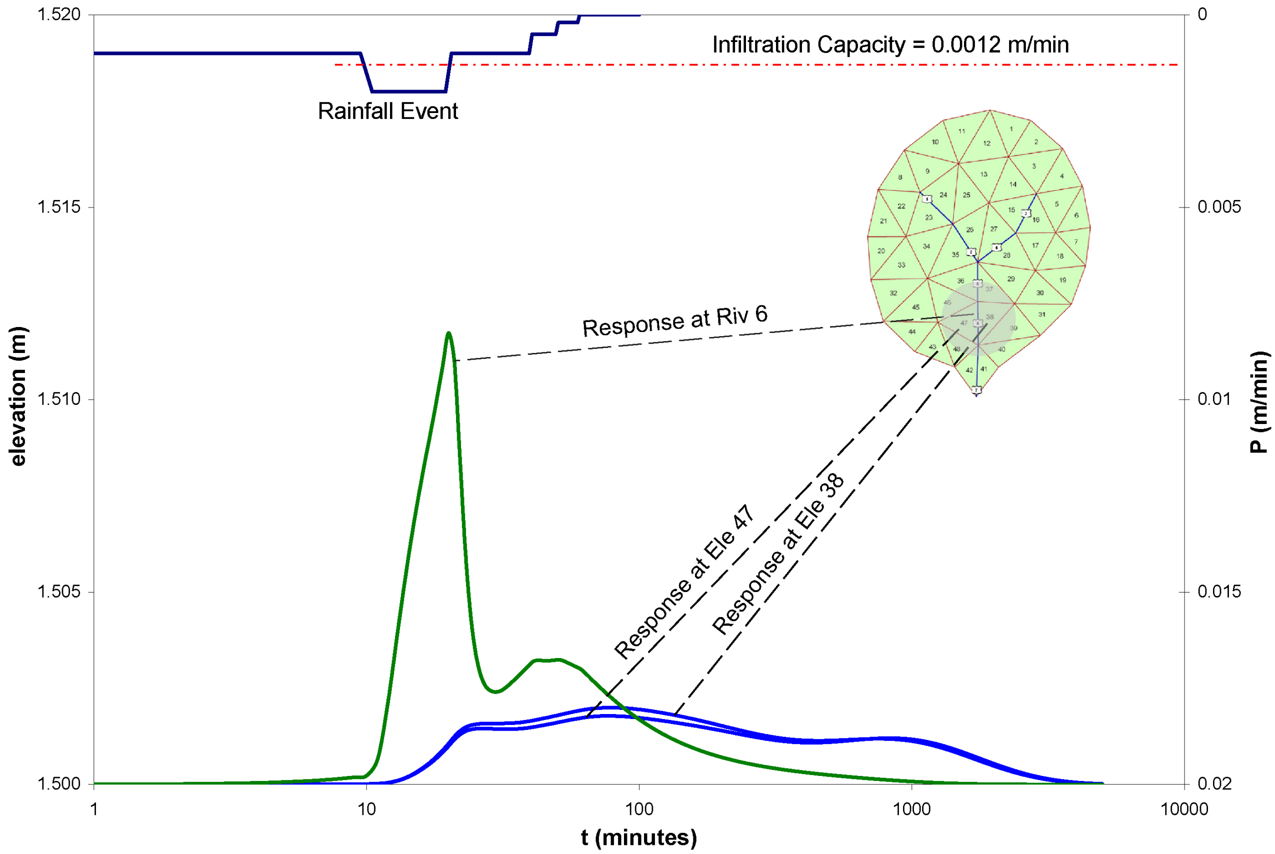

Figure 7 Groundwater elevation and channel stage responses in the lower region.

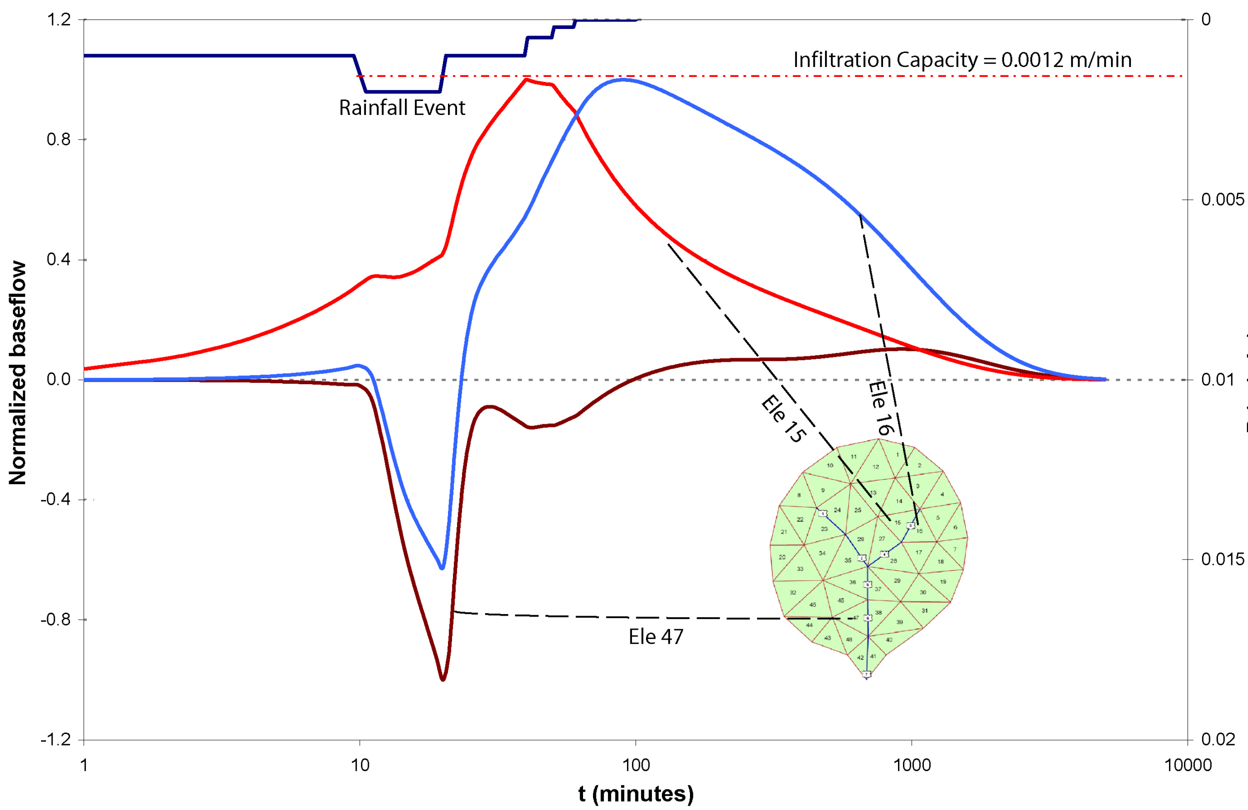

Figure 8 Base-flow responses in the upper and lower part of the watershed. Note that base-flow is negative (from channel to aquifer) at sites where the element dees not receive recharge.

2.7 CONCLUSION

A model strategy is proposed for a fully-coupled integrated hydrologic model. In this approach, governing PDE's for some processes, such as 2-D overland flow on the surface, 1-D flow in an adjacent channel, 1-D unsaturated flow and 2-D groundwater flow, are semi-discretized into ODE's with the FVM. By combining reduced ODE's and original governing ODE's, multiple processes are fully coupled and result in a local system of ODE's, i.e., model kernel, for a single prismatic element. Combining the local system of ODE's throughout the entire domain, results in a global ODE system and it is solved with a state-of-the-art ODE solver.

The strategy provides an efficient and flexible way to couple multiple distributed processes that can capture detailed "dynamics" with a minimum of elements.

The user can turn on/off processes or easily add new process equations in the model according to the simulation goal. The FVM guarantee's mass conservation during simulation at all cells. It allows flexible constitutive relationships in the kernel, and it is possible to apply this strategy to multi-scale applications.

GIS tools are conveniently used to decompose the domain into TIN's based on natural coordinates of the watershed. Constraints in the domain decomposition (e.g. hydrographic points and critical terrain points, catchments boundary and contours, etc), lead to an efficient representation of the domain with fewer elements than a finite difference approach.

This strategy has been implemented in a code PIHM (Penn State Integrated Hydrologic Model). Example results show how this strategy captures the dynamics of multiple processes in a simple watershed system. Field application of PIHM to a Pennsylvania watershed is the subject of another paper. Future versions of the model will incorporate multiple layers and transport processes. Large-scale computation (e.g. river basin) will require a parallel version of the code presently under development.

ACKNOWLEDGEMENTS

This research was funded by grants from the National Science Foundation, Science & Technology Center for Sustainability of Water Resources in Semi-Arid Regions (NSF EAR 9876800, L.D. James), and NASA_GAPP (ER020059) The Role of Soil Moisture & Water Table Dynamics in Ungaged Runoff Prediction in Mountain-Front Systems (J. Entin). This support is gratefully acknowledged.

REFERENCES

Abbott, M.B., J.A. Bathurst, and P.E. Cunge (1986), An Introduction to the European Hydrological System-Systeme Hydrologicque Europeen "SHE" 1: History and philosophy of a physically based distributed modeling system, *Journal of Hydrology*, *87*, 45-59.

Abbott, M.B., J.A. Bathurst, P.E. and Cunge (1986), An Introduction to the European Hydrological System-Systeme Hydrologicque Europeen "SHE" 2: Structure of a physically based distributed modeling system, *Journal of Hydrology*, *87*, 61-77.

Allen, R.G., L.S. Pereira, D. Raes, and M. Smith (1998), Crop evapotranspiration, FAO irrigation and Drainage paper No. 56.

Ascher, U.M., and L.R. Petzold (1998), Computer methods for ordinary differential equations and differential algebraic equations, SIAM, Philadelphia.

Beven, K.J. (2001), Rainfall-runoff modeling, the primer, John Wiley & Sons, New York.

Brandes, D. (1998). A low-dimensional dynamical model of hillslope soil moisture, with application to a semiarid field site, PhD thesis, the Pennsylvania state university.

Bras, R.L. (1990), Hydrology, An introduction to hydrologic science, Addison-Wesley publishing company.

Cohen, S.D., and A.C. Hindmarsh (1994), CVODE User Guide, Numerical Mathematics Group, LLNL. UCRL-MA-118618.

Delanunay, B. (1934). Sur la sphere vide, Bull. Acad. Science USST VII: Class Sci. Mat. Nat., b, 793.

Dingman, S.L (1994), Physical Hydrology, Prentice Hall, Upper Saddle River, NJ.

Du, Qiang, Max Gunzburger (2002). Grid generation and optimization based on centroidal voronoi tessellations, Applied Mathematics and Computations. 133(2002) 591-607. Elsevier.

Duffy, C.J. (1996), A two-state integral-balance model for soil moisture and groundwater dynamics in complex terrain, *Water Resources Research*, *32(8)*, 2421-2434.

Duffy, C.J. (2004), A Semi-Discrete-dynamical model for mountain-front recharge and water balance estimation: the Rio Grande of southern Colorado and New Mexico, AGU Monograph.

Eagleson, P.S. (1970), Dynamic Hydrology, McGraw-Hill, New York.

Garcia-Navarro, P., M.E., Hubbard, and A. Priestley (1995), Genuinely Multidimensional Upwinding for the 2D Shallow Water Equations, *Journal of computational physics*, *121*, 79-93.

Gottardi, G., and M. Venutelli (1993), A control-volume finite-element model for two-dimensional overland flow, *Advances in Water Resources*, *16*, 277-284.

Johnson, C. (1990), Numerical Solutions of Partial Differential Equations by Finite Element Methods, Cambridge University Press.

Kristensen K.J., S.E. Jensen (1975), A model for estimating actual evapotranspiration from potential evapotranspiration, *Nordic Hydrology*, *6*, 170-188.

Leveque, R.J. (2002), Finite Volume methods for hyperbolic problems, Cambridge University Press.

Madsen, N.K. (1975), The method of lines for the numerical solution of partial differential equations, Proceedings of the SIGNUM meeting on software for partial differential equations, Moffitt Field, California, USA.

Panday, S., and P.S. Huyakorn (2004). A fully coupled physically-based spatially-distributed model for evaluating surface/subsurface flow, *Advances in Water Resources*, *27*, 361-382.

Polis, M.F., and D.M. McKeown (1993). Issues in iterative TIN generation to support large scale simulations, 11th international symposium on computer assisted cartography (AUTOCARTO11), Minneapolis Mn, USA.

Shewchuk, J.R. (1997), Delaunay refinement mesh generation, PhD Thesis, Carnegie Mellon University.

Slattery, J. (1978), Momentum, energy, and mass transfer in continua, Krieger.

Sleigh, P.A., P.H. Gaskell, M. Berzins, and N.G. Wright (1998), An unstructured finite-volume algorithm for predicting flow in rivers and estuaries, *Computers and Fluids*, *27*, 4, 479-508.

Tarboton D.G., R.L. Bras, and I. Rodriguez-Iturbe (1991), On the Extraction of Channel Networks from Digital Elevation Data, *Hydrological Processes*, *5*, 81-100.

Vivoni E.R., V.Y.Ivanov, R.L. Bras, and D, Entekhabi (2004), Generation of triangulated irregular networks based on hydrological similarity, *Journal of hydrologic engineering*, *9*, 4. 288-302.

Voronoi, G. (1908), Nouvelles applications des parameters continues a la theorie des formes quadratiquess, dieuxieme memoire: researches sur les parallelloedres primitive. J. Reine Angew. Math., 134-198.

Xu, J. (1989), Theory of Multilevel Methods, PhD thesis, Cornell University.

Yeh, G.T. (1987), FEMWATER: A finite element model of water flow through saturated-unsaturated porous media – first revision, Oak Ridge National Laboratory, ORNL-5567/R1.

CHAPTER 3
THE PENN STATE INTEGRATED HYDROLOGICAL MODEL: CODE IMPLEMENTATION AND VERIFICATION

Yizhong Qu[1] and Christopher J. Duffy[1]

[1]Department of Civil and Environmental Engineering
The Pennsylvania State University
University Park, PA 16802

ABSTRACT

The Penn State Integrated Hydrologic Model (PIHM) is a fully coupled multi-process hydrologic model. Instead of coupling through artificial boundary conditions, major hydrological processes are fully coupled by the semi-discrete finite volume approach. For those processes whose governing equations are partial differential equations (PDE), we first discretize in space via the finite volume method. This results in a system of ordinary differential equations (ODE) representing those processess within the control volume. Within the same control volume, combining other processes whose governing equations are ODE's, (e.g. the snow accumulation and melt process), a local ODE system is formed for the complete dynamics of the finite volume. After assembling the local ODE system throughout the entire domain, the global ODE system is formed and solved by a state-of-art ODE solver.

PIHM implementation and code verification is the focus of this paper. The model is coded in C with an object-oriented data-model. The data model approach is widely used in geographic information system (GIS) products. With the object oriented data structure in data model, it is possible to seamlessly connect the hydrologic models with a GIS pre and post processor, all without the need of any intermediate text files. In such a seamless hydrologic model package, the numerical model and its pre/post-processor operate on the same data-model (often referred to as a geo-database). This not only results in faster access of data and model results, but also supports post visualization and complicated data inquiries.

Since published results for a fully coupled model are not yet available to the author, the PIHM code is verified against analytic and numerical solutions for independent hydrologic processes. For the groundwater components, it is shown that PIHM results converge to the analytic solutions for radial groundwater flow to a well. In another test case where surface overland flow was coupled with channel routing, the model results are shown to agree well with the numerical solution.

Key words: Integrated Hydrological Model, PIHM

3.1 INTRODUCTION

In hydrologic research as well as operational forecasting, there is an increasing need to evaluate the significance of fully-coupled physical processes. Traditional approaches have tended to adopt weak-coupling strategies: using uncoupling hydrologic processes first, and then assume artificial boundary conditions for data exchange purpose for all independent processes. A good example of this has been the implementation of groundwater models in watersheds where streams are handled as specified hydraulic head, i.e. Dirichlet-type boundary conditions. This strategy has been extended to multiple processes as well, where multiple processes are coupled through artificial boundary conditions, i.e. the output from one module is used as the forcing or boundary condition to another module. One example of this type is the European model, MIKE-SHE (Abbott, 1986). It is an integrated modeling environment that allows multiple model components to be loosely coupled through boundary conditions. MIKE-SHE uses a controller that manages the coupling by specifying and passing the potential or flux boundary condition among all components. One problem with this coupling technique is that large variations in the flux exchange across the element interface tends to lead to instability, since each sub-component runs at its own time step.

There are a few fully-coupled integrated hydrological codes which have been recently developed (VanderKwaak, 1999; Panday, 2004). In these approaches, the partial differential equations (PDE) are reformed as parabolic nonlinear diffusion equations. That is, the Saint Venant equations for surface flow are approximated with the same form as Richards' equation (e.g. a nonlinear diffusion equation) for subsurface flow and thus all can be assembled into one mass matrix within the finite element method (FEM) or finite difference method (FDM).

Qu and Duffy (2004) have developed a new fully-coupled technique based on semi-discrete finite volume method (FVM). Within a finite volume, the semi-discrete approximation reduces PDE's to ordinary differential equations (ODE) (Leveque, 2002). This technique also provides a convenient and efficient way to couple hydrological processes governed by mixtures of PDE's and ODE's as is common in many water resource applications. Compared with FEM or FDM, FVM guarantees mass conservation throughout simulation domain.

The large number of land-surface, subsurface and channel parameters as well as the distributed and multiple types of atmospheric forcing have moved the entire research and applied hydrologic community towards the use of geographical information system (GIS) as a powerful tool in supporting complex geospatial and geotemporal data. Beyond the complex data required for the modeling, PIHM also applies GIS tools for pre and post processing and visualization of data, parameters and model results. For example, terrain analysis tools are applied to develop constraints to decompose the domain into a triangular irregular network (TIN), a widely used data format in GIS. The TIN representation allows efficient domain decomposition for modeling and also serves as the most efficient way to visualize the model results.

Most hydrologic models still read and write output to intermediate text files. In PIHM, an object-oriented data-model is used such that all information exchanged with the model (data, parameters, etc.) is carried out efficiently. This makes it possible to have a consistent and seamless connection from the GIS pre-processor of the distributed parameters, to the unstructured grids for the hydrologic model, and finally to its post processor for visualization of the spatial and temporary model results.

3.2 MODEL DESCRIPTION

3.2.1 Model Strategy

The general form of mass conservation equation of incompressible fluid flow can be written as

$$\frac{\partial \rho}{\partial t} + \nabla \cdot u = 0 \tag{1}$$

where ρ is fractional mass (dimensionless) in an arbitrary control volume, and u is fluid flux [L/T]. Mass conservation implies that the change rate of ρ is exactly balanced by the divergence of the flux. The integral form over the control volume V is given by

$$\int_V \frac{\partial \rho}{\partial t} dV = -\int_V \nabla \cdot u dV \ . \tag{2}$$

Applying the divergence theorem to the right hand side yields

$$\int_V \frac{\partial \rho}{\partial t} dV = -\int_S u \cdot N dS \tag{3}$$

where S is surface of V, and N is the normal vector on S. Computing the right-hand-side of equation (3) using the finite volume formulation (Leveque, 2002) yields

$$-\int_S u \cdot N dS = \sum_{i=1}^{S} Q_i \tag{4}$$

where the net flux Q_i across surface i, is positive in and negative out.

Letting the integral form of the left hand side of (3) be $M = \int_V \rho dV$, leads to the semi-discrete form of the mass conservation equation

$$\frac{dM}{dt} = \sum_{i=1}^{S} Q_i \tag{5}$$

where M is mass storage of control volume. Q_i is evaluated as the normal flux to each surface of the control volume. The vector form of (5) represents the system of ODE's within a control volume. Substitution of appropriate constitutive equations to evaluate fluxes in equation (5) allows the flux to be evaluated across the element boundary. We note that the finite volume method guarantees mass conservation for each control volume and it has the convenient ODE form of balance equations for both parabolic and hyperbolic PDE's (Leveque, 2002).

Under circumstances where full coupling of multiple hydrologic processes is required, the model kernel approach described offers a simple, yet flexible numerical strategy. First, the user can incorporate the desired number of processes simply by setting on/off switches prior to simulation. Second, trial constitutive relationships are easily applied and tested with numerical experiments. Finally, the control volume can be in any shape as long as orthogonal flux across boundary is feasible to be evaluated with the FVM.

3.2.2 Governing Processes and Equations

PIHM has incorporated channel routing, surface overland flow, and subsurface flow together with interception, snow melt and evapotranspiration using the semi-discrete approach with FVM (figure 2). Table 1 shows all these processes along with the original and reduced governing equations. For channel routing and overland flow which is governed by St. Venant equations, both kinematic wave and diffusion wave approximation are included. For saturated groundwater flow, the 2-D Dupuit approximation is applied. For unsaturated flow, either shallow groundwater assumption in which unsaturated soil moisture is dependent on groundwater level or 1-D vertical integrated form of Richards's equation can be applied. From physical arguments, it is necessary to fully couple channel routing, overland flow and subsurface flow in the ODE solver. Snowmelt, vegetation and evapotranspiration are assumed to be weakly coupled. That is, these processes are calculated at end of each time step, which is automatically selected within a user specified range in the ODE solver.

Process	Governing equation/model	Original governing equations	Semi-discrete form	Approximation	Coupling technique	Reference
Channel Routing	St. Venant Equation	$\frac{\partial h}{\partial t}+\frac{\partial(uh)}{\partial x}=q$	$\left(\frac{d\varsigma}{dt}=P_c-\sum Q_{gc}+\sum Q_{oc}+Q_{in}-Q_{out}-E_c\right.$	Kinematic or Diffusion wave	Fully coupled	Chapter 2 2.3.1.3
Overland Flow	St. Venant Equation	$\frac{\partial h}{\partial t}+\frac{\partial(uh)}{\partial x}+\frac{\partial(vh)}{\partial y}=q$	$\left(\frac{\partial h}{\partial t}=P_o-I-E_o-Q_{oc}+\sum_{j=1}^{3}Q_s^{\ ij}\right)_i$	Kinematic or Diffusion wave	Fully coupled	Chapter 2 2.3.1.1
Unsaturated Flow	Richard Equation	$C(\psi)\frac{\partial\psi}{\partial t}=\nabla\cdot(K(\psi)\nabla(\psi+Z$	$\left(\frac{d\xi}{dt}=I-q^0-ET_s\right)_i$	Shallow groundwater assumption or 1-D integrated form	Fully coupled	Chapter 2 2.3.1.2
Groundwater Flow	Richard Equation	$C(\psi)\frac{\partial\psi}{\partial t}=\nabla\cdot(K(\psi)\nabla(\psi+Z$	$\left(\frac{d\zeta}{dt}=q^0+\sum_{j=1}^{3}Q_g^{\ ij}-Q_l+Q_{gc}\right)_i$	2-D Dupuit approximation	Fully coupled	Chapter 2 2.3.1.2
Interception	Bucket Model	$\frac{dS_I}{dt}=P-E_I-P_o$	$\left(\frac{dS_I}{dt}=P-E_I-P_o\right)_i$	N/A	Pre-calculated before Δt	Chapter 2 2.3.2.1
Snow melt	Temperature Index Model	$\frac{dS_{snow}}{dt}=P-E_{snow}-\Delta w$	$\left(\frac{dS_{snow}}{dt}=P-E_{snow}-\Delta w\right)_i$	N/A	Adjust after Δt	Chapter 2 2.3.2.2
Evapotranspiration	Pennman-Monteith Method	$ET_0=\frac{\Delta(R_n-G)+\rho_a C_p\frac{(e_s-e_a}{r_a}}{\Delta+\gamma(1+\frac{r_s}{r_a})}$	$\left(ET_0=\frac{\Delta(R_n-G)+\rho_a C_p\frac{(e_s-e_a)}{r_a}}{\Delta+\gamma(1+\frac{r_s}{r_a})}\right)_i$	N/A	Adjust after Δt	Chapter 2 2.3.2.3

Table 1 Major hydrologic process, governing equations, approximation and coupling technique in PIHM.

3.2.3 Domain Decomposition

The domain decomposition applies Delaunay Triangulation (Delaunay, 1934; Voronoi, 1908; Tucker, 2001) with constraints in 2-D. The unstructured grid is projected over the depth of the subsurface flow volume forming prisms, as shown in figure 1 and 2.

The circum-center is used to represent each triangle/prism. The advantage of the voroni triangle is that the flux across any edge with its neighbor is always normal to its common boundary by definition. For instance in figure 1, V_1V_2 is normal to D_4D_7. This reduces computational cost to evaluate flux across the volume boundary. Of course, this condition has the restriction that the circum-center must remain within the triangle under all circumstances. An algorithm that computes Delaunay triangulation satisfying this requirement from a set of points and constraints, in principal, is given by Shewchuk (2001) and we have adopted his algorithm in this research.

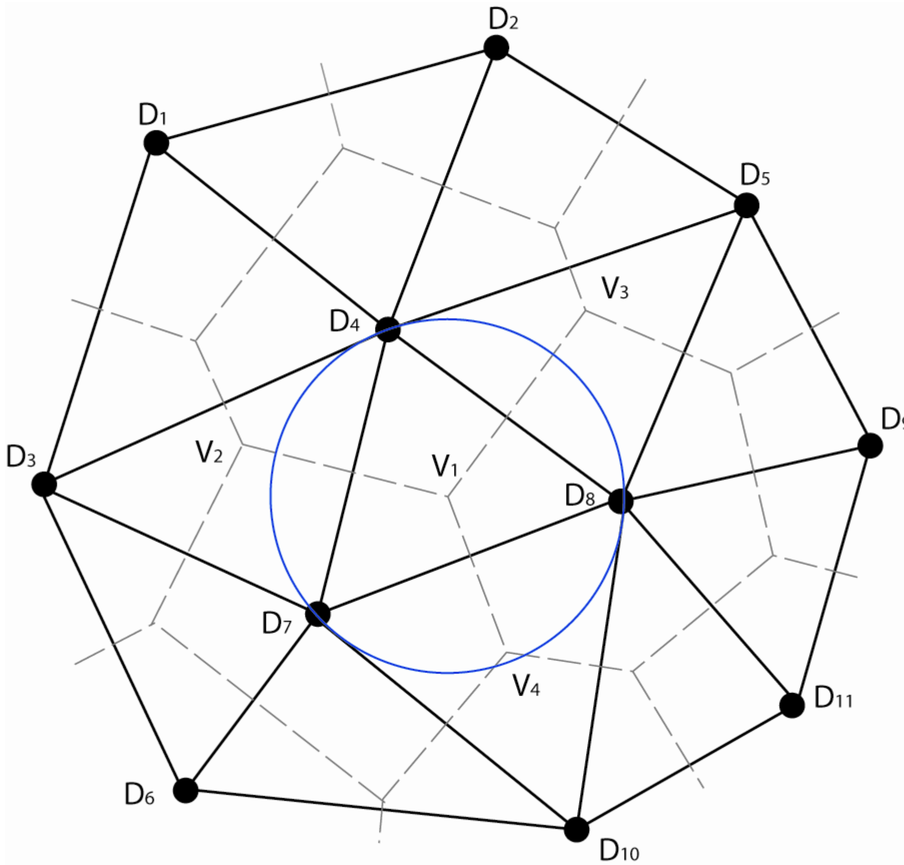

Figure 1 Delaunay triangulation (Delaunay, 1934) and Voronoi diagram (Voronoi, 1908). The solid lines form Delaunay triangulation, and the dashed lines form Voronoi diagram.

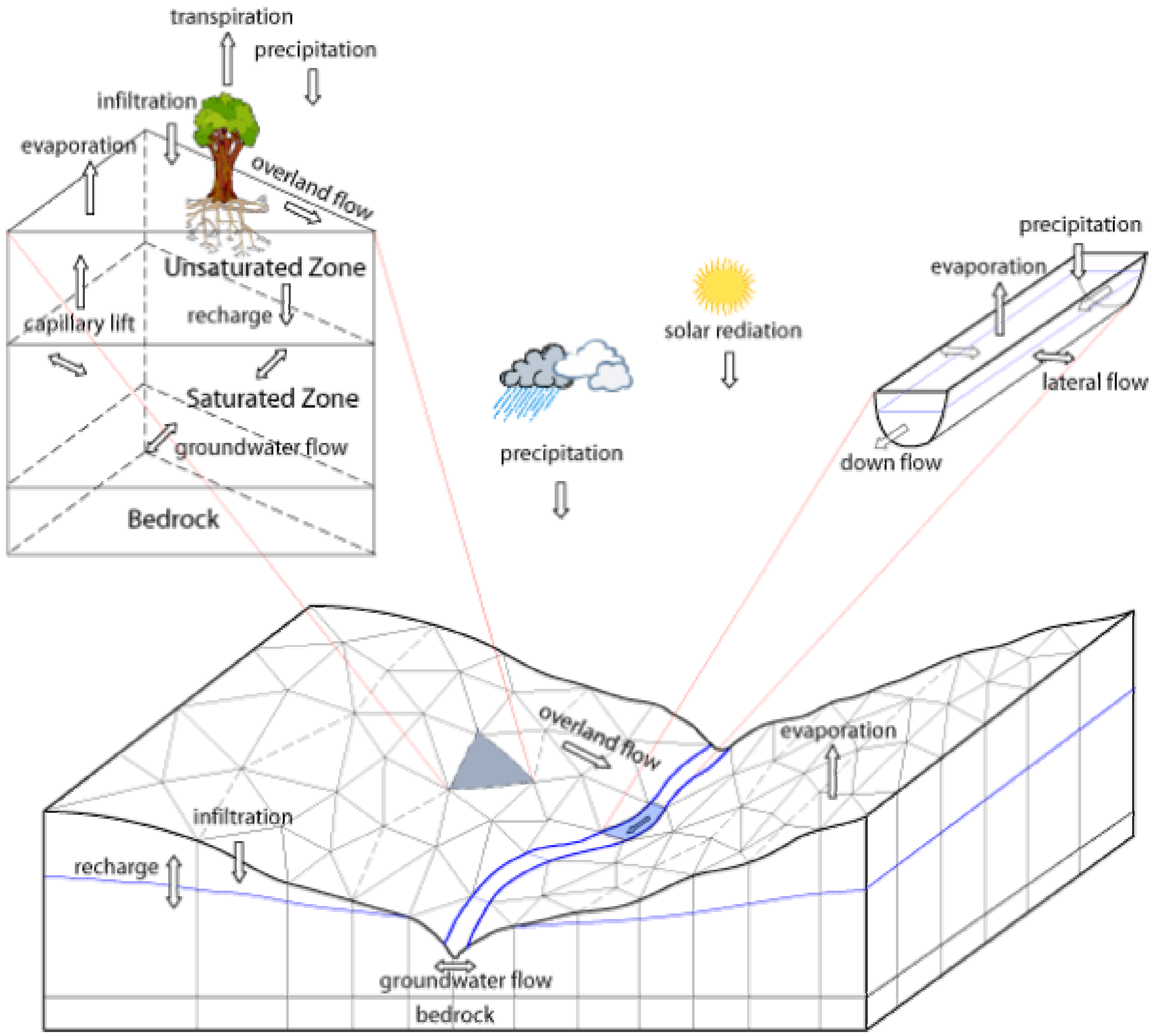

Figure 2 The Domain decomposition in a hillslope scale example. The basic prismatic element is shown to the left with multiple hydrological processes. The channel segment is shown to the right.

The large number of parameters, forcing and scale of water resource problems make GIS a powerful tool in developing watershed model solutions (Maidment, 2002). In PIHM, geographic information system (GIS) tools are frequently involved in domain decomposition, pre-processing of data and parameters and post-processing for model results and visualization. The unstructured grid used to decompose the domain is represented as a triangular irregular network (TIN format in GIS). The process starts with a digital elevation model (DEM) representing a grid of topographic data over the model domain. To better represent the terrain and meet simulation goal with TIN decomposition, hydrographic points (including hydraulic structures, such as gage stations and dams) and critical terrain points (including local surface maximum/minimum, convexity/concavity, or saddle points) are selected using terrain analysis tools in GIS as starting points. Research shows that much fewer total nodes are needed for a TIN than the original DEM to represent the terrain with acceptable error (Polis, 1993).

It is straightforward to refine a coarse unstructured TIN to produce a finer one. So, at the first stage, the goal of mesh generation is, in principle, to generate a mesh having the least number of elements and satisfying all requirements (minimum angle, maximum area, and constraints, etc). In large scale applications, this would involve determining the coarsest spatial scale that meets the goals of our hydrologic simulation.

In addition to the hydrographic constraint points, we also need line segments, including catchment boundaries, stream network and elevation contours, as constraints on the model domain. Figure 3 illustrates the sequence of procedures to generate the TIN and project the known parameters upon each element in the river basin. The decomposition process involves delineation of the catchments boundary and river network at the desired resolution. The constraints are formed by combining them with all other GIS layers, such as hydrographic points and elevation contours, etc. In general, the elevation contours, soil map layers, geologic layers, vegetation maps, or other GIS themes can in principal become a constraint in the domain decomposition and unstructured grid generations.

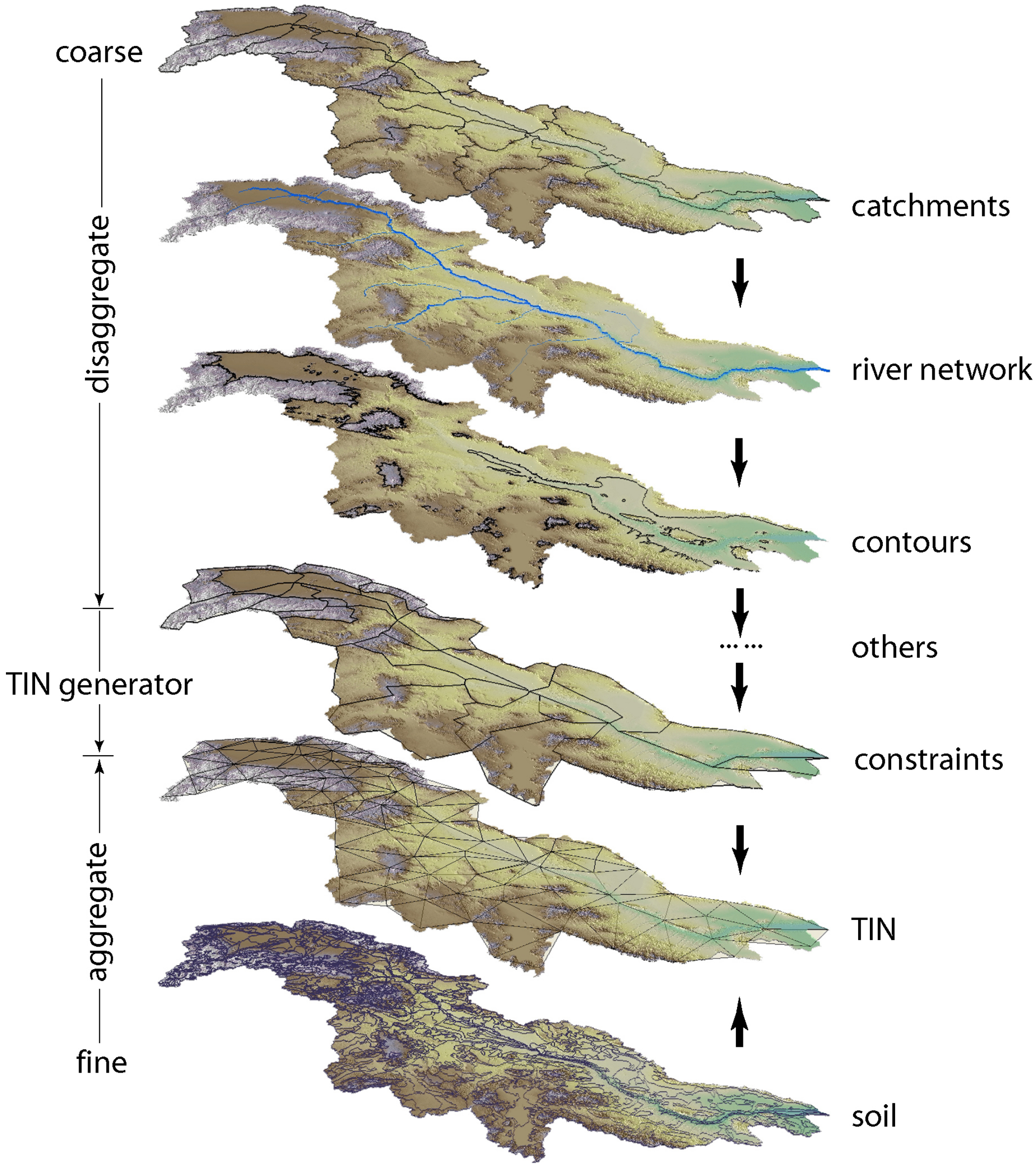

Figure 3 A schematic view of domain decomposition process. Within the disaggregating process, catchments boundary, river network and critical terrain points, etc, are introduced as constraints to generation of the TIN. Using GIS tools, detail coverage (soil map) is utilized to determine soil or geologic parameters for each model element. In this case ArcGIS (ESRI) software was used.

3.2.4 ODE Solver

In PIHM, The global ODE system is solved with the SUNDIALS (suite of nonlinear and differential/algebraic equation solvers) developed in the center for applied scientific computing at Lawrence Livermore National Laboratory. SUNDIALS is a family of closely related solvers, including CVODE, CVODES, KINSOL and IDA for ODE, ODE sensitivity analysis, algebraic equations, and differential algebraic equations, respectively. All these solvers share common code modules: vector kernels and generic direct and iterative linear system solvers. The solvers are designed to work in both serial and parallel environments.

CVODE (Cohen and Hindmarsh, 1994) is the primary solver to solve our global ODE system. CVODE is an ODE solver in C language that incorporates numerical methods for both stiff and non-stiff initial value problems. The integration methods in CVODE are multi-step methods, variable-coefficient Adams-Moulton for non-stiff problems and Backward Differentiation Formula methods for stiff problems respectively. In CVODE, the stiff non-linear system is solved with some variant of Newton iterations, which requires solve the linear system by a direct (dense or band) solver or a preconditioned Krylov solver, GMRES. In both cases, the user can either provide Jacobian or let the solver calculate it internally.

CVODE runs automatically with an adaptive time step during simulation, with the step chosen based on local error estimation. The user can control the maximum and minimum time step. Normally, the minimum time step should be automatically determined by the stiffness of the problem by the solver. The maximum time step can not be beyond the internal time step of the forcing data. Otherwise, the model will resample the forcing and produce errors.

3.2.5 Stability Analysis

In order to test the stability properties of a coupled ODE system, a simple test case of groundwater-channel interaction is investigated with Mathematica 5 (Wolfram Research Inc, 2004). For a general initial value ODE system in form of $y' = f(t, y)$, its solution $y(t)$ is stable if given any $\varepsilon > 0$, there is a $\delta > 0$ such that for any other solution $\hat{y}(t)$ satisfying the general ODE system, $|y(0) - \hat{y}(0)| \leq \delta$ and $|y(t) - \hat{y}(t)| \leq \varepsilon$. It is asymptotically stable if, in addition to being stable, the convergence condition is met: $|y(t) - \hat{y}(t)| \to 0$, as $t \to \infty$. The dimensionless test problem is shown as in figure 4: a hillslope is decomposed into 2 rectangular elements; the channel is decomposed into 2 segments. The surface overland flow is ignored. Precipitation/Conductivity is set to 1.0e-4; Depth of aquifer/Depth of channel is 4; channel manning coefficient is set 0.013.

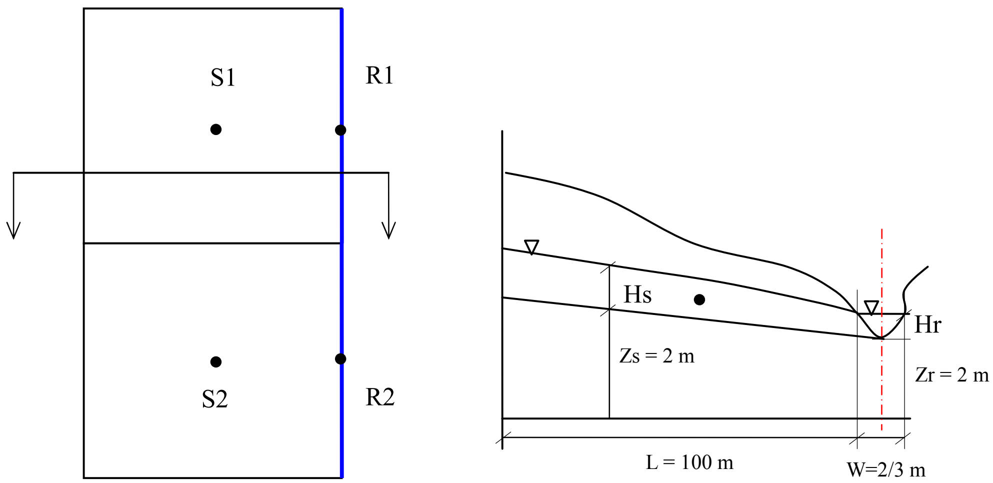

Figure 4 Stability test problem for PIHM

The relaxation of the groundwater levels and stream stage for four initial conditions are shown in figure 5. The initial groundwater levels in the 2 elements are arbitrarily set as unequal, while the two channel elements are initially set to be equal. In the upper illustration of figure 5, it shows that groundwater elevations in element 1 and 2 converge to the same equilibrium for all cases. The second illustration shows that channel stage converges to the equilibrium point following its own trajectory even though the initial conditions for channel part were the same. In other words, the phase plain plot shows 4 separate trajectories corresponding to the different groundwater level-channel level dynamic regimes before converging to the equilibrium point.

Figure 6 shows the solution trajectories for the groundwater and river stage (hs vs. hr). In case 1) the phase-plane plot shows a high groundwater table and high stream stage; 2) illustrates a high groundwater table and low stream stage; 3) low groundwater table and high stream stage; 4) low groundwater table and low stream stage. These four cases span the range of wet to dry conditions and may provide some important insight into the relative impact of flood and drought response in coupled watershed systems. The rapid convergence of the trajectories indicate that stream stages approach the equilibrium value much faster than the groundwater, or the stream is “enslaved” by the slower groundwater reservoir. In the long run, it is clear that the groundwater dominant the trajectories.

Figures 5 and figure 6 shows the ODE system is locally and asymptotically stable provide the initial conditions are physically reasonable. The investigation of PIHM stability is ongoing research.

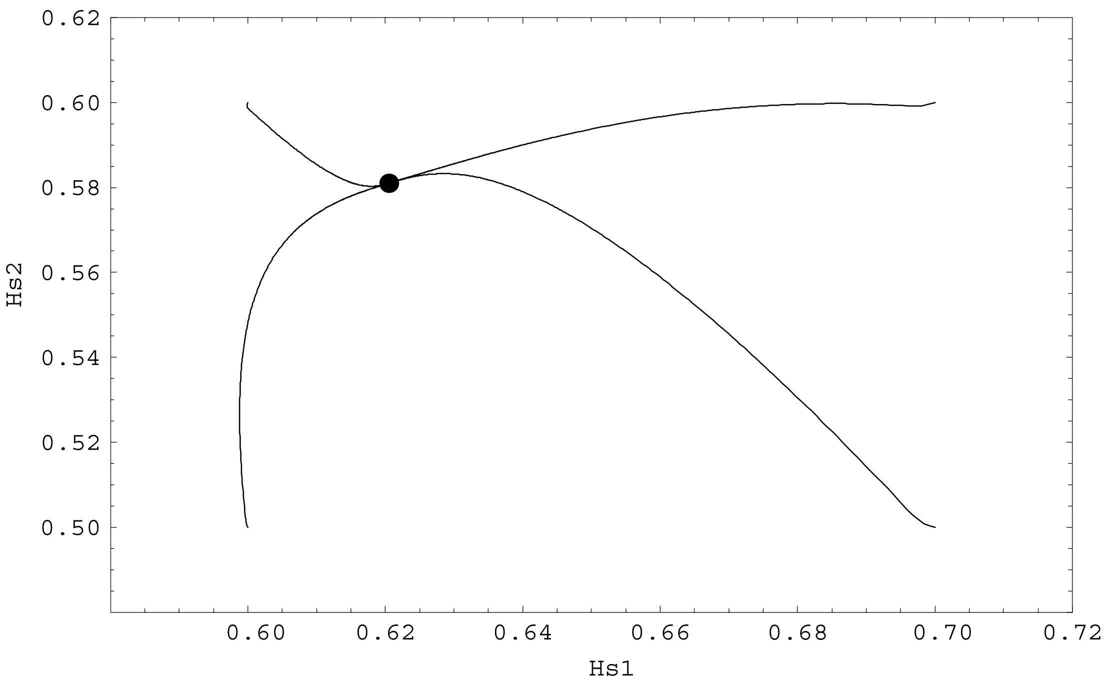

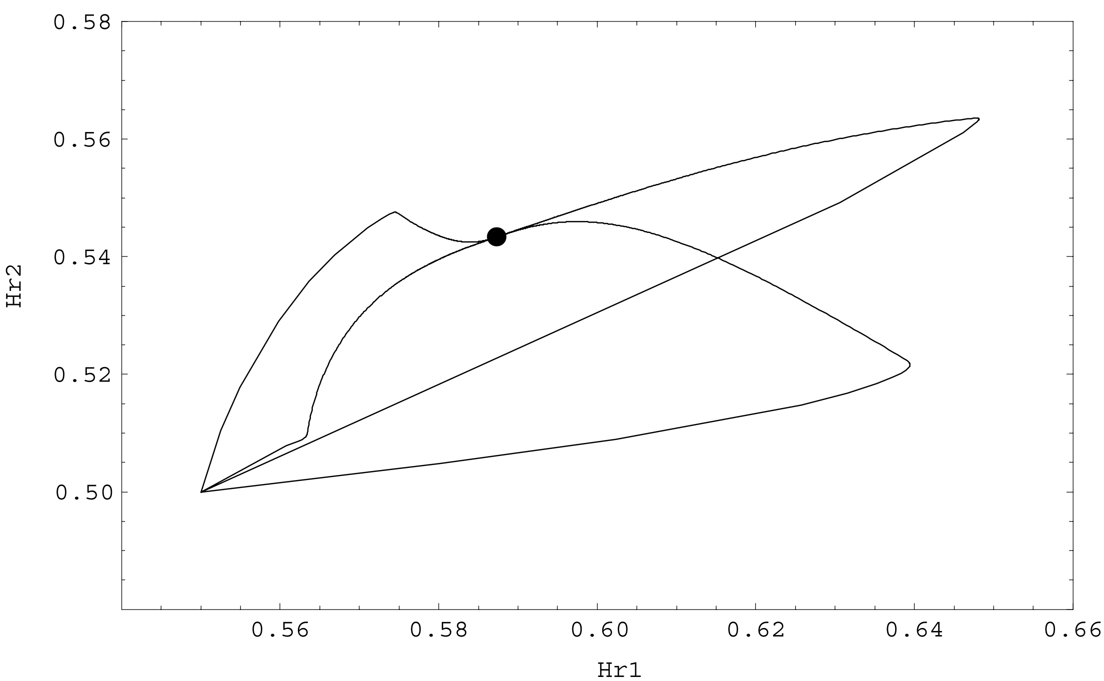

Figure 5 Solution trajectories with different initial conditions. The equilibrium points are from solving right hand algebraic equations. The initial condition is shown as starting points in figures.

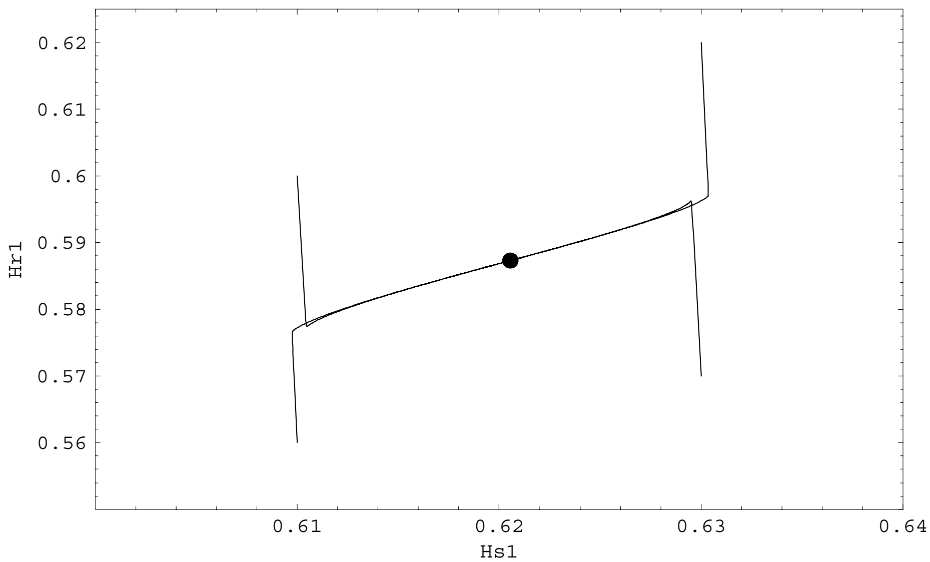

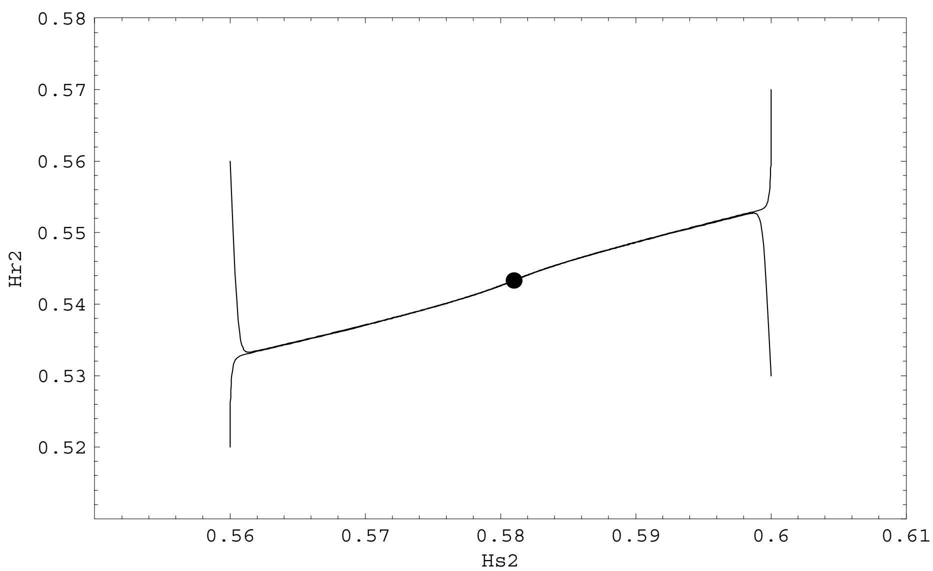

Figure 6 Solution trajectories with different initial conditions. The equilibrium points are from solving right hand algebraic equations. The initial condition is shown as starting points in figures.

3.2.6 Kinematic Wave and Diffusion Wave Approximations

PIHM use either diffusion wave approximation or kinematic wave approximation to full Saint Venant equations. Figure 7 shows a division of the application field for the model into 3 zones, where approximations are made for zero-depth-gradient lower boundary conditions. This figure is excerpted from Vieira (1983). Similar figures can also be found from the same reference for other boundary conditions.

In figure 7, $F_0 = C(\tan\theta / g)^{1/2}$ is Froude number, and $k = (g^3 L \sin\theta / C^4 q^2)^{1/3}$ is the kinematic wave number where C is Chezy roughness of the plane, θ is the slope, L is normalized length and q is the lateral flow. Generally, on natural slopes where the kinematic number is larger, the kinematic wave approximation can be used. On the smooth urban slopes where the kinematic number is between 5 and 20, the kinematic or diffusion wave approximation may be used depending on the value of Froude number. For lower kinematic wave number, the full St. Venant equations must be solved if Froude number is greater. The lower boundary condition may also have a significant effect on the solution in some cases.

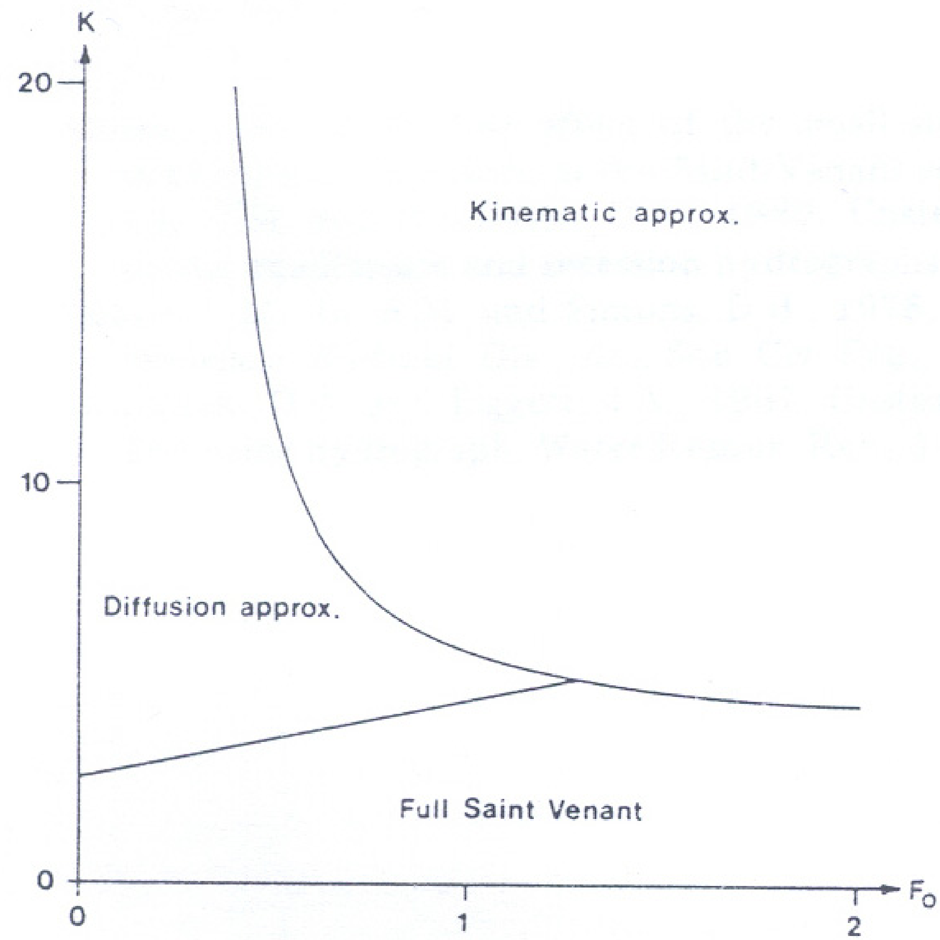

Figure 7 Division of 3 zones where approximation is valid for zero-depth-gradient boundary conditions. F_0 and k are Froude number and kinematic wave number respectively. (After Vieira, 1983)

3.3 CODE IMPLEMENTATION

3.3.1 Schematic View

PIHM is an implementation of a new strategy for integrated hydrological model (Qu and Duffy, 2004) in the C language. The schematic view of PIHM is shown in figure 8. The input files are a product of the GIS pre-processor which maintains a consistent data format. The memory is dynamically allocated based on problem size. After that, the initialization module initializes all the data for new simulation. Next the global ODE system is assembled and the right hand side of ODE system is evaluated. The user can modify this module as necessary to turn on/off some processes. Finally, the ODE solver, CVODE, is ready to solve the global ODE system as an initial value problem with the control information provided in the input files. During the simulation, the solver evaluates the right hand side of the ODE system as needed. Whenever the solver meets an output point, it outputs the model results.

Based on the basic GIS data architecture, pre- and post processing, including input files generation, and visualization, is currently being designed as a plug-in of ArcGIS to take advantage of the existing data-model (Mckinney, 2002). An example of this software product is the ArcHydro software (Maidment, 2002). The implementation of this part is under-development.

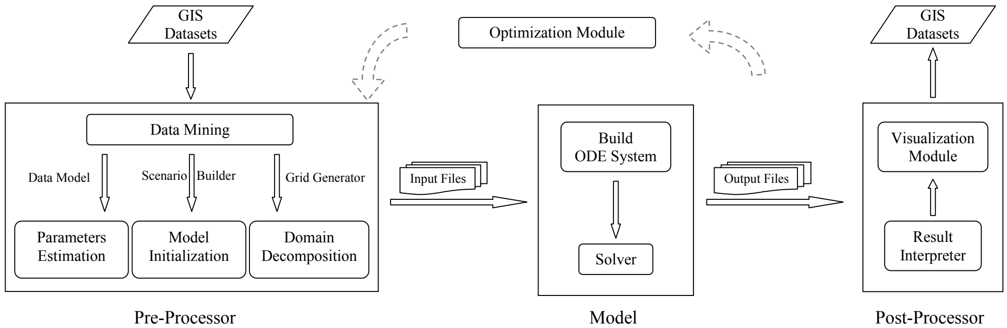

(a)

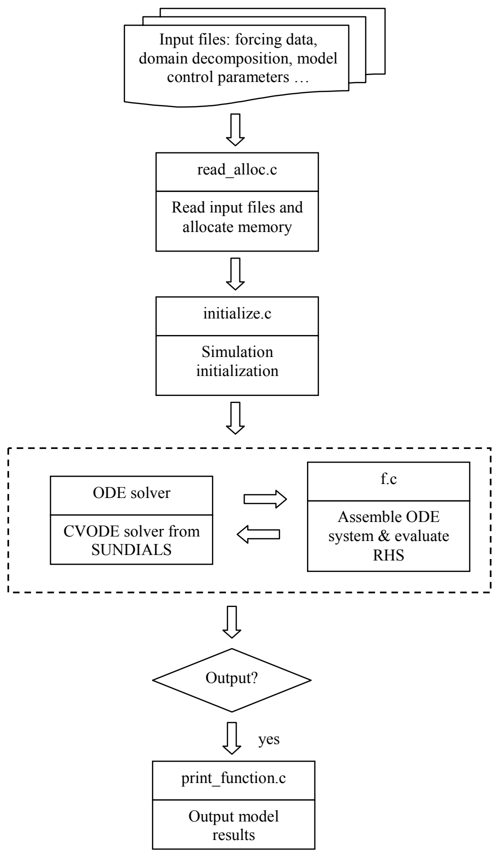

(b)

Figure 8 Illustration (a) shows the complete hydrologic package including pre processor, hydrologic model and post processor. Illustration (b) shows the schematic view of PIHM code implementation

3.3.2 Data Structure

The data structure of PIHM is shown as in figure 9. The basic element, as shown in figure 1 and 2, is a prism projected by a triangle with 3 nodes as vertices. It has 3 neighbor elements unless it is on the boundary. The ELEMENT has pointers pointing to the soil, vegetation data type and other forcing information associated. The SOIL data type has hydraulic conductivity, porosity and vertical variation information, etc. For those variables varying in time, such as leaf area index data and precipitation, a TIME SERIES RECORD data type is designed to contain them.

The CHANNEL represents a channel segment flowing along the edge of an element between 2 nodes. There is a down channel segment unless it is the last one. A channel segment has one left element and one right element unless it is on the boundary. A channel segment could have one of the following 4 boundary conditions: Dirichlet, Nuemann, Critical-depth or Zero-depth-gradient. The channel has a pointer pointing to its SHAPE data. By default, the channel process is governed by Sanit Venant equations. However, if it is controlled by man-made structure, e.g. dam, it becomes a reservoir, then the discharge is a specified time series data regulated.

The object-oriented data structure not only save space in a large application, but also share the fundamental data models with those in GIS product, such as ArcHydro. This fundamental basis leaves the door open to build a seamless hydrologic model package: e.g. the GIS pre- and post-processor and hydrologic model operate on the same data model. The data-model discrepancy in GIS product and model has been a hassle in large application. Intermediate text files for input information and model results could be huge and hard to handle in large scale simulations. If hydrologic models are capable of access object-oriented data model, it is possible to get rid of huge intermediate text files, and make it possible to support friendly inquiry to model results. It will also be easy to take advantage of product from GIS community.

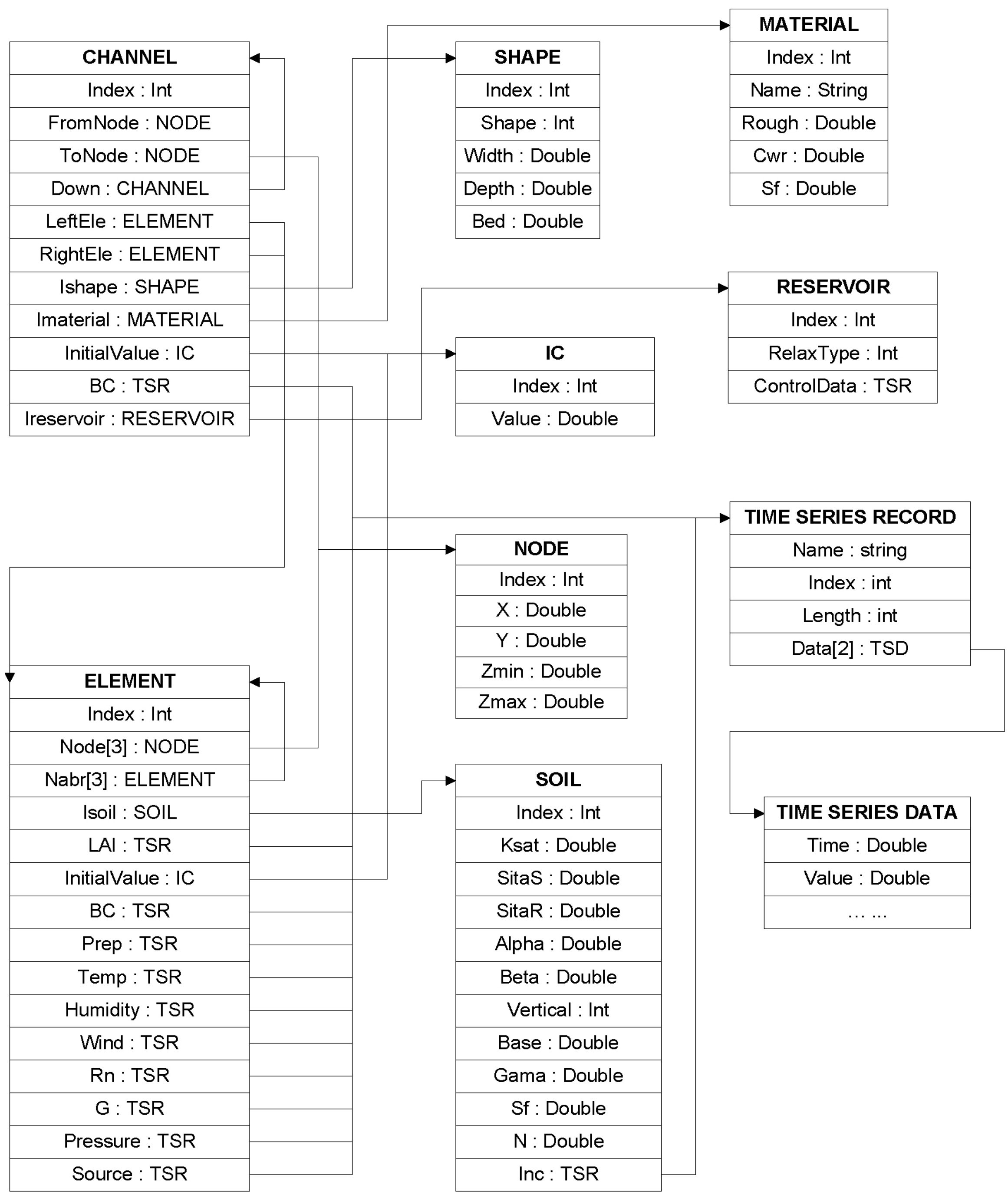

Figure 9 Data Model in PIHM

3.4 VERIFICATION

It is difficult to construct a test problem for coupled channel routing, overland flow and groundwater flow that has an analytic solution. PIHM code is verified against close form solution and other model results in several cases, each is designed for one or two processes. First, a radius groundwater flow test problem is shown to verify groundwater flow component. Another problem in which surface overland flow and channel routing are coupled is discussed to verify the processes governed by St. Venant equations.

3.4.1 Groundwater Flow Process

To verify the implementation of semi-discrete approach with FVM for groundwater flow, a radial ground flow example is set up as shown in figure 10. There is uniform rainfall P applies on top of a rounded aquifer with radius R. Its boundary condition is a specific head, h_0. If a constant pump rate of Q is applied to the well in the center, then an analytic solution of groundwater head h, in terms of r, is given by

$$h^2 = {h_0}^2 + \frac{P}{2K}(R^2 - r^2) + \frac{Q}{\pi K}\ln\left(\frac{r}{R}\right) \tag{6}$$

where the first term in the right hand side is boundary effect; the second term is recharge effect, and the last term is pumping effect caused by radial flow. Since the analytic solution becomes singular when r approaches 0, we can not treat well as a point in numerical simulation. To ease the domain decomposition procedure, we assume the well has radius of 10 meters in this example, i.e. the forcing P applies to uniformly to the surface of the well. The other parameters are: $R = 1000$ meter; $h_0 = 8$ meter, and $Q/K = 5$ square meter. The domain is decomposed into 2588 elements with radial constraints as shown in figure 10. The spatial decomposition is shown in figure 11.

Figure 12 and 13 show numerical results which approach the analytic solution except near the well where a singular point exists. If local error is defined as $\frac{\left|h_{PIHM} - h_{theory}\right|}{h_{theory}}$, figure 14 indicates that the average error approaches to zero as time increases.

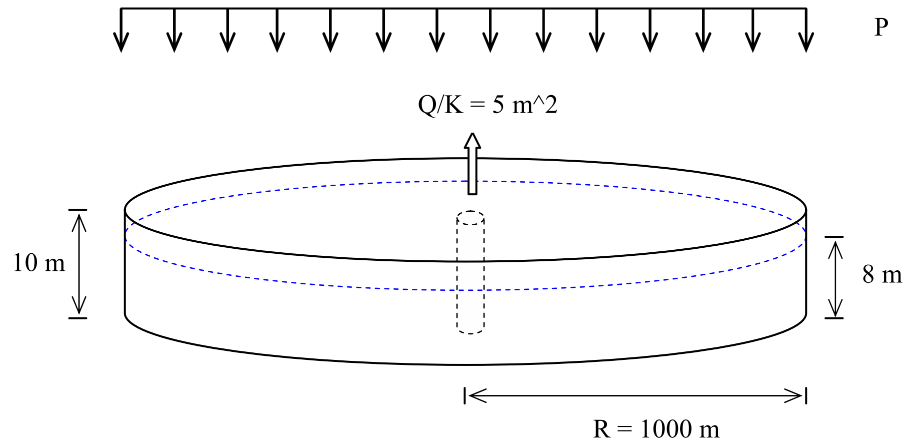

Figure 10 Radial groundwater flow problem

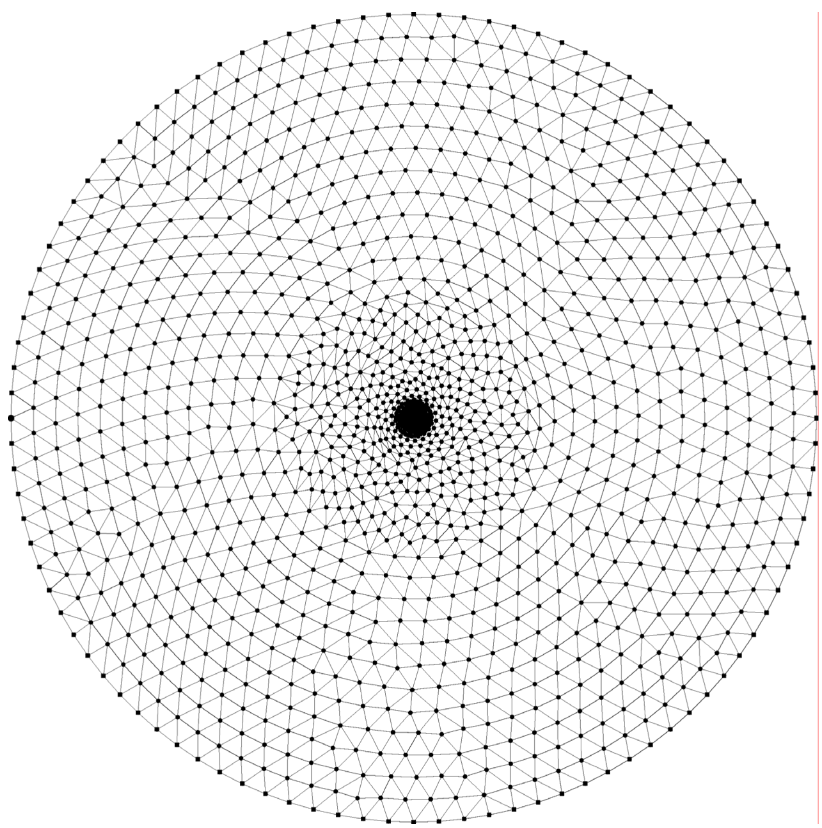

Figure 11 Domain decomposition for the radial groundwater-flow problem

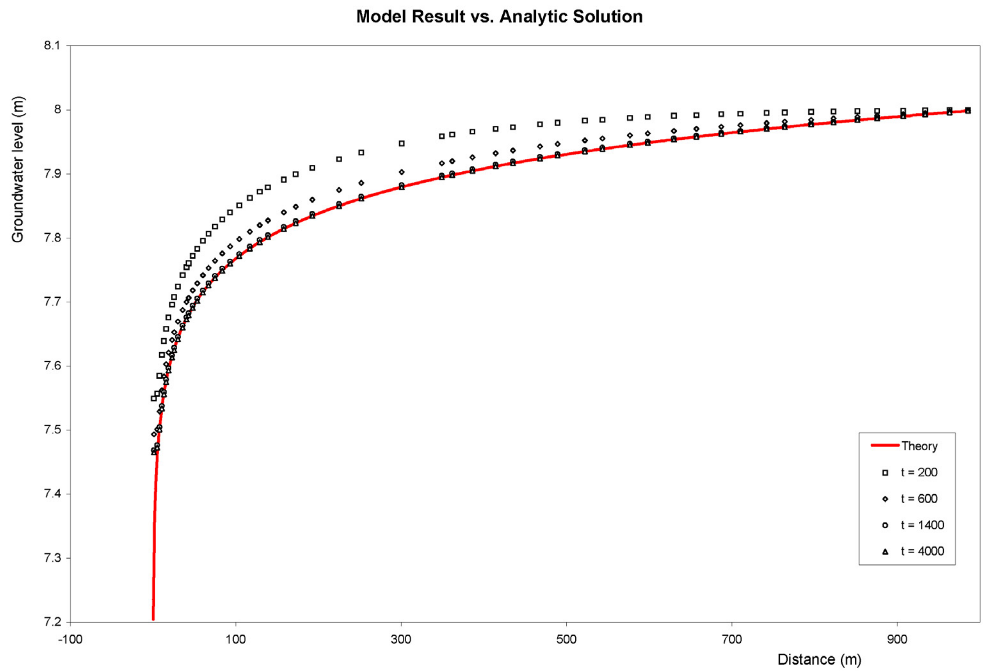

Figure 12 PIHM results and analytic solution when P = 0

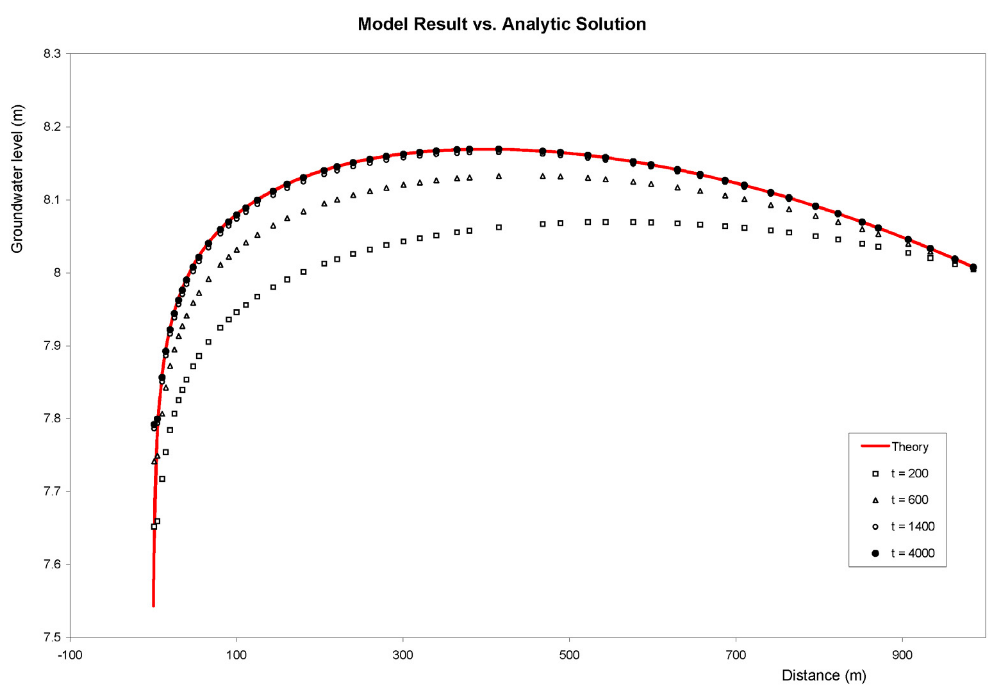

Figure 13 PIHM results and analytic solution when P/K = 1e-5

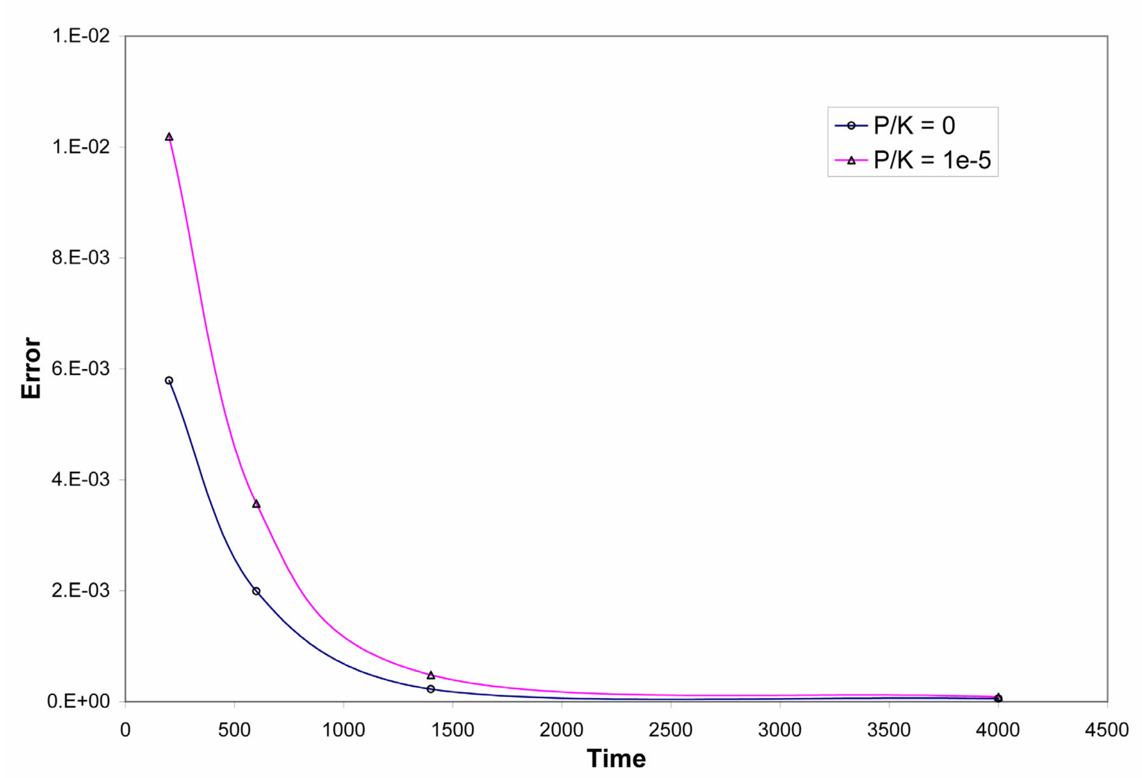

Figure 14 Average model errors in radial groundwater flow case

3.4.2 Surface overland flow and channel routing

2-D overland surface flow coupled with channel routing is verified using rainfall and runoff example of diGiammarco (1996). In the example, overland flow from a tilted V-shape catchment is generated by one 90-minute duration, 3e-6 m/s intensity rainfall event. The dimension of V-shape is shown in figure 15. The domain is two 1000 meter by 800 meter planes connected to a 1000 meter length of channel 20 meter wide. Surface slope are 0.05 and 0.02, perpendicular to and parallel to the channel respectively. Manning roughness are 0.015 for the slope and 0.15 for the channel. The boundary conditions are no flow at plane and critical depth at the outlet. Due to symmetry, only half of the domain is decomposed and simulated.

DiGiammarco (1996), VanderKwaak (1999), Panday and Huyakorn (2004) present simulation results by various model and approach. Those are compared with the present model results as in figure 16. IFD (integrated finite difference, DiGiammarco, 1996) and MIKE-SHE (DiGiammarco, 1996) applies finite difference scheme. In the simulation, it decomposes the domain with 160 squares with a side length of 100 meters. MODHMS (Panday and Huyakorn, 2004) uses 50 meters by 50 meters squares, total of 640, in its simulation. In PIHM, only half of the domain is simulated due to symmetry. The half-domain is decomposed with 408 triangles. All the other model parameters are the same as above.

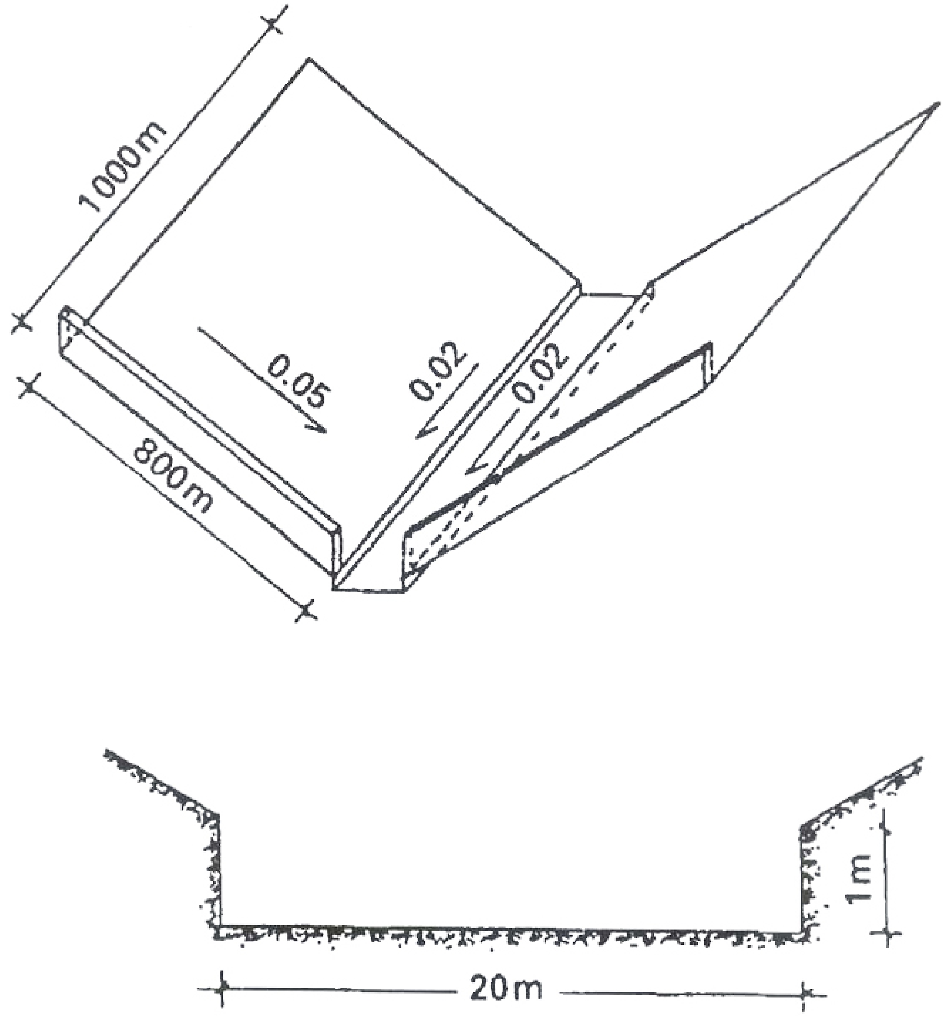

Figure 15 Tilted V-shape catchment (after DiGiammarco, 1996)

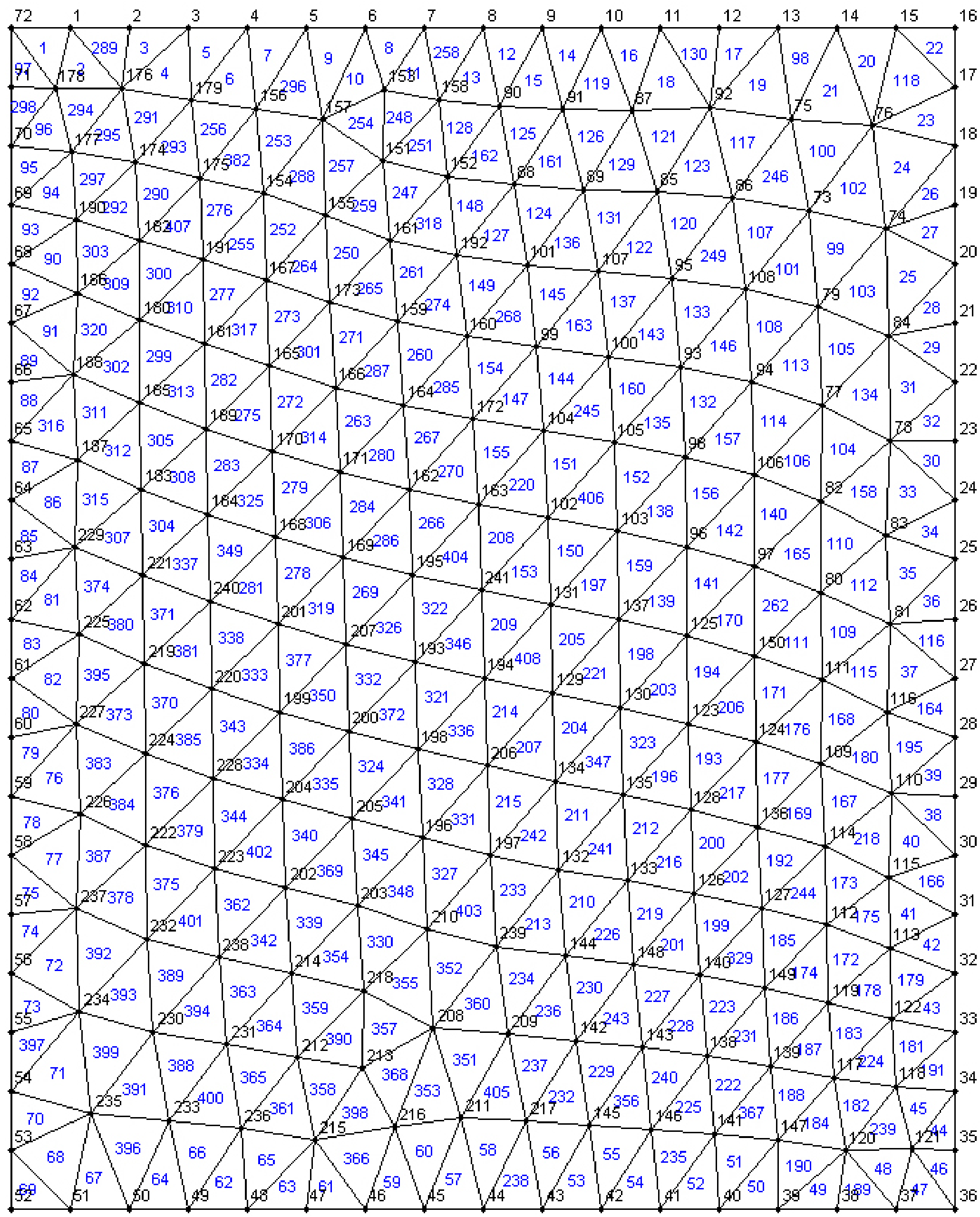

Figure 16 Domain decomposition for tilted V-shape catchment problem

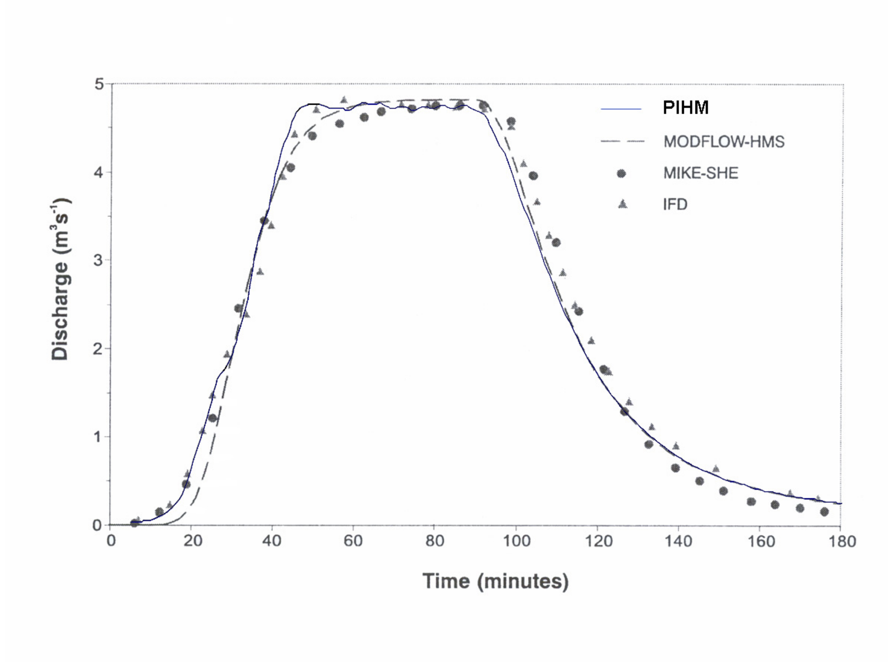

Figure 17 Comparison of modeled hydrograph by PIHM, study of DiGiammarco (1996) and Panday & Huyakorn (2004)

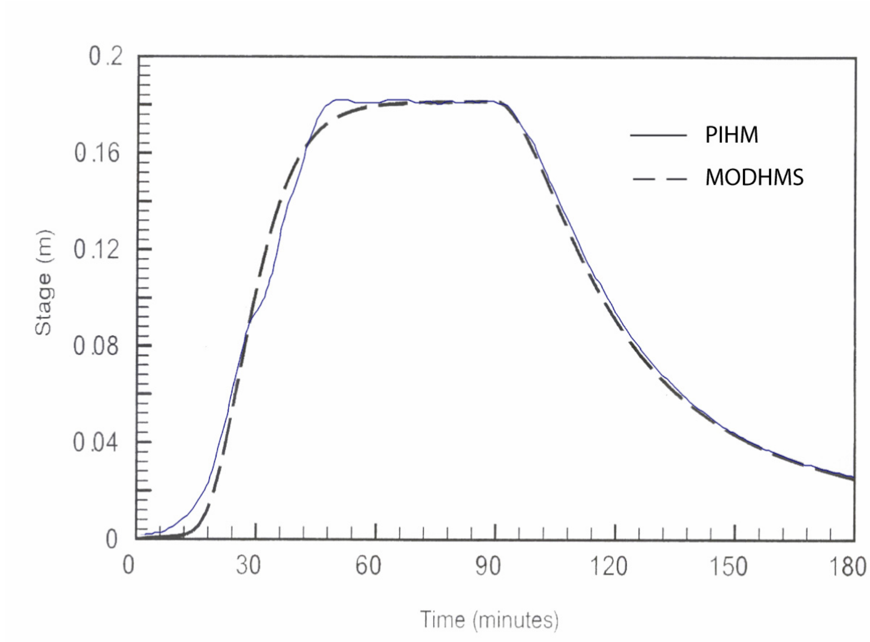

Figure 18 Comparison of modeled stage by PIHM, study of DiGiammarco (1996) and Panday & Huyakorn (2004)

The hydrograph in figure 17 and 18 can be viewed as 3 sections: the rising limb, the stable limb and the receding limb. It appears the all models agree well for the receding limbs. For the rising limbs, there is a delay in MIKE-SHE. Both IFD and PIHM have a shift in the middle of rising limbs. Detailed investigation shows that it is caused by the weir structure we apply between the channel and the hillslope. At that moment, the weir switches from submerged to a free surface condition. However, MODHMS result does not have this effect even though it is reported that the same weir structure is applied. The MIKE-SHE model result is a little far away from the other results for the stable limb. PIHM has some oscillations in its stable limb, which are not present in MODHMS, but it is shown in IFD and CVFE (controlled volume finite element, DiGiammarco, 1996). The no flow boundary applied in the V-shaped problem imposes an invisible wall on the left end of the plane. Due to the slope along the channel, the overland flow is blocked and reflected. This “wall” effect or the instability of the algorithms could cause the oscillations. Further investigations about this will be attempted in future.

3.5 CONCLUSION

The Penn State Integrated Hydrologic Model, PIHM, is an integrated model designed for multiple hydrologic processes simulation. The PIHM is written in C and is designed to exchange I/O with an object oriented data model. Because it operates on the same type of data model, it will ultimately be possible to achieve seamless connection between pre/post processor and the hydrologic model. This will not only save space for model results, it will also allow complex inquiries to be handled efficiently.

PIHM is verified against close form solutions and other model results in several cases. For groundwater flow, the PIHM result is compared with analytic solutions in a radial groundwater flow problem. The results show that model converges to the analytic solution. In a V-shape catchment simulation, PIHM results are compared with two other numerical models. In general, PIHM compares reasonably well to the CVFE and FD models. However, there are small oscillations in the stable limbs as with CVFE method. Further investigation will be focus on these oscillations in the future.

REFERENCES

Abbott, M.B., Bathurst, J.A., Cunge, P.E., 1986. An Introduction to the European Hydrological System-Systeme Hydrologicque Europeen “SHE” 1: History and philosophy of a physically based distributed modeling system. Journal of Hydrology, 87, 45-59.

Abbott, M.B., Bathurst, J.A., Cunge, P.E., 1986. An Introduction to the European Hydrological System-Systeme Hydrologicque Europeen “SHE” 2: Structure of a physically based distributed modeling system. Journal of Hydrology, 87, 61-77.

Allen, R.G., Pereira, L.S., Raes, D., Smith, M., 1998. FAO irrigation and Drainage paper No. 56, Crop Evapotranspiration.

Beven, K.J., 2001. Rainfall-runoff modeling, the primer. John Wiley & Sons.

Brandes, D., 1998. A low-dimensional dynamical model of hillslope soil moisture, with application to a semiarid field site. PhD thesis, the Pennsylvania state university.

Bras, R.L., 1990. Hydrology, An introduction to hydrologic science. Addison-Wesley publishing company.

Cohen, S.D., and A.C. Hindmarsh, 1994. CVODE User Guide, Numerical Mathematics Group, LLNL. UCRL-MA-118618.

Di Giammarco P., Todini, E, Lamberti, P., 1996. A conservative finite elements approach to overland flow: the control volume finite element formulation. Journal of Hydrology, 175(1996) 267-291.

Dingman, S.L., 1994. Physical Hydrology. Macmillan.

Duffy, C.J., 2004. A Semi-Discrete-dynamical model for mountain-front recharge and water balance estimation: the Rio Grande of southern Colorado and New Mexico. AGU Monograph.

Maidment, David, 2002. Arc Hydro, GIS for water resources, ESRI Press. Redlands, CA.

McKinney, Daene, Cai Ximing, 2002. Linking GIS and water resources management models: an object-oriented method, Environmental Modeling & Software, 17(2002) 413-425.

Panday, S., Huyakorn, P.S., 2004. A fully coupled physically-based spatially-distributed model for evaluating surface/subsurface flow. Advances in Water Resources 27, 361-382.

Tucker, Gregory, Lancaster, Stephen, et al, 2001. An object-oriented framework for distributed hydrologic and geomorphic modeling using triangulated irregular networks, Computers & Geosciences 27(2001) 959-973.

VanderKwaak, J., 1999. Numerical simulation of flow and chemical transport in integrated surface-subsurface hydrologic systems. Ph.D Thesis in Earth Sciences, University of Waterloo, Waterloo, Ontario, Canada, 217pp.

Vieira, J.H., 1983. Conditions governing the use of approximations for the Saint-Venant equations for shallow surface water flow. Journal of Hydrology, 60, 43-58.

CHAPTER 4
NUMERICAL SIMULATION OF RUNOFF GENERATION FOR THE SHALE HILLS EXPERIMENT WITH A FULLY-COUPLED INTEGRATED MODEL

Yizhong Qu[1] and Christopher J. Duffy[1]

[1]Department of Civil and Environmental Engineering
The Pennsylvania State University
University Park, PA 16802

ABSTRACT

In 1974, a field experiment was conducted at the Shale Hills watershed in central Pennsylvania to experimentally investigate the role of antecedent moisture (initial conditions) on hillslope runoff response to artificial rainfall events. The data collected from Shale Hills experiment has been extensively used in teaching and research at Penn State University. However, to date there is no distributed numerical model applied to this field experiment because of its complicated rainfall-runoff generation and ephemeral channel. In this paper, the field data is re-analyzed, and a new integrated hydrologic model, PIHM (Penn State Integrated Hydrologic Model), is applied to simulate the hillslope responses to a series of 6 artificial rainfall events. Examination of the field data reveals that a large percentage of rainfall (more than 37%) is stored in the shallow groundwater after each rainfall event. After each storm,

the water table and base-flow relax over a relatively long time scale (~weeks). Although it was clear that the percentage of rainfall stored in the saturated groundwater depends on the antecedent soil moisture, it is shown from experiment and the model that the soil moisture storage (equivalent of depth of moisture) increases as the water table relaxes after each storm. This effect shows the competitive relationship between soil moisture storage above the water table and saturated storage below the water table. As the water table rises, the total storage of soil moisture decreases. As the water table relaxes the volumetric storage of soil moisture per unit surface area decreases. The explanation is that surface tension holds moisture against gravity, while below the water table gravity alone affects the flow.

Another important feature of the model results is the simulation of the ephemeral stream-flow. The ephemeral channel in the upland region as the name implies, alternates from wet during rainfall events, to dry as the water table relaxes following the storm event. The ephemeral state (flowing-nonflowing) cannot be predetermined from experimental data. Thus one challenge of the fully coupled model is to reproduce this effect with the coupled effects of overland flow, channel flow, and groundwater flow.

Both field data and numerical results show that saturation overland flow (saturation from below near the stream channel) is the most important contributor to the total runoff. The model clearly shows that during rainfall events, subsurface hydrologic processes play a fundamental role in surface runoff generation. A final interesting feature of the model result is that, even though the soil properties were assumed homogenous, the model surface saturation areas during and just after each storm event tended to be discontinuous. That is because continuous surface was limited and much of the overland flow “re-infiltrated”. The patches of saturation grew as the soil moisture increased and connectivity of the patches also increased.

Keywords: Integrated Hydrologic Model, runoff generation, PIHM

4.1 INTRODUCTION

We can think of the watershed response to a storm as having two fundamental categories: the hillslope response and the stream network response. The hillslope response transforms areal rainfall to channel runoff through the physical processes of surface flow or subsurface flow. Within these categories there are three critical physical mechanisms which control the flow: 1) Overland flow is generated when rainfall exceeds the conductance of the soil (Horton, 1933); 2) Overland flow is also generated when the soil becomes saturated from below, due to a rising water table, this is called saturation overland flow (Dunne, 1970); and 3) Subsurface runoff to the channel occurs where the water table drains by gravity to the channel. The latter is referred to as base-flow (Freeze, 1972). For the most part, each mechanism has been extensively studied, and a number of models have been developed (Freeze, 1980; Robinson and Sivapalan, 1996). Among them, only a few are capable of simulating the multiple mechanisms of rainfall-runoff (VanderKwaak and Loague 2001; Panday and Huyakorn, 2004).

The stream network serves to collect all contributions from hillslope and routes the flows to the outlet. The channel transport processes are described by St. Venant equations (e.g. shallow water equations). As stated, most models assume the hillslope response and channel network response are independent or weakly coupled (Robinson and Sivapalan, 1996), which is an acceptable assumption when the time scale separation between them is significant. However, there are cases that require a fully-integrated simulation of both hillslope and channel network response. For instance, in upstream region where channel is ephemeral, water depth may be totally dependent on the subsurface contribution to the channel and the conditions for "flow" or "noflow" cannot be determined a-priori. Lower down in the watershed, it is also possible that the channel may lose or gain water from the groundwater during and after the storm. Given that almost all watersheds have only a single gage at the outlet, most models ignore these physical processes and local complexities of the exchanges between hillslope and channel.

Integrated hydrologic model have recently become a more active research topic in numerical simulation. VanderKwaak (1999) developed an integrated surface-subsurface hydrologic system called, InHM. In his approach, 2-D diffusion wave governing equation is fully coupled with 3-D subsurface governing equation in one frame work, and the whole system is discretized and solved with finite element method. Panday and Huyakorn (2004) have constructed the integrated hydrologic model, MODHMS, which includes 1-D channel routing, 2-D overland flow and 3-D groundwater flow. MODHMS solves fully coupled diffusion wave approximation of St. Venant equation and Richards' equation with finite difference method. Qu and Duffy (2004) apply semi-discrete finite volume approach to develop Penn State Integrated Hydrologic Model, PIHM. PIHM has incorporated 1-D channel routing and 2-D overland flow on the surface. For subsurface, it has incorporated integrated 1-D vertical unsaturated flow and 2-D groundwater flow. PIHM, fully couples hillslope response and channel network response. Within PIHM, all coupled governing equations are integrated over the finite volume reducing the PDE's to semi-discrete form (discrete in space, continuous in time). In this form a state-of-art ODE solver can be used to solve the integrated system. One advantage of PIHM is its flexibility for adding or subtracting process models. The user can turn on/off hydrologic processes based on the particular need of the modeler. It also allows flexible constitutive relationships. For instance, either kinematic wave approximation or diffusion wave approximation can be used. Next, the utility of PIHM is demonstrated with a watershed field experiment from central Pennsylvania.

In 1974, a comprehensive field experiment was conducted, at Shale Hills, PA, to investigate rainfall-runoff generation mechanisms. The focus of this paper is to apply the PIHM to a well measured field experiment, where both the hillslope and channel network response are important.

4.2 SHALE HILLS FIELD EXPERIMENT

The Shale Hills hydrologic experiment was conducted on a 19.8 acre watershed in the Valley and Ridge physiographic province of central Pennsylvania in 1974 by the Forest Hydrology group at the Pennsylvania State University. The goal of the study was to experimentally determine the physical mechanisms of runoff and stream-flow generation at the upland forested catchment, and to evaluate the effects of antecedent soil moisture on the runoff peak and timing. The data collected during the experiment has been used to benefit teaching and research for many years. Recently, a new effort has begun to re-instrument the watershed and to make available the historical data as a "test-bed" for watershed modelers. The new instrumentation will focus on real-time, automated measurements of continuous stream flow, groundwater levels, soil moisture, soil tension, temperature, and precipitation.

The experiment consisted of a comprehensive network of piezometers (~40), neutron access tubes for soil moisture (40) and four weirs. The distribution of sampling sites is shown in figure 1. The watershed was implemented with a spray irrigation network, shown in figure 2, to precisely control the amount of rainfall over the entire watershed. The stream in figure 2 is delineated from a 1-meter resolution digital elevation model (DEM). The upper part of the channel is ephemeral, and flows during storms or snowmelt periods. The artificial precipitation forcing is applied below the tree canopy and above the surface vegetation. Therefore, it is not intercepted by the tree canopy. Besides the grass, the hillslope is also covered by a layer of leaves and forest litter. It is known that macrospores from decayed root and worm holes underneath this layer may contribute to high hydraulic conductivity of the in the soil as shown in figure 3. The soil profile at Shale Hills is typically a silt loam, ranging from 0.6 meter thickness at the ridge top, to 2.5 meters deep near the channel. Specifically, the main soil types are: Ashby soil type, a shaley-silt-loam in the upland portion of the watershed; the Blairton silt loam on the intermediate elevation slopes; and the Ernest silt loam in the lower region along the channel.

From July to September 1974, there were a series of 9, equal artificial rainfall events (0.25 inch/hr for 6 hours) applied to the entire watershed. The events were conducted such that the antecedent moisture gradually increased from very dry in the first storm, to very wet in the 9th. Along with the artificial rainfall, natural rainfall events also occurred which slightly complicated the experiment. To reduce the impact of the natural events, 6 consecutive rainfall events were selected and simulated in this paper.

The primary questions we are trying to answer by the numerical simulation are: (1) It is often speculated that runoff has the same pattern for the hillslope response regardless of which overland flow mechanism occurs, overland flow from rainfall exceeding the hydraulic conductivity of the soil, or overland flow from water table saturation from below. Thus, one of the questions to answer is: what is the impact of groundwater flow and soil moisture in both cases? (2) Closing the water budget is a major challenge with both scientific and practical implications. So, under what conditions is it possible and/or is it useful to maintain a distributed mass balance for all rainfall-runoff mechanisms? (3) What is the role of complex terrain in producing runoff in Shale Hills? (4) To date models of ephemeral and intermittent channels have not met with much success. Can fully coupled models improve the ability to simulate catchments that have ephemeral and/or intermittent channels?

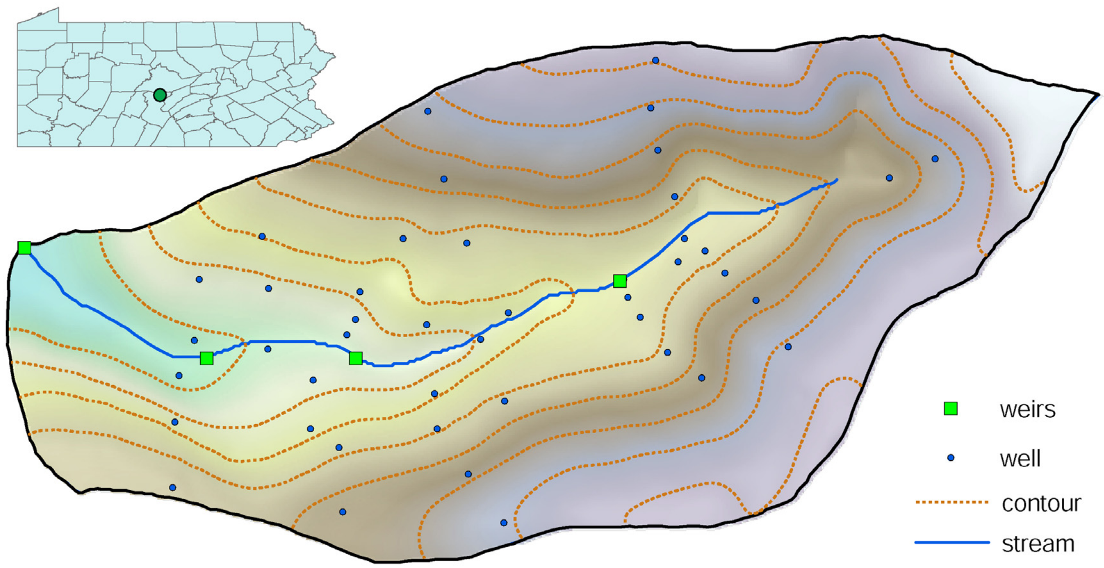

Figure 1 The Shale Hills watershed and measurement locations. It consists of 44 wells and 4 weirs distributed across a 19 acre hillslope.

Figure 2 Spray irrigation devices are spraying a controllable rate of irrigation under the tree canopy in Shale Hills experiment.

Figure 3 "Macro pores" underneath the surface vegetation layer at Shale Hills, PA may lead to an intermediate time scale process, slower than surface overland flow but faster than porous media subsurface flow.

4.3 MODEL DESCRIPTION

4.3.1 Semi-Discrete Approach with FVM

The general form of mass conservation equation of incompressible fluid flow can be written as

$$\frac{\partial \rho}{\partial t} + \nabla \cdot u = 0 \tag{1}$$

where ρ is fractional mass (dimensionless) in an arbitrary control volume, and u is fluid flux [L/T]. Mass conservation implies that the change rate of ρ is exactly balanced by the divergence of the flux. The integral form over the control volume V is given by

$$\int_V \frac{\partial \rho}{\partial t} dV = -\int_V \nabla \cdot u dV \ . \tag{2}$$

Applying the divergence theorem to the right hand side yields

$$\int_V \frac{\partial \rho}{\partial t} dV = -\int_S u \cdot N dS \tag{3}$$

where S is surface of V, and N is the normal vector on S. Computing the right-hand-side of equation (3) using the finite volume formulation (Leveque, 2002) yields

$$-\int_S u \cdot N dS = \sum_{i=1}^{S} Q_i \tag{4}$$

where the net flux Q_i across surface i, is positive in and negative out.

Letting the integral form of the left hand side of (3) be $M = \int_V \rho dV$, leads to the semi-discrete form of the mass conservation equation

$$\frac{dM}{dt} = \sum_{i=1}^{S} Q_i \tag{5}$$

where M is mass storage of control volume. Q_i is evaluated as the normal flux to each surface of the control volume. The vector form of (5) represents the system of ODE's within a control volume. Substitution of appropriate constitutive equations to evaluate fluxes in equation (5) allows the flux to be evaluated across the element boundary. We note that the finite volume method guarantees mass conservation for each control volume and it has the convenient ODE form of balance equations for both parabolic and hyperbolic PDE's (Leveque, 2002).

Under circumstances where full coupling of multiple hydrologic processes is required, there are several reasons that the model kernel approach described above offers a simple, yet flexible numerical strategy. First, the user can incorporate the desired number of processes simply by setting on/off switches prior to simulation. Second, trial constitutive relationships are easily applied and tested with numerical experiments. Finally, the control volume can be in any shape as long as orthogonal flux across boundary is feasible to be evaluated with the FVM.

In this paper the necessary hydrological processes included in Shale Hills field experiments are: vegetation layer interception, evapotranspiration, overland flow, infiltration, vertical unsaturated flow, and lateral groundwater flow. Shale Hills watershed is decomposed into a triangular unstructured grid and the finite volume element is a prism while the channel segment is represented as uniform as shown in figure 4. A prism element may have channel segments along any edge.

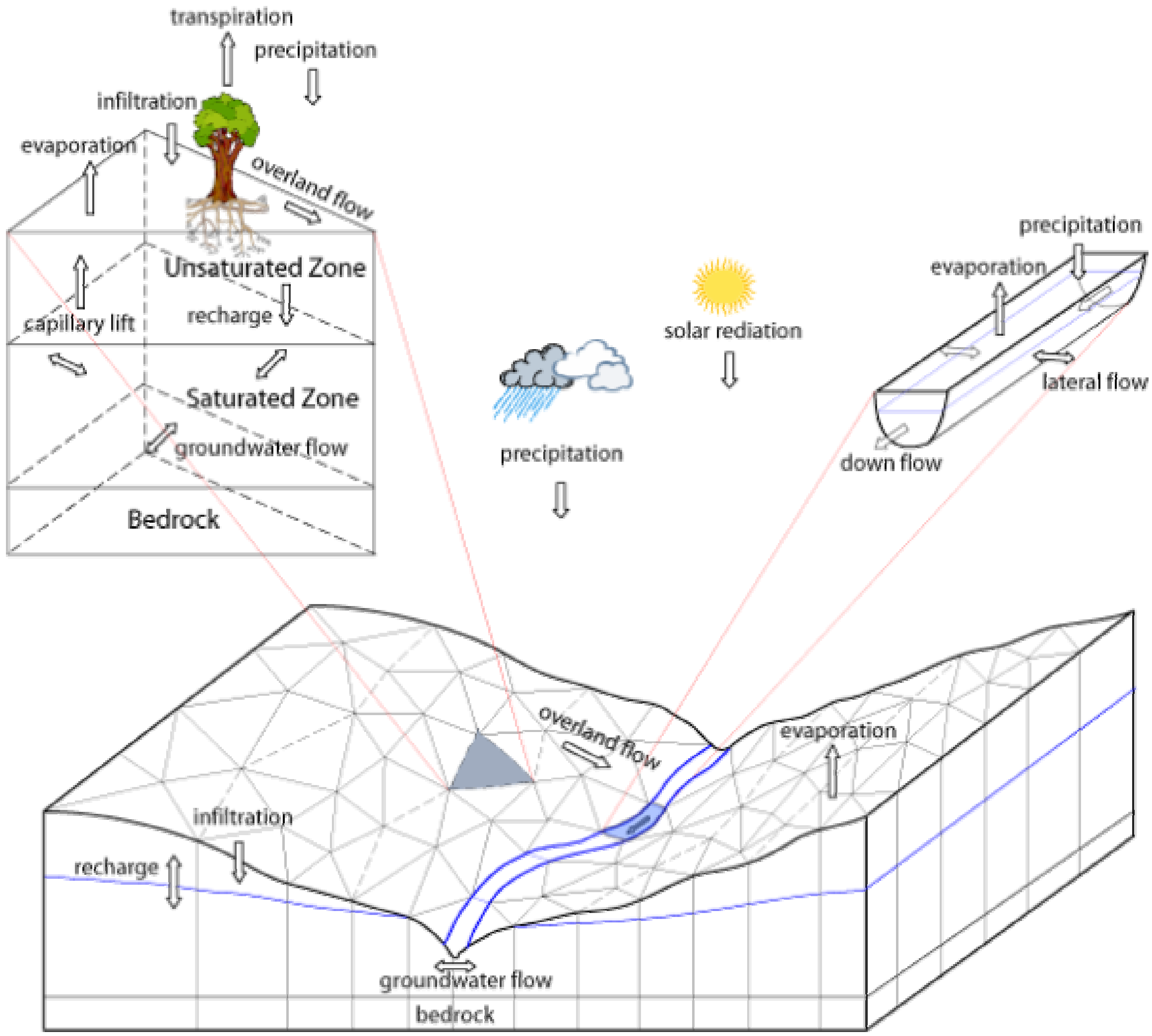

Figure 4 The Domain decomposition in a hillslope scale example. Basic prism element is shown to the left with multiple hydrological processes. Channel segment is shown to the right.

4.3.2 Governing Equations for Hydrologic Processes

The governing equation for channel routing, overland flow and subsurface flow are PDE's. The governing equations for interception and evapotranspiration are either ODE or algebraic equations. For those PDE's, semi-discrete finite volume method is applied and ODE's is yielded with respect to a control volume. Over each finite volume, we combine these with the remaining ODE's for vegetation, snow, etc. to form a global system of ODE's. The system is them solved using CVODE (cohen and Hindmarsh, 1994). Only derived governing equations in ODE form with respect to a control volume are discussed in this paper. Those interested in the details of the derivation are referred to Qu and Duffy (2004).

Assuming there is no spatial interaction between interception storage between control volumes, the interception process is controlled by

$$\left(\frac{dS_I}{dt} = P - E_I - P_o \right)_i \tag{6}$$

where S_I is interception storage. P is total water equivalent precipitation, E_I and represents evaporation from surface vegetation, P_o is through-fall precipitation, which is also the input of overland surface storage. The upper bound of S_I is a function of vegetation type, canopy density and even the precipitation intensity. When the canopy reaches the upper threshold, all precipitation becomes through-fall.

The 2-D overland flow is estimated by the following ODE derived by applying semi-discrete approach on St. Venant equations

$$\left(\frac{\partial h}{\partial t} = P_o - I - E_o - Q_{oc} + \sum_{j=1}^{3} Q_s^{\ ij}\right)_i \tag{7}$$

where h is overland storage. $Q_s^{\ ij}$ is surface flow from element i to its neighbor j, evaluated by equation (7.1) and (7.2). P_o, I and E_o are net precipitation, infiltration and evaporation respectively. Q_{oc} describes interaction between overland flow and channel routing. Please note all fluxes are normalized by projected surface area of the prismatic element.

The fluxes across the element boundary is evaluated with the diffusion wave approximation (Gottardi and Venutelli, 1993) by

$$Q_s = hk_i \frac{\partial H}{\partial x} \tag{7.1}$$

with

$$k_i = \frac{h^{\frac{2}{3}}}{n_i} \frac{1}{\left|\partial H/\partial s\right|^{\frac{1}{2}}} \tag{7.2}$$

where H is total hydraulic head. n is Manning roughness coefficients. s is a vector along the direction of maximum slope.

Another method known as the kinematic wave approximation [Eagleson, 1970], defines the stage and discharge in terms of

$$Q = \alpha A^m \tag{7.3}$$

where α and m are empirical parameters.

Similarly, the governing equation for 1-D channel routing is derived from 1-D St. Venant equation as

$$\left(\frac{d\varsigma}{dt} = P_c - \sum Q_{gc} + \sum Q_{oc} + Q_{in} - Q_{out} - E_c\right)_i \tag{8}$$

where ς is volumetric water in channel. P_c is precipitation applying to channel element i. E_c is evaporation from channel segment. $\sum Q_{gc}$ is the summation of the lateral interaction between aquifer and channel, which is evaluated by Darcy's law. Q_{oc} refers to interaction between overland flow and channel routing. Q_{in} is inflow from other channel segments. Q_{out} is outflow to other channel segments. Again, all the fluxes are normalized by segment surface area.

Like 2D overland flow, the kinematic wave or the diffusion wave approximations can also be applied to reduce the complexity of solving full St. Venant equations.

The governing equations for subsurface flow is derived in integral form Richards' equation (Duffy, 2004)

$$\left(\frac{d\xi}{dt} = I - q^0 - ET_s\right)_i \tag{9}$$

$$\left(\frac{d\zeta}{dt} = q^0 + \sum_{j=1}^{3} Q_g{}^{ij} - Q_l + Q_{gc}\right)_i \tag{10}$$

where ξ [L] is unsaturated moisture storage of element i. ζ [L] is saturated moisture storage. q^0 is internal flux between unsaturated zone and saturated zone, referred to as capillary lift for upward flow from the water table or recharge for downward flow to water table. I and ET_s are incoming infiltration and outgoing evapotranspiration at land surface, respectively. $Q_g{}^{ij}$ is lateral groundwater flow from element i to its neighbor j . Q_l is vertical leakage through an underlying confining bed. Q_{gc} is discharge/recharge from/to aquifer to/from channel. In this approach all fluxes are normalized by surface area of the element with units [L/T].

In the case where the groundwater table is shallow, equation (9) and (10) can be further simplified into a single state (Bierkens, 1998) by applying the "enslaving principal" (Duffy , 2004)

$$\frac{d\xi}{dt} = G_1(h)\frac{dh}{dt} \tag{9.1}$$

$$G(h)\frac{dh}{dt} = I - ET_s + \sum_{j=1}^{3} Q_g{}^{ij} - Q_l + Q_{gc} \tag{10.1}$$

with

$$G(h) = \varepsilon_0 + (\theta_s - \theta_r)(1 - (1 + (\alpha(z_s - h))^n)^{-((n+1)/n)}) \tag{10.2}$$

and

$$G_1(h) = -(1 + (\alpha(z_s - h))^n)^{-((n+1)/n)} \tag{10.3}$$

where h and z_s are height of phreatic surface and surface elevation relative to some reference. ε_0 is a extreme parameter to obtain stable solutions. θ_s and θ_r are saturated and residual moisture content. α and n are soil parameters.

The central point of the integrated model is that all interaction terms and coupling are specified within the local ODE system and kernel incorporating equations (6), (7), (8), (9) and (10).

Lateral groundwater fluxes are evaluated using a volume-average version of Darcy's law [Duffy, 2004]. Before normalization, it is in form of

$$Q_g^{ij} = B_{ij} K_{eff} \frac{H_i - H_j}{D_{ij}} \frac{\zeta_i + \zeta_j}{2} \tag{11}$$

where B_{ij} is length of common boundary and D_{ij} is distance between element i and j. $H_i = \zeta_i + z_i$ is hydraulic head where z_i is elevation of datum of element i. The effective hydraulic conductivity K_{eff} is harmonic mean of element i and j. The storage-discharge relation in equation (10) is a non-linear one due to vertical integration.

For the internal flux q^0 between unsaturated zone and saturated zone, i.e. recharge or capillary lift, Duffy [2004] has shown that a simplified form based on integration over the finite volume can be approximated by

$$q^0(\xi, \zeta) = K_s \frac{1 - e^{-\alpha(z_s - \xi)} - \alpha\zeta}{\alpha(z_s - \xi) - (1 - e^{-\alpha(z_s - \xi)})} \tag{12}$$

where K_s is saturated hydraulic conductivity. α is a parameter for the exponential soil model. Z_s is total aquifer depth. We note that the integrated flux at the water table (11) is a nonlinear function of the water table position and the depth of soil moisture above the water table.

The interaction item between the overland flow process and subsurface processes, i.e. infiltration I in equation (7) and (9), is expressed by either of the two overland flow runoff generation mechanisms. The interaction between overland flow and channel routing, i.e., lateral flow Q_{oc} in equation (7) and (8), is approximated by the weir equation [Panday and Huyakorn, 2004], with free-flowing or submerged conditions. The interaction item between aquifer and channel routing, i.e. Q_{gc} in equation (8) and (10) is controlled by volumetric integration of Darcy's law like equation (11).

Evaporation from vegetation interception, overland flow, snow pack and river surfaces is estimated using the Pennman Equation [Bras, 1990], which represents a combined mass-transfer and energy method.

$$\left(E = \frac{\Delta(R_n - G) + \rho_a C_p (e_s - e_a)}{\Delta + \gamma} \right)_i \tag{12}$$

Potential evapotranspiration from soil and plant is estimated using Pennman-Monteith equation

$$\left(ET_0 = \frac{\Delta(R_n - G) + \rho_a C_p \dfrac{(e_s - e_a)}{r_a}}{\Delta + \gamma(1 + \dfrac{r_s}{r_a})} \right)_i \tag{13}$$

here, ET_0 refers to potential evapotranspiration. R_n is net radiation at the vegetation surface. G is soil heat flux density. $e_s - e_a$ represents the air vapor pressure deficit. ρ_a is the air density. C_p is specific heat of the dir. Δ is slope of the saturation vapor pressure- temperature relationship. γ is the psychometric constant. r_s and r_a are the surface and aerodynamic resistances. Actual evapotranspiration is a function of potential ET and current plant, climatic and hydrologic conditions, such as soil moisture. In this approach, coefficients are introduced to calculate actual ET from potential following Kristensen and Jensen [1975]. Allen et al. [1998] provides guidelines for computing those coefficients for different vegetation.

Combining equation (6), (7), (8), (9) and (10) together leads to a local system of ODE's representing multiple hydrological processes within element i. One advantage of this strategy is its flexibility. It allow to use flexible constitutive relationships. There is no intrinsic limitation to the number of hydrologic processes. The users can easily turn on/off processes based on their needs.

The domain decomposition uses Delaunay Triangulation. In our model, the circum-center is used to represent its triangle. In the Shale Hills simulation, the domain is represented by 566 nodes and 315 elements. The channel is decomposed into 21 segments, including both ephemeral and perennial channel segments.

The global ODE system is solved with SUNDIALS (suite of nonlinear and differential/algebraic equation solvers) developed in the center for applied scientific computing at Lawrence Livermore national laboratory. SUNDIALS is a family of closely related solvers, including CVODE, CVODES, KINSOL and IDA, for ODE, ODE sensitivity analysis, algebraic equations, and differential algebraic equations respectively. Among them, CVODE is an ODE solver that has methods for both stiff and non-stiff initial value problems. The integration method in CVODE is a multi-step method, called variable-coefficient Adams-Moulton and Backward Differentiation Formula methods. For a stiff ODE system in PIHM, the linear system in CVODE is solved by either a direct (dense or band) solver or a preconditioned

Krylov solver, GMRES. In both cases, the user can either provide Jacobian or let the solver calculate it internally. CVODE uses adaptive time step during simulation based on a local error estimation scheme. However, the user can control the maximum and minimum time step it works in. Normally, the minimum time step is determined by the stiffness of the problem automatically, and maximum time step can not be greater than the interval of forcing data. Otherwise, the model will not capture the exact forcing numerically.

4.4 DATA ANALYSIS

The Shale Hills experiments datasets can be accessed at http://www.cee.psu.edu/Shale_Hills/. Among all 9 experiments done in 1974, 6 consecutive events in August with less interference of natural rainfall are selected in this paper for analysis and simulation.

4.4.1 Shallow Groundwater Assumption

A vertical profile of soil moisture is measured at each neutron probe site. The spatial average of soil moisture across the entire site is calculated and plotted against saturated groundwater storage as in figure 5. Figure 5 also validates shallow groundwater assumption with reasonable Van Genuchten silt loam soil parameters: $\alpha = 2.0$, $n = 1.8$ based on equation (9.1) and (10.3). Therefore, shallow groundwater assumption is adopted in the simulation to save computational cost.

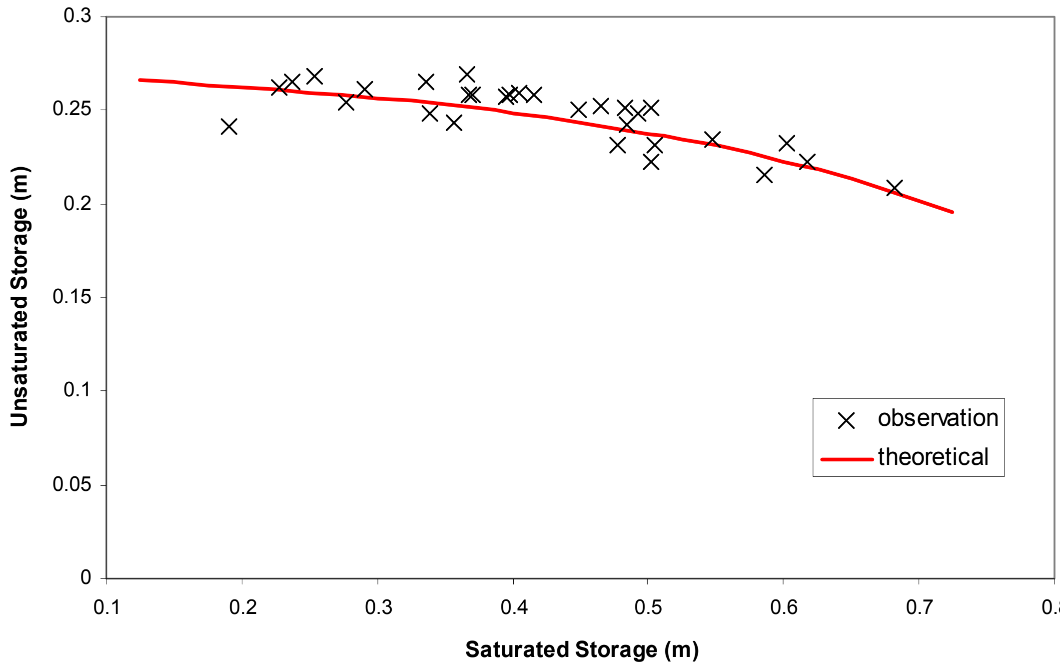

Figure 5 **The spatial average saturated-unsaturated storage relation for Shale Hills experiment. The red line represents theoretical "steady-state" saturated-unsaturated storage relationship (Bierkens, 1998, Duffy, 2004) in shallow groundwater assumption with Van Genuchten soil parameters:** $\alpha = 2.0$ **,** $n = 1.8$.

4.4.2 Water Budget

As shown in figure 6, the forcing and runoff is measured at 15 minutes interval for almost a month. Among those 6 equal rate artificial rainfall (irrigation) events, there is some interference of natural rainfall. Please note that natural rainfall applies directly on the top of canopy, while the equal rate experiment forcing applies below the tree canopy and above vegetation layer. Our experiment instruments are not able to measure the natural rainfall which falls directly above the canopy. Rather it measures through-fall (the fraction which makes it through the canopy) for those natural events. Because of that, we only select the six events with a minimum of natural storms.

The mass balance is calculated for each rainfall events from August 1, 1974 to September 1, 1974 in table 1. The research area is totally 77703.5 square meters. The total input to the system is 0.2789 m, i.e. 21670.88 cubic meters. The total discharge is 0.1210 m, i.e. 9404.31 cubic meters. By averaging groundwater table and soil moisture data spatially, aquifer storage, including both saturated and unsaturated storage, increases 0.146 m, i.e. 11348.6 cubic meters during this period of time. There is about 4.2% of total rainfall missing. It could be lost due to evapotranspiration or groundwater flow underneath the weirs. Numerical simulation will help to figure out this.

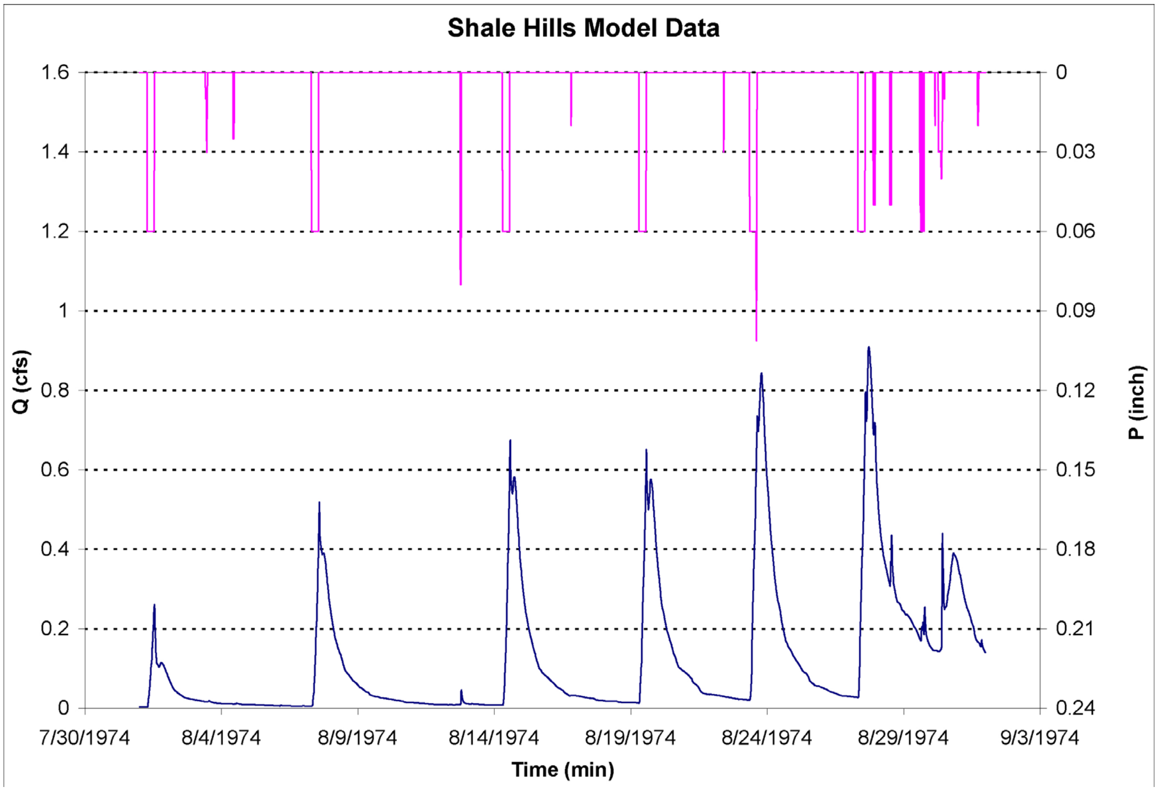

Figure 6 The 6 Rainfall events and it corresponding runoff in Shale Hills experiment

Storm	Duration	Irrigation (m)	Input (m^3)	Output (m^3)	Discharge Percentage (%)
1	08/01-08/07	0.04318	3355.236	407.4109	12.1
2	08/07-08/14	0.045974	3572.339	998.8983	27.9
3	08/14-08/19	0.038608	2999.975	1287.057	42.9
4	08/19-08/23	0.038862	3019.712	1340.731	44.4
5	08/23-08/27	0.04064	3157.869	1839.37	58.2
6	08/27-08/31	0.071628	5565.744	3530.845	63.4
total	08/01-08/31	0.2789	21670.88	9404.31	43.4

Table 1 The mass balance for all rainfall events in Shale Hills experiments

4.4.3 Antecedent Soil Moisture Effect

The 6 rainfall events are approximately equal in rate, about 0.25 inch/hour for 6 hours. There is no significant infiltration-excess overland flow observed in the experiment. This implies that the infiltration capacity is large enough to accommodate most of the rainfall. However, the runoff response increases, as shown in figure 6 and table 1, due to antecedent moisture gradually increased preceding each rainfall event from very dry to very wet. Table 1 shows the water budget for each event. We sum up the rainfall and runoff during interval for each storm event, it shows that only 12% of rainfall becomes runoff for the 1st storm when the antecedent soil moisture (including saturated and unsaturated storage) is very dry at the beginning, and the percentage increase gradually to 63.4 percent when the antecedent soil moisture becomes very wet. More rainfall quickly turns into runoff as antecedent soil moisture increases. However, at least 40% percent of the total rainfall infiltrates into the aquifer and is released as base-flow. The relaxation for the 6th event indicates significance of groundwater and soil moisture effects on rainfall-runoff generation.

For the subsurface, a two-state dynamical model proposed by Duffy (1996) is used, which is based on spatial integration of the unsaturated and saturated moisture over the catchment volume. The analysis of model results reveals: 1) the integrated soil-moisture storage and saturated storage are competitive state variables or they are inversely correlated. 2) Convex-concave topography creates near-stream conditions of surface saturation, overland flow and rejected rainfall. The latter process represents a nonlinear storage-feedback loop which dramatically enhances runoff under high water table conditions. 3) Base flow to the channel is found to be a nonlinear function of saturated groundwater storage. The overall role of shallow groundwater and its relation to soil moisture is found to be a critical factor in peak flow generation and flood duration.

4.5 SIMULATION RESULTS

4.5.1 Simulation Setup

The surface terrain is derived from 1 meter resolution DEM digitized from a detail topology map. There are 44 monitoring wells covering the entire domain as shown in figure 1. The aquifer bottom elevation at well location can be calculated by subtraction well depth from surface elevation. A bedrock DEM is determined by interpolation of bottom elevation at well locations. The domain is decomposed into 566 triangle elements with 315 nodes. The channel is delineated from DEM and further decomposed into 21 segments, including both ephemeral and permanent segments. The silt loam soil property used in the simulation is $\theta_s = 0.40$, $\theta_r = 0.05$, $\alpha = 2.0 \;\; 1/m$, $\beta = 1.8$, $k_s = 1e-5m/s$. Surface infiltration capacity is set to be the same as saturated hydraulic conductivity. Due to roughness of leaves and grass, the surface effective roughness for overland flow is estimated to be $0.83\min/m\text{^}(1/3)$. The main driven forcing, irrigation rate, is about 0.25 inch/hour for 6 hours. The reader is reminded that this forcing is applied under tree canopy, above ground vegetation. However, there are irregular natural rainfall took place during experiments, which applies on top to tree canopy. It is possible that experiment underestimates the natural rainfall rate because it measures only the through-fall. Temperature and other climate data collected are from USGS website for Huntingdon County, PA. It is impossible to get 15 minute climate data by all means. So daily data is used and therefore, evapotranspiration is just roughly estimated in this simulation.

The channel is assumed to be rectangular, 1.5 meter wide and 0.5 meter deep. The hydraulic roughness for the channel is set to $0.5\min/m\wedge(1/3)$. The boundary condition is set to be no flow at catchment boundary. At the outlet, it is critical depth boundary condition. The initial condition is estimated from neutron and well data preceding the experiment.

4.5.2 Closing Water Balance

As mentioned in the data analysis section, the research area is 77703.5 square meters. The total input to the system is 0.2789 m, i.e. 21670.88 cubic meters. The total discharge is 0.1210 m, i.e. 9404.31 cubic meters. By averaging the groundwater table and soil moisture data spatially, aquifer storage, including both saturated and unsaturated storage, increases 0.146 m, i.e. 11348.6 cubic meters during this period of time. There is about 0.012 meter, i.e. 4.2% of total rainfall missing.

The potential ET estimated from average daily temperature using Penmann Method is about 0.4 cm/day. Assuming actual ET is approximately 20% of potential ET during 6 events, the total ET is about 0.024 meter, which is higher than 4.2 %. Therefore, it is plausible to assume there is no significant groundwater flow underneath the outlet weir.

4.5.3 Simulation Results

Figure 7 compares modeled well elevation against observed well elevation data on Aug 1, Aug 16 and Aug 30. It reflects a pretty good match with slope of 1.05, and $R = 0.965$.

Figure 8 shows modeled runoff and observed data. The first event does not match as well as others possibly because the initial condition we used may be in error. There are several natural rainfall event involved as shown in figure 8, among them the one following the 6^{th} event is intense. Again, our experiment instrument is designed to measure rainfall rate under the canopy, while the natural rainfall applies on the top of it, which results in underestimate the natural intensity. This may explain the departure in the tail of the 6^{th} event.

Figure 9 shows those 6 peak-flows in figure 8. It is noticeable that there are 2 peaks for each rainfall event in both modeled results and observed data, which is caused by the complex terrain of the hillslope. The low dimensional model can not capture this, while PIHM successfully models it.

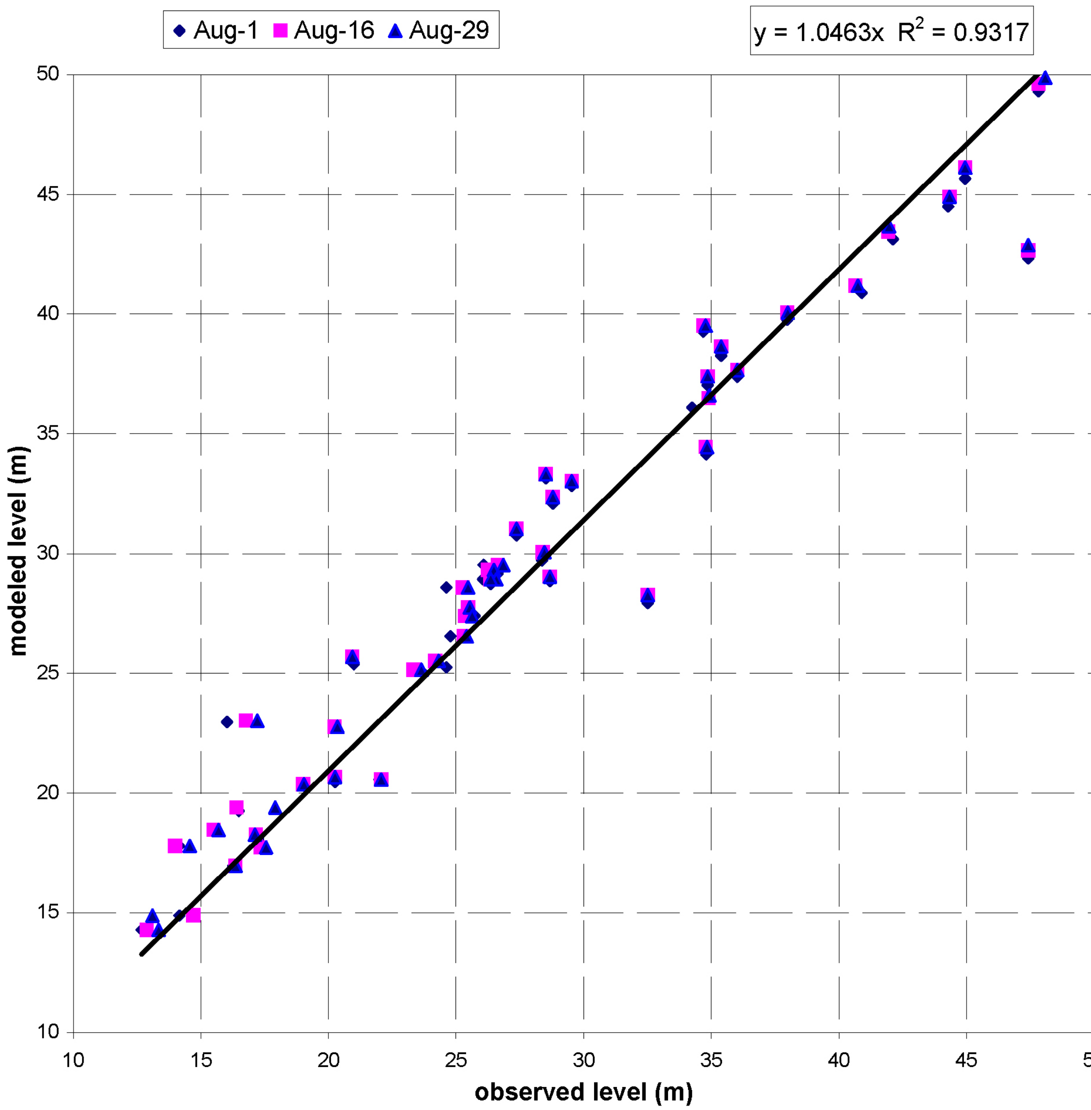

Figure 7 Modeled groundwater level and observed. Data at Aug 1, Aug 16, and Aug 29 are picked in this plot. It is ideally 1 to 1 relation if they are perfectly matched.

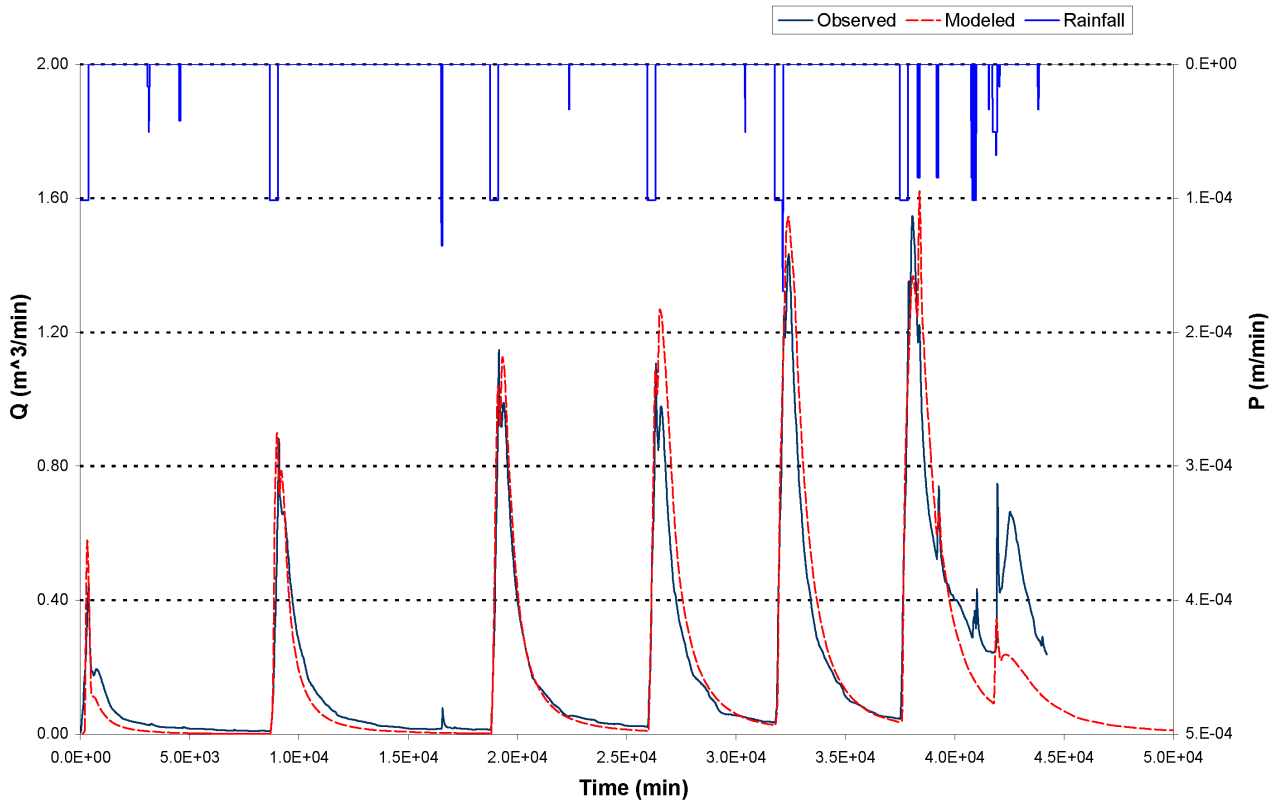

Figure 8 Modeled runoff vs. observed runoff for Shale Hills experiments, PA

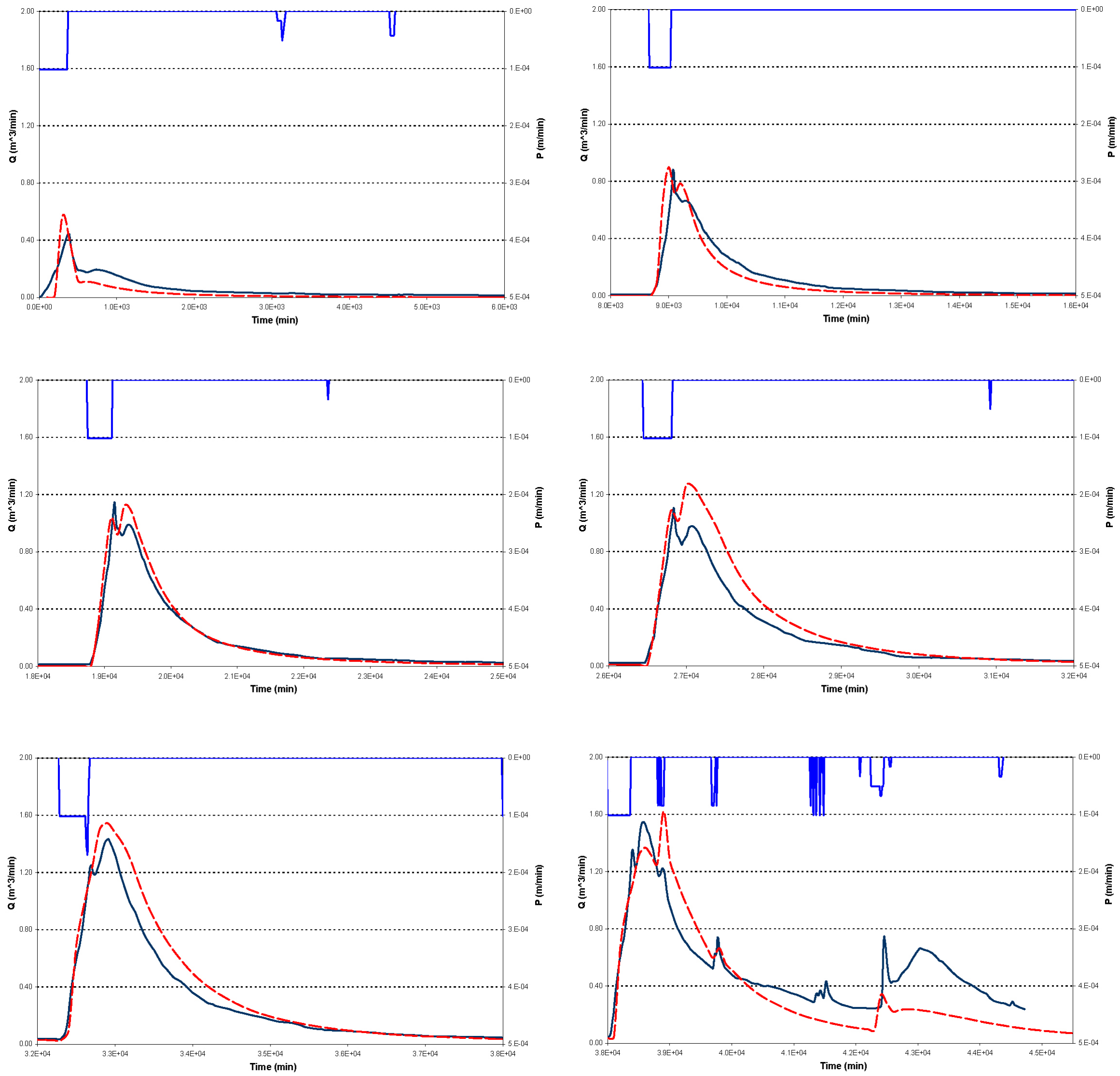

Figure 9 runoff peaks for 6 consecutive events. There are 2 peaks for each rainfall event.

4.6 DISCUSSION

4.6.1 Rainfall-runoff Generation Mechanism

PIHM incorporates 3 rainfall-runoff generation mechanisms. All of them take place in field of Shale Hills Experiment, as shown in figure 10.

Horton overland flow (precipitation excess) occurs when rainfall intensity exceeds infiltration capacity of surface soil. In Shale Hills experiment, the soil infiltration capacity is large enough to accommodate controlled rainfall, so Horton overland flow only happens during 5th event when a natural storm falls during artificial irrigation.

Saturation overland flow occurs generally at locations where water table saturates the land surface from below. For a hillslope, like Shale Hills, with less intensive rainfall, it takes place at the toe of hillslope. The saturation area right after each storm grows, and normally will not completely relax before next rainfall event. This leads to increasing antecedent soil moisture and saturation area preceding each rainfall event. The rejected rainfall over those saturated area produces most of runoff peak during or shortly after storm event. Figure 11 shows the saturation area after each storm event. First of all, because groundwater relaxes in a longer time scale than storm intervals, saturation area continues to increase from 4% at the beginning to 78% after 6th rainfall event. This reflects that antecedent soil moisture is increasing and runoff response due to saturation overland flow grows as well. On the other hand, rainfall infiltrates into aquifer results in higher soil moisture and partial saturated area. A quasi-linear relationship between percentage of rainfall stored in aquifer and its result, saturated area after storm, is shown in figure 12. Saturation area location distributes in a somewhat random fashion on local saddle, or concave patches during the first 4 storm events. Thus the effect is largely due to local complexity in the terrain. The impact of non-contiguous patches of saturation and overland flow alters the time scale of runoff significantly, as water infiltrates and exfiltrates the surface before it finally enters the channel. Starting from the 5th event, the saturation area becomes more continuous at least in the center. This is confirmed at other northeastern sites by the observation of Amerman (1965) and Dunne (1970). The saturation area of the numerical simulation is noticeable higher than the field data. This seems to be a complication of the surface layer covered by vegetation and leaves. In this analysis, saturation overland flow is the most important contributor to the peak runoff in Shale Hills experiment.

4.6.2 Runoff Responses

There are natural rainfall events among 6 artificial events. In figure 8 and figure 9, one can see the runoff responses to the rainfall events depend on its intensity and duration. First, there is significant runoff responses to every artificial storm, which is stronger than most of natural one and has a longer duration. For some of the natural storms, either because they are less intensive or short duration, all the forcing infiltrates and there is no instant runoff response. Again, at the tail of the 6th storm, the runoff response is off because of possible underestimate of the natural rainfall.

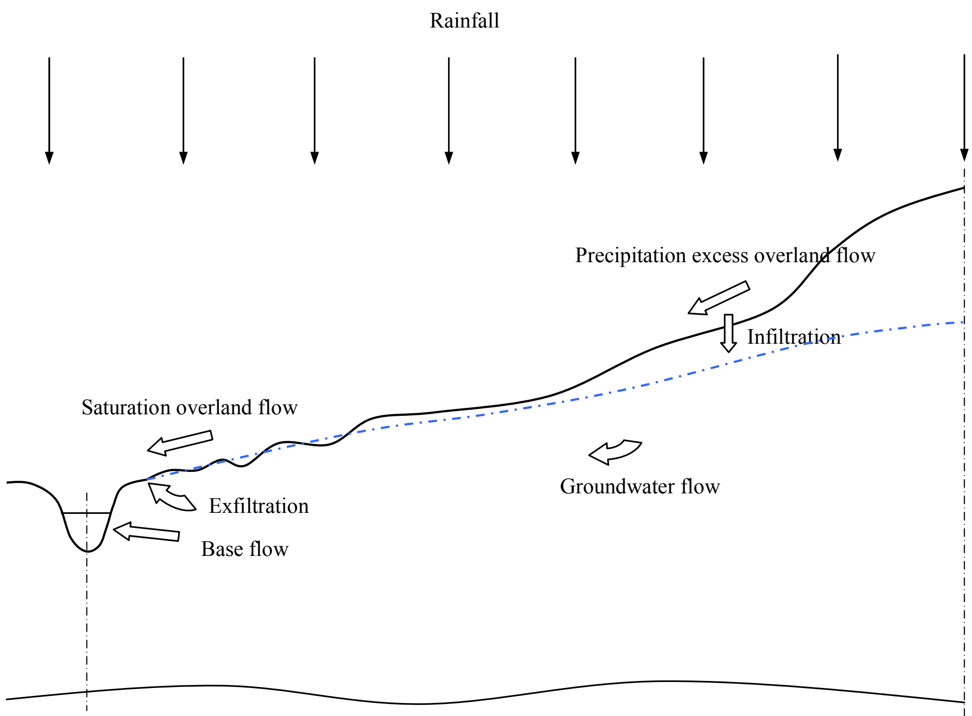

Figure 10 rainfall-runoff generation mechanisms at Shale Hills experiment, PA.

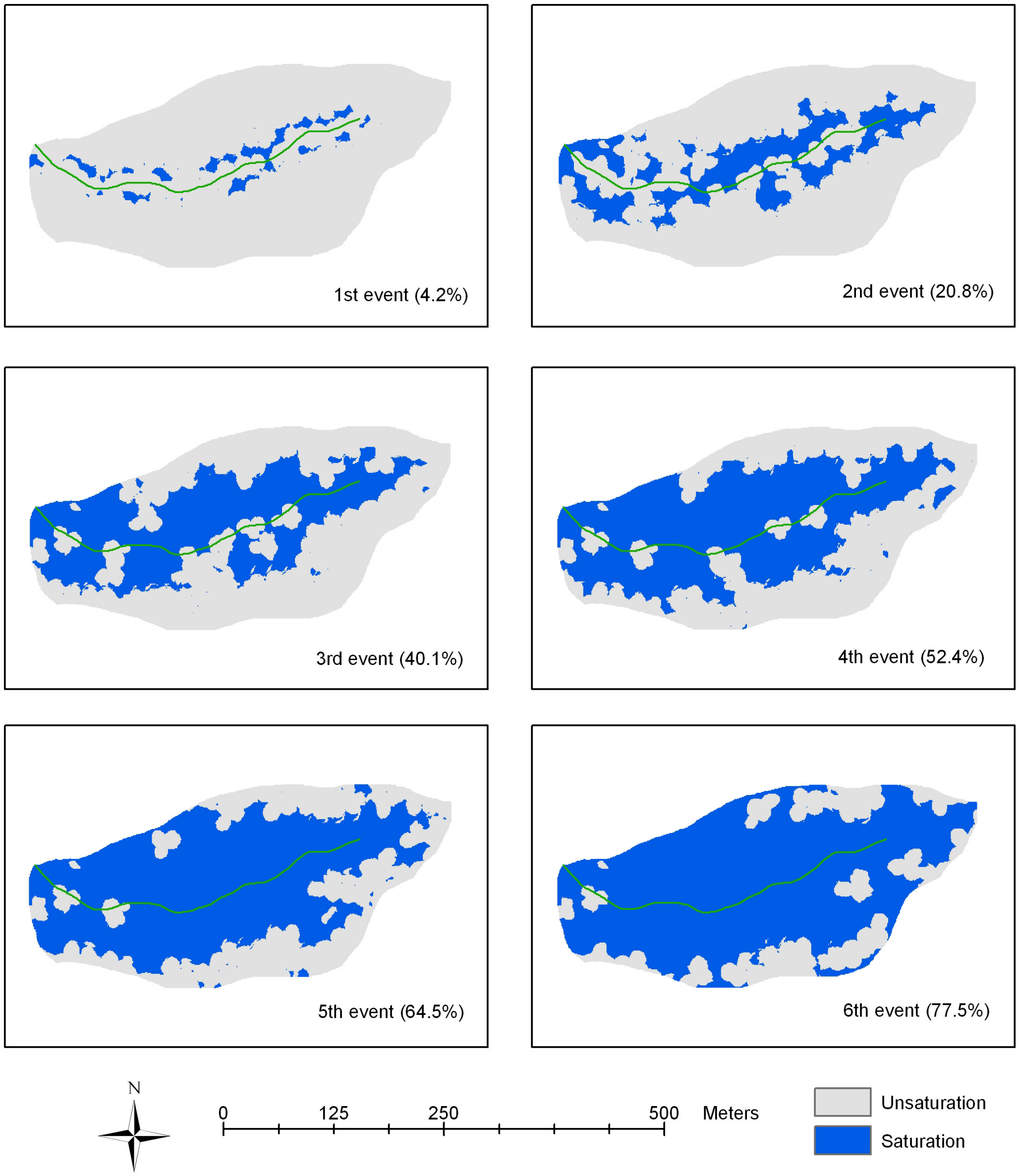

Figure 11 **The saturation area location after each rainfall event. It shows saturation area increases and cause high runoff peaks due to Dunne overland flow. It also reveals that saturation area is not continuous for the 1st 4 events, which leads to longer time scales in surface overland flow.**

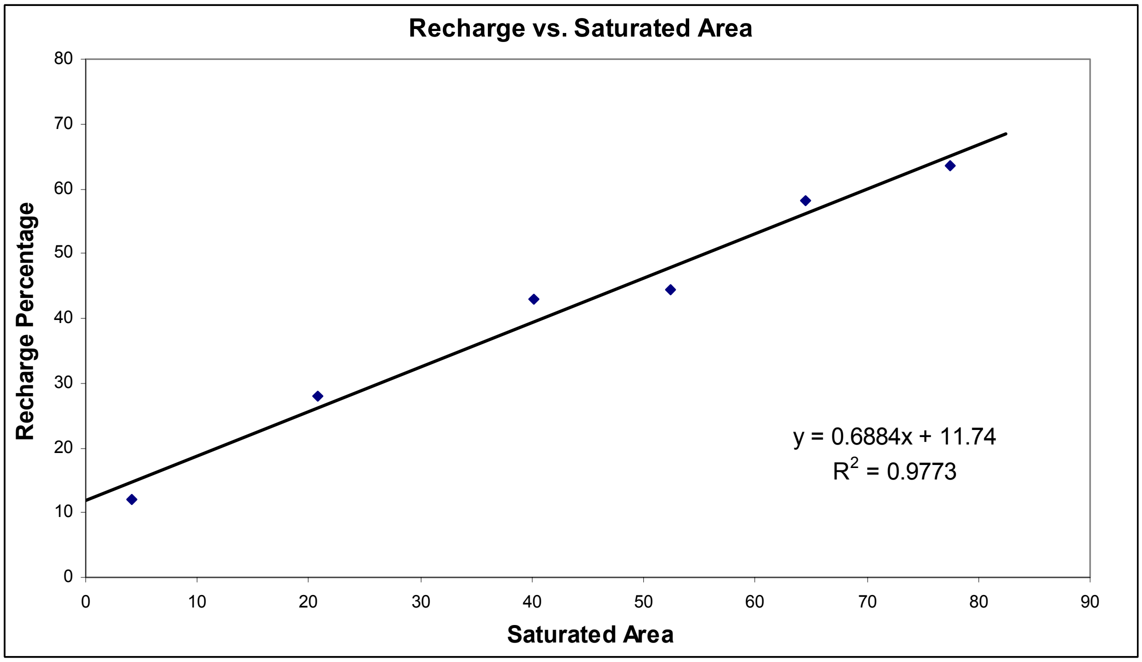

Figure 12 Recharge areas vs. saturated area

The figure 13 and 14 indicates the channel responses to the 3rd rainfall events. Before the rainfall, the channel is almost dry out. It starts to accumulate flow right after the rainfall applies. The dot-dash black line in figure 14 shows the snapshot of channel responses during the rainfall. After 6 hours when the rainfall stops, the channel keeps growing until about 10 hours it reaches its maximum. Since then, the flow depth and channel length begin to shrink back to where it was. This reflects that PIHM is capable of simulating watershed with ephemeral or ungaged channel.

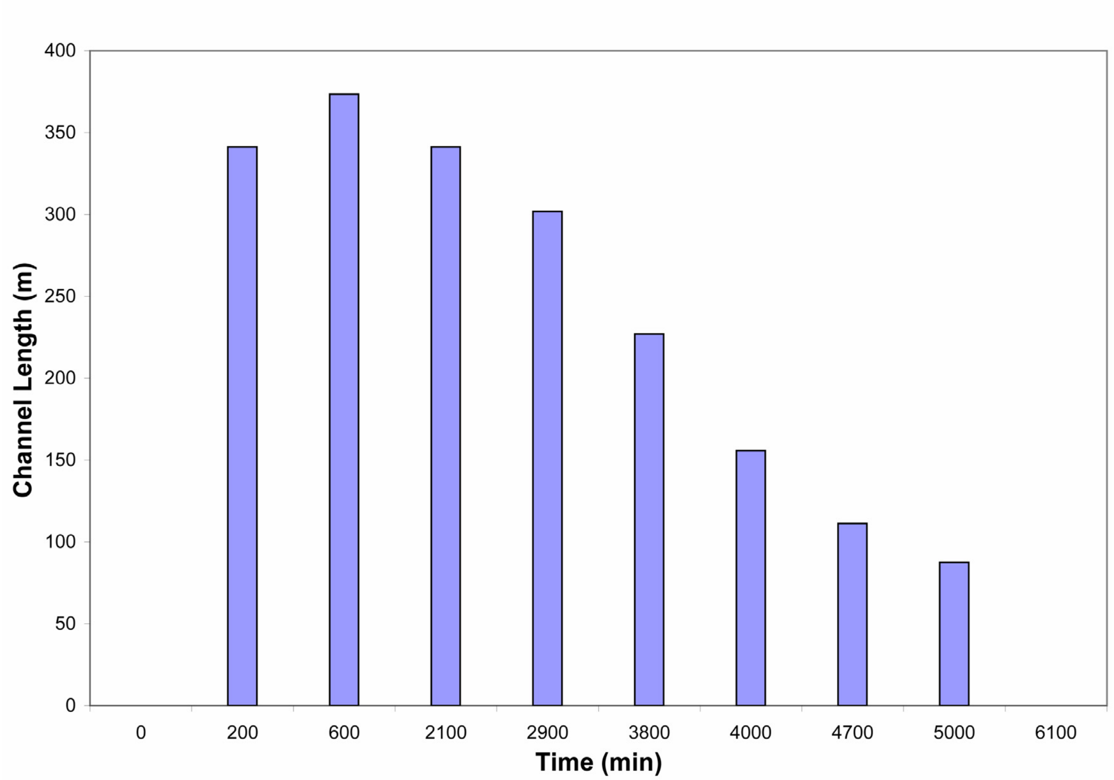

Figure 13 the length of ephemeral channel during 3rd rainfall event.

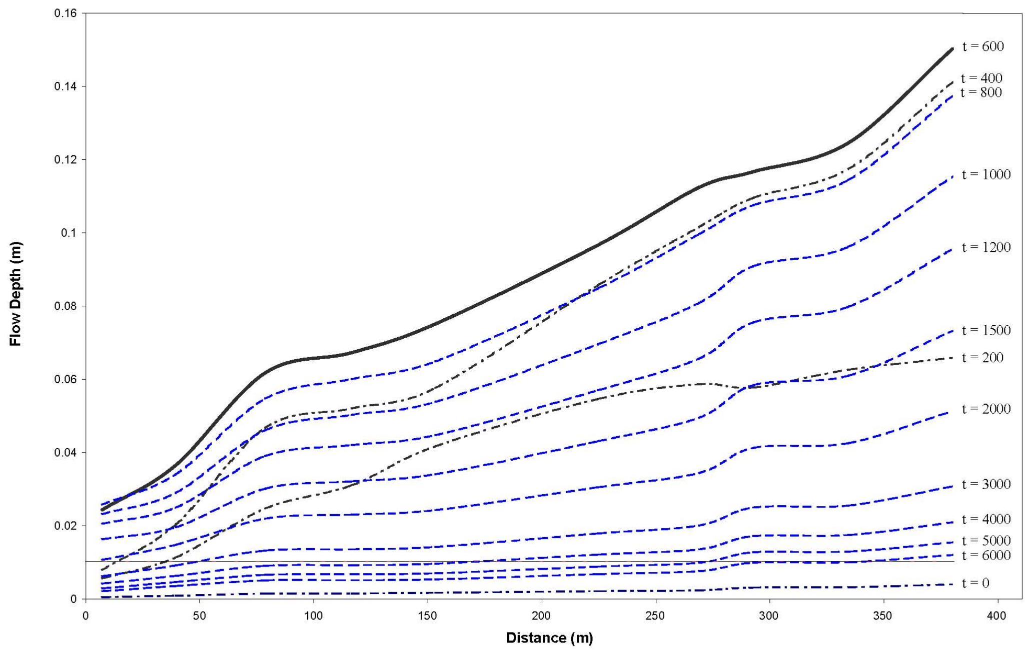

Figure 14 the snapshot of ephemeral channel during 3rd rainfall event.

4.6.3 Predict with Lower Antecedent Soil Moisture

One of goal of hydrological models is to predict. To simulate what will happen in case of dry antecedent soil moisture, we run the model with dry initial condition: there is no rainfall during dry season; the aquifer has been relaxed for half a year. The response of Shale Hills, runoff, is shown in figure 15. The first 3 responses of rainfall events are less intensive than observations both in peaks and tails. However, the latter 3 responses catch up and look almost the same as observations. This implies that the deficit of antecedent soil moisture is made up.

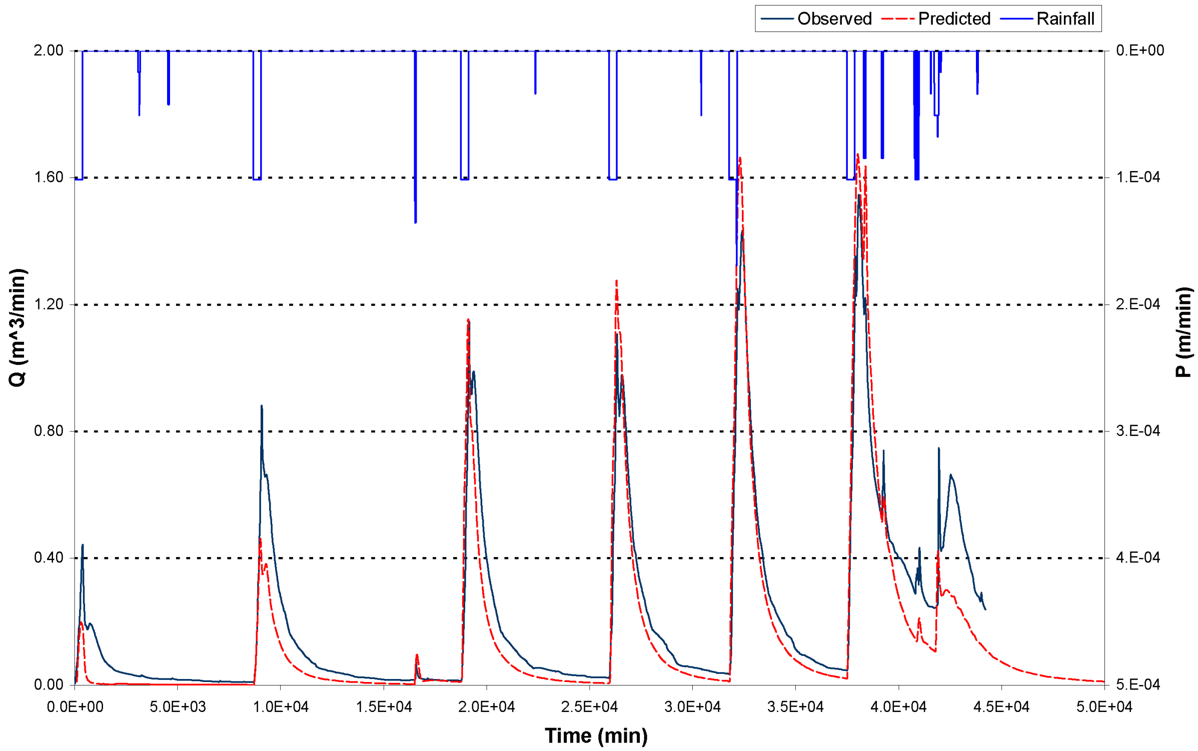

Figure 15 predict runoff with lower antecedent soil moisture

4.7 CONCLUSION

Experiment data of Shale Hills experiment are analyzed in this paper. It reveals that subsurface hydrologic processes play an important role in runoff generation. Runoff response increases as antecedent soil moisture gradually grows. In all six rainfall events, at least 37% of rainfall is stored in aquifer, and releases in a very long time scale as base-flow.

This is the first application of PIHM. It successfully simulates Shale Hills experiments with reasonable match of groundwater level and runoff at outlet. The numerical simulation illustrates the rainfall-runoff mechanisms are a mixture of all four: Horton overland flow; Dunne overland flow; Interflow and Base flow. Among them, Dunne overland flow is the most important mechanism. Those infiltrates in aquifer results in partly saturated area during and after rainfall events. When the antecedent soil moisture is low, the saturated zone is not continuous due to complex terrain. In addition to its flexibility, PIHM show its capabilities in Shale Hills simulation by captures the dynamics of ephemeral channel, which is also possible to be applied to ungaged watershed.

PIHM is used to predict runoff under extreme dry condition, i.e., there is no rainfall during dry season. It shows that only the first 3 runoff response is reduced in this situation. The last 3 remains the same since the antecedent soil moisture is made up.

REFERENCES

Amerman, C.R., 1965. The use of unit-source watershed data for runoff prediction, water resource research, 1(4), 499-508, 1965.

Bierkens, M.F.P., 1998. Modeling water table fluctuations by means of a stochastic differential equation, water resources research, vol. 34. no. 10, 2485-2499.

Bras, R.L., 1990. Hydrology, An introduction to hydrologic science. Addison-Wesley publishing company.

Cohen, S.D., and A.C. Hindmarsh (1994), CVODE User Guide, Numerical Mathematics Group, LLNL. UCRL-MA-118618.

Duffy, C.J., 1996. A two-state integral-balance model for soil moisture and groundwater dynamics in complex terrain. Water Resources Research, Vol. 32, No. 8, 2421-2434.

Duffy, C.J., 2004. A Semi-Discrete-dynamical model for mountain-front recharge and water balance estimation: the Rio Grande of southern Colorado and New Mexico. AGU Monograph.

Dunne, T., Black, R.D., 1970. An experimental investigation of runoff production in permeable soils, water resources research, vol. 6, no. 2 478-490.

Dunne, T., Black, R.D., 1970. Partial area contributions to storm runoff in a small New England watershed, water resources research, vol. 6, no. 5, 1296-1311.

Freeze, A.R., 1972. Role of subsurface flow in generating surface runoff 1. base flow contributions to channel flow, water resrources research, 8(3), 609-623.

Freeze, A.R., 1972. Role of subsurface flow in generating surface runoff 2. upstream source areas, water resources research, 8(5), 1272-1283.

Freeze, A. R., 1980. A stochastic-conceptual analysis of rainfall-runoff processes on a hillslope, water resources research, vol. 16, no. 2, 391-408.

Gottardi, G., and M. Venutelli (1993), A control-volume finite-element model for two-dimensional overland flow, *Advances in Water Resources*, *16*, 277-284.

Haken, H., 1978. Synergetics, an introduction, 2nd edition. Springer Verlag.

Horton, R.E., 1933. The role of infiltration in the hydrologic cycle, Transactions-American Geophysical Union, 14, 446-460.

Leveque, R.J., 2002. Finite Volume methods for hyperbolic problems. Cambridge University Press.

Panday, S., and P.S. Huyakorn (2004). A fully coupled physically-based spatially-distributed model for evaluating surface/subsurface flow, *Advances in Water Resources*, *27*, 361-382.

Robinson, J.S., Sivapalan, M, 1996. Instantaneous response functions of overland flow and subsurface stormflow for catchment models, Hysrological Processes, Vol. 10, 845-862.

VanderKwaak, J. E., 1999. Numerical simulation of flow and chemical transport in integrated surface-subsurface hydrologic systems. Ph.D thesis, University of Waterloo.

VanderKwaak, J. E., Loague, K., 2001, Hydrologicl-response simulations for the R-5 catchment with a comprehensive physics-based model, water resource research, vol. 37, no. 4, 999-1013.

Whipkey, R.Z., 1965. Subsurface storm flow from forested slopes, Bulletin International Association of Scientific Hydrology, 15(3), 25-33.

CHAPTER 5
SUMMARY AND FUTURE WORK

5.1 SUMMARY

In addition to three papers presented in this thesis, a C code implementation named PIHM is developed. The model kernel includes all rainfall-runoff generation mechanisms, channel routing and overland flow with diffusion wave and kinematics wave approximation, 1-D vertical unsaturated zone flow and 2-D groundwater flow. There are 4 types of boundary conditions at outlet: Dirichlet, Neumann, zero-depth condition and critical-depth condition. The model kernel is connected to CVODE, the ODE solver of SUNDIALS. The user has options to use dense, band or iterative solver in CVODE with selectable detail output.

As an implementation of semi-discrete finite volume approach, the ultimate goal of PIHM is not only an efficient research code for full coupled hydrologic simulation, but also a convenient and reliable software/package for wide real application. The development and maintenance of such code demands long term and well organized efforts: the more it has been done, the more it needs to do. So it is necessary for me, as the original author, to write down what I will do if I have plenty of time.

5.2 FUTURE WORK

A graphical user interface is needed to drive PIHM as pre and post processors. The main functions for pre-processor are: retrieve information from GIS data sets; delineate channel network from DEM; Domain decomposition and assign model parameters for elements and control parameters for the simulation. For the post-processor, it will convert model results to GIS datasets, and then we will rely on widely used GIS product for visualization. It is important to include the algorithm by Shewchuk (1997) for domain decomposition.

The structure of PIHM leaves the door open for further refinement. It is necessary to keep hydrologic modules updated. For example, incorporate state-of-art snow module and dynamic vegetation module whenever it is available. Another possible improvement could be a 3-D groundwater flow components, sediment and chemical transport modules.

Computational cost is always a big concern in such a model. It is suggested to use GMRES iterative solver if possible. A pre-conditioner for this solver may dramatically reduce the cost. In large (continent or basin scale) scale simulation, two options of improvement can be attempted. Reduce of complexity of the model kernel towards VIC model is one option. By this approach, this model will become spatial connection of many low dimensional models each representing a sub-watershed. It is possible to achieve such simulation by a PC. Another possibility is parallel version of PIHM. Either Open MP on multiple processor machine or MPI on distributed system can be explored. Since sub-watershed is relative independent region in a large domain, it may be a good idea to distribute load by watersheds.

The SUNDIALS has CVODES for parameter optimization and sensitivity analysis. These tools may be helpful in model calibration and parameter estimation later. It also has a DAE solver in case the ODE system can be reduced.

The scale and scope of hydrologic simulations make GIS a very attractive pre and post processor. However, the current intermediate text files between GIS tools and hydrologic models dramatically slow down the pre-process and limit the capability of post visualization and inquiry in large scale application. The ultimate goal in the long run is to make PIHM works on the same data model as GIS products so that we will have a seamless hydrologic package, i.e., empower the hydrologic model with capability to access the geo-database so that model read directly from database and write simulation results directly back. In this strategy, it is possible to take full advantage of current general database software/technology and make the connection between hydrologic model and GIS tools seamless.